UNIVERSITY OF SOUTHAMPTON

FACULTY OF SOCIAL AND HUMAN SCIENCES

Mathematical Sciences

Neutron Stars and their Terrestrial Analogues

by

Michael Hogg

Thesis for the degree of Doctor of Philosophy

January 2014

UNIVERSITY OF SOUTHAMPTON

ABSTRACT

FACULTY OF SOCIAL AND HUMAN SCIENCES
Mathematical Sciences

Doctor of Philosophy

NEUTRON STARS AND THEIR TERRESTRIAL ANALOGUES

by Michael Hogg

When we consider in detail the behaviour of a fluid consisting of two (or possibly more) interpenetrating components, the likelihood of dynamical instabilities induced by coupling between the two fluids cannot be ignored. The phenomenon is generic to all such multifluid systems and as such is appellated the two-stream instability. Mathematically this class of instability is somewhat akin to the more well known Kelvin Helmholtz instability, but is distinguished by the fluids flowing through each other rather than having a clearly defined interface between them. In this thesis we describe in some detail the mechanisms underlying this instability in a simple linear flow scrutinising in particular the growing (unstable) solutions for small harmonic perturbations. We further consider the application of this genre of instabilities to other physical systems, most conspicuously to that of a rotating superfluid body with rotational lag between the components. This case is of particular interest in neutron star physics, where it offers possibilities for exploring behaviour within the core. There also seems to be the chance of exploring this example in laboratory systems. We also take a tentative first step to extending the application and understanding of the two-stream instability by flirting with the analogous observations in a laboratory realisable binary Bose-Einstein Condensate. This laboratory realisation is a first step towards being able to explore physically issues relating to neutron star dynamics. We further discuss general analogue systems for modelling key features of neutron stars in terrestrial laboratories. The possible applications, along with some of the difficulties in using these analogues, are explored.

Contents

List of Figures

Declaration of Authorship

I, Michael Hogg , declare that the thesis entitled *Neutron Stars and their Terrestrial Analogues* and the work presented in the thesis are both my own, and have been generated by me as the result of my own original research. I confirm that:

- this work was done wholly or mainly while in candidature for a research degree at this University;
- where any part of this thesis has previously been submitted for a degree or any other qualification at this University or any other institution, this has been clearly stated;
- where I have consulted the published work of others, this is always clearly attributed;
- where I have quoted from the work of others, the source is always given. With the exception of such quotations, this thesis is entirely my own work;
- I have acknowledged all main sources of help;
- where the thesis is based on work done by myself jointly with others, I have made clear exactly what was done by others and what I have contributed myself;
- parts of this work have been published as: [9]

Signed:.....

Date:.....

Acknowledgements

There are so many people to whom I should express my gratitude that it is inevitable that I will miss somebody. To those whose names I omit, my apologies.

None of this would have been possible without my foundation year and undergraduate studies. So firstly I should like to express my gratitude to all who lectured, tutored or mentored me in any way. I particularly thank Dr James Renshaw, my personal tutor and Professor James Vickers, who obtained a Nuffield Research Scholarship for me - probably the major reason that I undertook my Ph.D.

I should like to thank all staff and students who, at some time in the last four years have been members of the General Relativity Group. In no particular order I should like to express my thanks to Dr Sam Lander, Dr Steve Millmore and Dr Cesar Lopez-Monsalvo who helped me considerably with the transition from undergraduate to postgraduate study. My thanks also to those others with whom I have shared an office over the years: John Muddle; Tim Lemon; and Stuart Wells. Their friendship and encouragement have helped more than I can say. I would like in particular to thank two people who have been constant companions throughout my time as a postgraduate, Lucy Keer and Justin Lovegrove. Although our areas of study have been different, we have shared a journey and they have put up with me for that long.

I also express appreciation to all of my family. Their personal support has been invaluable. My thanks to my children, Stephanie, James and Elissa, who have all made sacrifices because of my choice to study rather than go out and earn money.

Also thanks to my friends outside of academia. My thanks go especially to the lads from the darts team who understood that I had to take a couple of seasons sabbatical to concentrate on work. Shame they got relegated the first year that I wasn't there.

I reserve my greatest appreciation for two people. The first is Professor Nils Andersson, my supervisor. Nils has always been there. He has remained friendly and supportive, even when things have gone not so well. His personal understanding during some difficult times in my life was invaluable. It's fair to say that without Nils, I wouldn't be here today.

Finally, I should like to give posthumous thanks to my father. Although not an educated man, he saw the value in education for his offspring. I always felt that I let him down in my youth and my only regret about this whole process is that he is not here to share this with me.

Nomenclature

All abbreviations used in this thesis are fully explained at the appropriate juncture in the text.

Chapter 1

Introduction

1.1 Prelude

In studying and extending our knowledge of neutron stars, we are very much at the mercy of nature. The extreme conditions present cannot be reproduced on Earth and, as a consequence, we can not instigate experiments that directly replicate the behaviour of these bodies. We can only watch and wait, hoping that some event will occur, that can be observed and dissected. We watch, for example, for changes in rotation or increases in activity that might further our understanding and improve our model. We are impotent to initiate change in the prevailing conditions of the stars, such as a large accretion of matter or the gravitational effects of nearby bodies. We can only make our observations and interpret.

There is a bitter irony in this state of affairs. Neutron stars are, in themselves, ideal laboratories for the physics of extreme environments. Nowhere else in our Universe are such severe temperature, pressure and gravity combined in a single body. Under this inimitable combination of conditions, we can learn much that can not be studied elsewhere. Yet, we are and will remain (for any foreseeable future time) unable to influence; powerless to set in chain some required set of circumstances designed to further our knowledge.

Considering our purely passive role in the operation of these distant laboratories, it seems remarkable how much has been learned. Through observation alone of the stars, their influence on surrounding bodies and behaviour when influenced by said bodies, we have built an amazing store of knowledge. When combined with known physics, our measurements have enabled an accepted model of the structure of a neutron star to be constructed; allowed us to make testable predictions of their future behaviour. Yet so much remains hidden, impenetrable, in the nature of these Lilliputian, but awe inspiring,

stars.

Yet, what we have learned through observation of these stars and their environs suggests that, even in the ferocious conditions prevailing, much of the physics remains recognisable. From this familiar nature of a star's behaviour, one can infer that key features of this might be successfully modelled using materials that share these features. Let us assume that materials can be found that, in a terrestrial laboratory, can mimic elements of neutron star physics. Then one might realistically produce laboratory experiments that could enhance our understanding of the observed phenomena associated with neutron stars.

Much of this thesis focusses on the ubiquitous two-stream instability [2]. This is described in some detail below. In Chapter 4 we demonstrate an important application of this instability in neutron stars. Elsewhere we explore this instability in other fluid systems and consider whether these might be used to model the behaviour of neutron stars. We further consider different low temperature systems and demonstrate how advances in these fields have led to the possibility of using them as models of some aspects of neutron star behaviour.

1.2 Neutron Stars

Since this thesis is concerned with neutron stars and their laboratory analogues, we commence with a brief overview of their standard model. We include a brief history of how this model was built up over the last eighty years and describe its principal features.

1.2.1 A Brief History of Neutron Stars

In 1932, Sir James Chadwick, working at the Cavendish Laboratory in Cambridge, showed experimentally the existence of the neutron [10]. Only a year later Walter Baade and Fritz Zwicky proposed a star composed of these neutrons [11]. They further suggested, with remarkable prescience, that such stars were born in super-nova explosions. They hypothesised that these bodies would be very dense and much smaller than other stars, with very high gravitational binding.

The earliest theoretical calculations regarding the proposed neutron stars were published in 1939 by Oppenheimer and Volkoff [12]. In these calculations it was assumed that the

stars were composed of an ideal gas of free neutrons at high density. The work was chiefly motivated by the idea that massive normal stars might have cores that consist largely of free neutrons. The behaviour of these neutrons might contribute a significant portion of the stars energy output [10].

As the mechanisms relating to nuclear fusion within stars became better understood, interest in these 'neutron cores' faded somewhat. However, several physicists continued to produce theoretical works, for example [13][14][15], where such topics as the composition and the equation of state of these still unconfirmed bodies were discussed. This work was very much at the fringes of the astrophysics community as it was believed that such stars were unlikely to be visible to the optical telescopes of the time [10].

The discovery of non solar x-ray sources in 1962 [16][17] and the first identification of a quasi stellar object (quasar) in 1963 [18] triggered further interest in neutron stars. It was speculated that the x-ray source might be a young warm neutron star and this inspired theoretical work on neutron star cooling [10]. The observation of the high red-shift of the quasar led to suggestions that this was associated with a compact object. However it was shown, as more quasars were detected, that the red-shift from these exceeded the maximum gravitational red-shift from a stable neutron star [19]. With this observation any link between quasars and neutron stars was dispelled [10].

It was the discovery of pulsars in 1967 [20] that brought neutron stars to the fore. The original observations were made by Jocelyn Bell, who was working as part of a team using a radio telescope to study quasars. She noted a signal pulsing with great regularity at a rate of approximately one pulse per second. This pulse was so regular that it was even suggested that it might be artificial in nature. This led to the source being given the cognomen LGM-1 (Little Green Men -1). This observation, along with its astrophysical interpretation, was seen to be of such significance that Anthony Hewish, the leader of the group that made the detection was awarded the Nobel Prize in 1974. It was proposed that this pulsar, along with others that had been observed, was a rapidly rotating neutron star [21]. However, it should be noted that this discovery was not made in a theoretical vacuum. It had previously been surmised that neutron stars, as the remnants of super-novae explosions, would be rapidly rotating [22][23][24]. It had also been proposed that they would possess strong magnetic fields [22][25] and that a neutron star might be the energy source of the Crab nebula [26]. Further a simple magnetic dipole model for the conversion of a neutron stars rotational energy to electro-magnetic radiation had already been produced at the time of Hewish's discovery [27].

After the first observation of a pulsar, progress in neutron star physics was rapid. A review of the subject published in 1971 [28] gave a description of the structure for these stars that contains most the features in today's standard model. Such features as a superfluid core, a solid crust, an atmosphere, a strong magnetic field and its associated braking were included (See Figure 1.1)

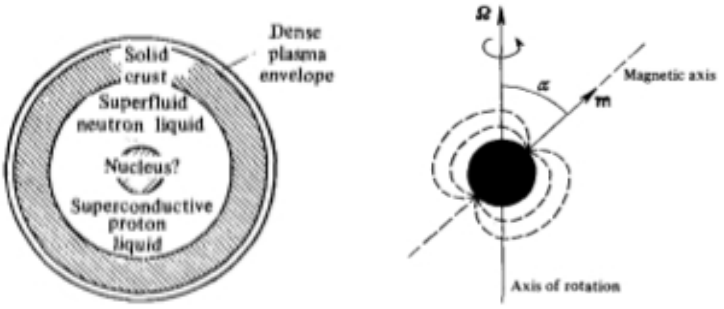

Figure 1.1: *Figures from 1971 review showing basic structure of a pulsar. It can be seen that within a few years of the discovery of pulsars, most of the features of today's standard model were already included.* V.L.Ginzburg, Soviet Physics Uspekhi **14** 83

As was noted in the review, neutron stars undergo continuous spin-down through magnetic braking. However, in 1969 a significant and rapid increase in the rotational velocity of the Vela pulsar was observed [29]. Similar phenomena, which were referred to as glitches, were observed in many other pulsars, as well as regular occurrences in both the Vela and Crab pulsars [30][31]. Several explanations were originally put forward for these glitches. The two most likely candidates are the star quake model [32][33] and the vortex unpinning model [34][35][36]. These two mechanisms are discussed in more detail later in this thesis. However, it is worth noting that they are not mutually exclusive. It is possible that both may be causes of glitches at differing times in a neutron stars life [37][38].

Whilst this by no means brings us up to the present in terms of neutron star research; most of the standard model had been established by the early 1970s. The structure and formation of the stars had been explained. As described in [39], research became more diverse and specialised, focussing on individual elements of a star's behaviour.

1.2.2 The Standard Model of Neutron Star Structure

Whilst predominantly 'text book' material, it is of some value to include a description of the main components of a neutron star's structure at this point. Throughout this thesis, references are made to various parts of the star and a synopsis of the structure provides a useful context. Before proceeding to the specifics of the structure of a neutron star,

we include some more general points.

The mass of an 'average' neutron star is approximately 1.4 solar masses, although more massive stars, close to two solar masses have been observed [40]. The radius is of the order of 10^4 m and the average density, depending on the mass, is approximately 10^{17} kg m^{-3}. Of course, the density is not constant throughout the star and increases markedly as one approaches the centre. It has been theorised that this increase in density is roughly quadratic in nature [41]. (This density profile will prove useful when we discuss modelling elements of the superfluid core using Bose Einstein Condensates, as quadratic profiles can be relatively easily achieved in the latter). This high density, alongside the resulting pressures and gravitational fields, are not found anywhere else in our known Universe. The average density of a neutron star is of the order of 10^{14} times that of our sun and, within the interior of the star, it is greater than that of atomic nuclei. Under such extreme conditions much of the physics we use to describe the rest of the Universe is inadequate. Neutron stars are also observed to spin rapidly with rotation rates up to the order of tens of thousands of revolutions per minute. A neutron star also possesses a strong magnetic field, of the order of 10^{12} Gauss, compared to a strength of one tenth of a Gauss for the Earth's field and one Gauss for the Sun. There also exists a class of neutron star with magnetic fields one thousand time stronger. These are referred to as magnetars.

These intense magnetic fields are a simple consequence of the conservation of magnetic flux from the progenitor star. As the star shrinks, its magnetic field intensifies by an inverse square law.[91]

The misalignment between the rotational and magnetic axes is more problematic. There is as yet no explanation for the evolution of the magnetic fields that account for this. Our evidence for this misalignment is purely observational. It is worth noting that without such a misalignment, pulsars would not pulse.

The strong magnetic fields lead to charged particles from the star magnetosphere being concentrated at the poles. These particles are highly energetic, owing to the strength of the field and the rapid rotation of the star, and cause emissions at the poles that are very bright in the radio and x-ray bands. Since the magnetic poles are not necessarily aligned with the rotation of the stars, these jets give us the regular pulses by which neutron stars are most easily observed. Matter may also be accreted from the detritus of a star's progenitor or a nearby companion. This accretion can also contribute to the concentration of charged particles.

An illustration of a neutron star's structure is given in Figure 1.2. It is interesting to compare this with image from 1971, Figure 1.1. It can be seen that the earlier image displayed most of the features (with the notable exception of a distinct atmosphere) of the now, universally accepted model. We continue with a concise description of each layer of the star. We note that Figure 1.2 shows the crust as a single layer, whereas we separate this into inner and outer crusts for reasons that will become apparent.

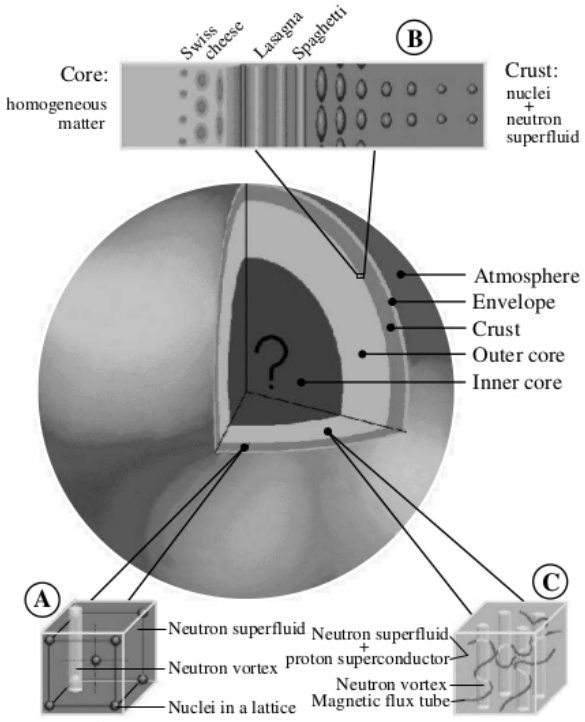

Figure 1.2: *The Structure of a neutron star, indicating the different regions of the star and the basic internal properties.* Dense Matter in Compact Stars: Theoretical Developments and Observational Constraints. Page and Reddy 2006.

Atmosphere. Owing to the very strong gravitational field at the surface of the star, the atmosphere is compressed down to less than a metre thick. The composition of the atmosphere can vary, but is most commonly made up from hydrogen, Helium or gaseous iron in plasma form. Recently a neutron star with an atmosphere composed largely of carbon has also been observed [42].

Envelope This is a thin dense Coulomb liquid, consisting of partially and completely ionised atoms surrounded by free electrons. Whilst the bottom interface of this 'ocean' layer with the solid crust is clearly defined; the interface with the atmosphere is more tenuous. For this reason the atmosphere and the envelope are not distinguished from each other in some descriptions [39].

Outer Crust This is composed largely of a lattice of iron ions. There are few free nucleons, although free electrons are abundant. This lattice is, at most, a few hundred metres thick.

Inner Crust This layer is up to one kilometre thick. As pressure increases, so the lattice ions are compressed further, leading to heavier nuclei being formed. As we go deeper into the star and there is a further increase in pressure, it becomes energetically favourable for neutrons to 'drip' out of the nuclei. It is the region where this process begins that we define as the boundary between the outer and inner crust. As the pressure continues to increase, so the number of free neutrons also increases. So the inner crust is composed of a sea of free neutrons coexisting with atomic nuclei and free electrons.

Outer Core At higher still pressures, atomic nuclei can no longer exist and we have a region composed entirely of superfluid neutrons, superconducting protons and free electrons. Within the outer core, the density can exceed that of atomic nuclei. This layer may be up to nine kilometres thick, although estimates for this are largely hypothetical and depend on the mass of the star.

Inner Core. At and very close to the centre of the neutron star the density may exceed nuclear density to such a degree that even the nucleons decompose into their constituent parts. At such densities, with the resultant pressures, our understanding of the composition of the star becomes problematic. Some have hypothesised that this part of the star consists of a quark-gluon 'soup'[43], although this is almost pure conjecture.

The insets in Figure 1.2 also show interesting features of the neutron stars interior. The top inset shows the interface between the inner crust and the outer core. Here the structure changes from that of a lattice surrounded by superfluid neutrons to a multi-component fluid of said superfluid neutrons, superconducting protons and highly energetic free electrons. The two lower insets show the existence of vortices in both the inner crust (left) and the outer core (right).

It is interesting at this point to consider the evidence for the existence of superfluid neutrons within the core of a neutron star. The assumption of a core consisting of such a superfluid is the basis for much of the work in this thesis and, as such, it is appropriate to briefly expand on the theory underlying this assumption.

The first major piece of evidence comes from the post glitch relaxation times. Early work by Alpar et al [44][45] indicated that the relaxation times were consistent with the

presence of a superfluid core rather than a normal fluid or solid core. This is discussed further in Chapter 2.

Further evidence emerged from studies of the cooling rates and subsequent calculations of neutrino emission rates. These were consistent with the formation and separation of neutrons into Cooper pairs. Such behaviour is consistent with the likely formation of a superfluid by the neutrons [46].

1.3 Superfluidity

We now move on to a short introduction to superfluids and their relation to neutron star physics. Again much of this section is text book material with any additions clearly indicated. The major sources for this section are Putterman [47], Li & Lam [48] and Khalatnikov [49].

Superfluidity is a state of matter in which the material under consideration behaves like a fluid with zero viscosity (under some circumstances [50]) and zero entropy. This occurs when the temperature of a material, which obeys Bose statistics, drops below some critical value. At temperatures below this critical value, a macroscopic proportion of the particles occupy the lowest energy, or ground, state for that material. Such a circumstance can only occur with a bosonic fluid, since the energy levels of fermions are restrained by Pauli's exclusion principle, as shown in Figure 1.3.

Since the first discovered and most widely known superfluid is that produced from Helium (^{4}He), much of the research into superfluidity has been based upon this.

1.3.1 Superfluidity in Helium-4

The superfluidity effect was first observed in 1937 [51][52] within liquid ^{4}He. Instead of freezing, as might be expected, the Helium underwent a phase transition. Before this change of state the experimenters were looking at a clear colourless liquid, whilst after the change, they were looking at a clear colourless liquid. But there were clearly observable changes in the liquids characteristics. The most easily observable was the way in the evaporation of the liquid. Above the critical temperature the liquid boiled like water in a saucepan. Below this temperature the fluid became still, with no visible bubbles rising through it [50]. This phenomenon is explained by the enormously

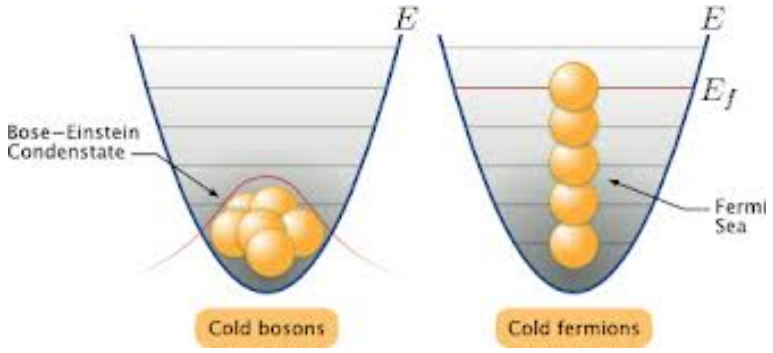

Figure 1.3: *Comparison of Possible Energy States of Bosons and Fermions. In the case of bosons, there is no limit to the number of particles that may occupy any energy level. Whilst only one fermion with a particular spin may occupy each state. We note that, in the case of the fermions, the highest occupied energy state, E_f, is referred to as the Fermi energy.* www.quantum bits.org

increased thermal conductivity below the critical temperature. In a normal liquid local hotspots develop, causing the vapour pressure to rise; resulting in a bubble, which rises to the surface. However, below the critical temperature, the high thermal conductivity does not allow such hot spots to form. So, even though evaporation continues at the surface, the bulk of the liquid appears undisturbed.

The cognomen superfluid comes from the most spectacular property of this new state of matter. This is the ability of the liquid to flow through fine holes without resistance. This has some interesting consequences. If an ordinary liquid were allowed to flow through a capillary, we would observe a pressure gradient across the tube to overcome the effect of shear viscosity. In the case of superfluid Helium, no such pressure gradient is observed. This suggests that, in this sense, the Helium has zero viscosity.

The differences between the two states of Helium are so great that it became necessary to distinguish between them in any discussion. To this end normal Helium is indicated by He I, whilst its superfluid cousin is indicated by He II. We use this method of distinguishing the two materials throughout this thesis.

We can see from Figure 1.4 that this critical temperature is somewhat pressure dependent and that there is a maximum pressure at which this phase transition occurs. Figure 1.5 shows the change in specific heat capacity of Helium with temperature. The shape of this plot resembles the Greek lambda and so, for Helium, this phase transition temperature has become known as the λ-point. This occurs, at normal atmospheric

pressure at about 2.17 K.

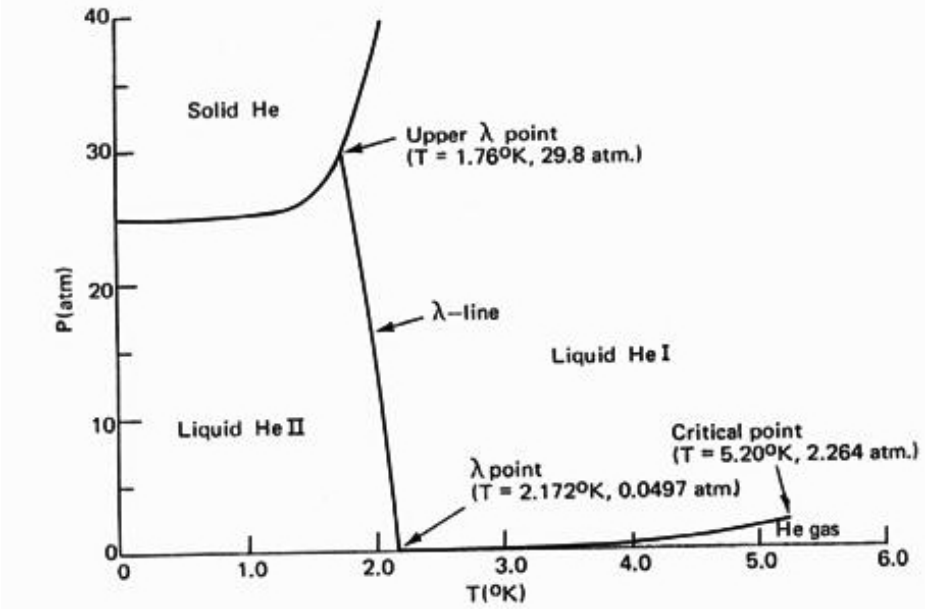

Figure 1.4: *Pressure/Temperature plot for* ^{4}*He indicating phase transition.*[1]

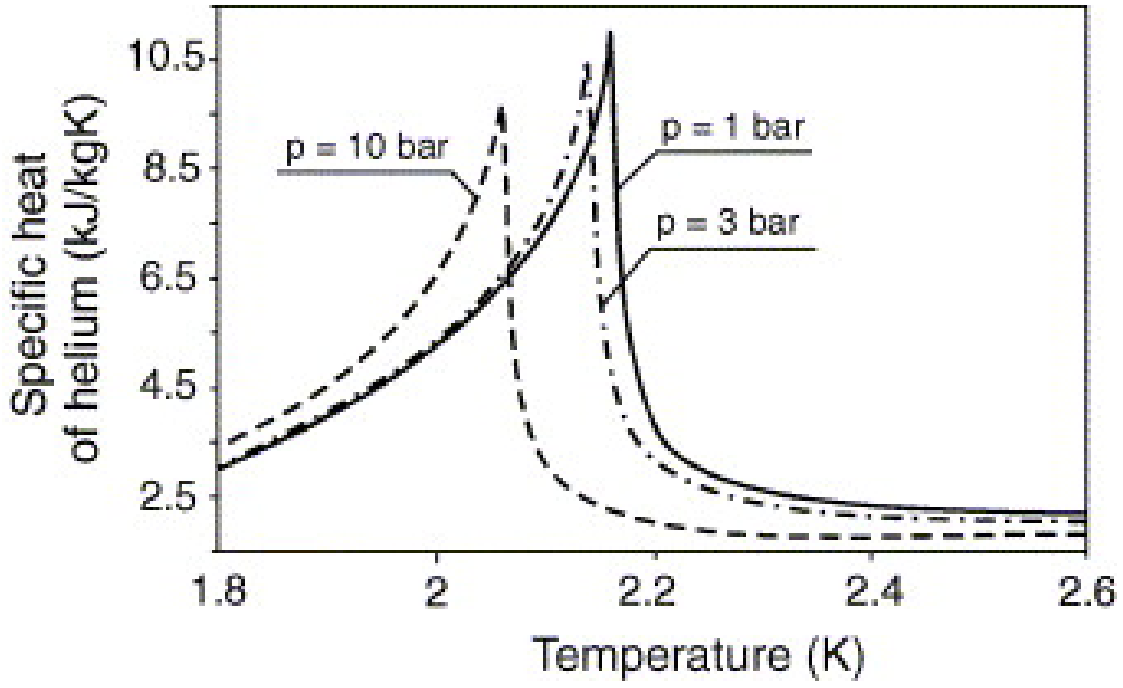

Figure 1.5: *Plot of specific heat vs. temperature for* ^{4}*He indicating the* λ *point. So named because of the shape of the curve. This figure also demonstrates the dependence on pressure of the onset of superfluidity.* [1]

As mentioned, superfluidity occurs when a proportion of the particles of a material occupy the lowest energy (or ground) state. As temperature decreases further, the fraction of particles in this ground state increases until, at about 1 K the overwhelming majority of particles are at their lowest energy. Between the λ-point and 1 K there exists

a mixture of normal fluid and these lowest energy particles. This coexistence of two differing groups of particles is the basis for the two fluid model for He II as put forward by Landau [53]. In this model He II is assumed to consist of two inter-penetrating fluid components. The first an ideal superfluid, the second a normal fluid component with which the entropy is associated. This is discussed in more detail in Chapter 2. In Chapter 6 we consider the entropy as a dynamical quantity in its own right.

As a final feature of superfluidity in this section we discuss the existence of quantised vortices in He II. Vorticity, itself, is not a unique feature of superfluids. The generation of vortices in a normal fluid can most easily be described as the result of shear when a fluid flows past a solid boundary. Vorticity is one of the properties of shear [54] and so, as a result of the no-slip condition and resulting velocity gradient, vortices are formed at the boundary. In a normal fluid the motion of such vortices (vorticity transport) can be considered somewhat analogous to heat conduction and convection [55]. This can be seen by considering the Navier-Stokes equation;

$$\rho\left(\partial_t \boldsymbol{v} + \boldsymbol{v}\cdot\nabla\boldsymbol{v}\right) = -\nabla p + \nabla\cdot\boldsymbol{T} + \boldsymbol{f}, \tag{1.1}$$

where $\boldsymbol{v}$ is the fluid velocity, ρ is the density, p is the pressure, $\boldsymbol{T}$ is the (deviatoric) component of the total stress tensor and $\boldsymbol{f}$ represents the body forces per unit volume acting on the fluid.

The vorticity, $\boldsymbol{\omega}$, of the fluid is defined as the curl of the velocity. So we can express this by

$$\boldsymbol{\omega} = \nabla\times\boldsymbol{v}. \tag{1.2}$$

So, if it is assumed that the fluid is incompressible, taking the curl of the Navier-Stokes equation, (1.1), and assuming no external forces, gives us the equation for vorticity transport equation in a two dimensional plane.

$$\partial_t\omega + \left(\boldsymbol{v}\cdot\nabla\right)\omega = v\nabla^2\omega. \tag{1.3}$$

Here ω is the vorticity component perpendicular to the plane. This equation is analogous for the heat equation for vanishing dissipation [54]. The $\boldsymbol{v}\cdot\nabla$ term is representative of the convection, whilst the ∇^2 represents the diffusion.

This is clearly a two-dimensional projection onto a plane. A full three-dimensional analysis would be considerably more complicated. However, this serves as a proof of principle and, since this subject does not form a critical part of the thesis, suffices for our purpose.

However, in the case of the superfluid component, the absence of viscosity does not enable vortices to form in this way. In this case the rotation of part of the fluid is not past to an adjoining region. We can regard the rotation as being 'captive' in one part of the fluid. If the energy of the rotation is high enough, a vortex becomes the lowest energy state and forms in the area of rotation. If the energy reaches a sufficient level another vortex forms and so on. The energy steps between the formation of an extra vortex are quantised, although there are different energies associated with individual configurations [54]. The lowest energy configuration in the absence of boundaries (hence the most common) is the Abrikosov lattice[1] where, in an idealised case, the vortices form equilateral triangles [54].

Whilst superfluidity has been observed in other materials, their critical temperatures are generally much lower than the λ-point of ^{4}He. In the cases of fermionic materials there are other effects that allow superfluidity to occur. These are discussed below. In chapter 3 we also examine Bose-Einstein Condensates which also exhibit superfluidity.

1.4 The Superfluid Two-Stream Instability

In considering the physics of a neutron star core, one of the key features is the existence of two distinct components, superfluid neutrons and superconducting protons, sharing the same physical space. Any full description of the dynamics of the core must include an analysis of the behaviour of such a composite fluid. In this section we describe a class of dynamical instabilities pertaining to such a composite superfluid. We reference much of the work on this subject of Andersson et al. [2], which itself references seminal works relating to other dynamical instabilities in fluid dynamics and plasma physics [57], [58].

In their paper [2], Andersson et al. describe a new dynamic instability in a two component superfluid, which they christen the superfluid two-stream instability. They assume the existence of a fluid consisting of two interpenetrating superfluid components with some form of coupling between them. They go on to show that this instability can occur when the relative motion of the two components exceeds some critical velocity. As is

[1] Whilst in the absence of boundaries, the Abrikosov lattice is the lowest energy configuration, this is not necessarily true for bounded or distorted superfluids. In these cases some deviation from the pattern of regular equilateral triangles is observed [56].

shown here the instabilities are somewhat analogous with the Kelvin-Helmholtz instability along the interface between two fluids [59], although in this case the two fluids occupy the same space.

Since the example which we cite in this thesis [2] was predominantly motivated by research into neutron stars, we assume a two component superfluid consisting of interpenetrating superfluid neutrons and superconducting protons indexed in equations by n and p respectively. This choice of materials is almost arbitrary since the initial model makes no mention of the charge in relation to the fluids in question. It does have one advantage that simplifies the algebra considerably, in that the particle masses of the two components can be treated as identical [60] without unduly affecting the result. As a further simplification it is assumed that there are no entrainment effects between the two fluid components. The inclusion of entrainment is discussed in both the paper under discussion and, in more detail, in later work by the paper's authors [61]. This leaves only the chemical coupling between the components as given by the variation,

$$\mathrm{d}\varepsilon = \mu_{\mathrm{n}}\mathrm{d}n_{\mathrm{n}} + \mu_{\mathrm{p}}\mathrm{d}n_{\mathrm{p}}, \tag{1.4}$$

where n_{x} and μ_{x} are respectively the particle density and chemical potential of the indexed fluid component, and ε is the total internal energy.

With regard to the environment, it is assumed that any gravitational field is constant and unperturbed, and that the protons are at rest in the reference frame being used; whilst the neutrons flow with constant velocity, v_0. A new variable, $\tilde{\mu}_{\mathrm{x}}\,(=\mu_{\mathrm{x}}/m_{\mathrm{x}})$, the chemical potential per unit mass, is also defined. Whilst it is true that these assumptions may not be valid when we come to apply this work to neutron stars, at this stage they simplify the problem, enabling the main features of the instability to be studied.

These assumptions lead to two dynamical equations for each fluid. A conservation equation,

$$\partial_t n_{\mathrm{x}} + \boldsymbol{\nabla}\cdot(n_{\mathrm{x}}\mathbf{v}_{\mathrm{x}}) = 0, \tag{1.5}$$

and an Euler-type equation,

$$\frac{\partial \mathbf{v}_{\mathrm{x}}}{\partial t} + (\mathbf{v}_{\mathrm{x}}\cdot\boldsymbol{\nabla})\,\mathbf{v}_{\mathrm{x}} + \boldsymbol{\nabla}\tilde{\mu}_{\mathrm{x}} = 0. \tag{1.6}$$

It is assumed that the background state is disturbed by sufficiently small perturbations, such that the two component velocities may be written as:

$$\mathbf{v}_{\mathrm{n}} = \left[v_0 + \delta v_{\mathrm{n}}\left(t, x\right)\right]\hat{\mathbf{x}} \tag{1.7}$$

and

$$\mathbf{v}_{\mathrm{p}} = \delta v_{\mathrm{p}}\left(t, x\right)\hat{\mathbf{x}}, \tag{1.8}$$

where $\hat{\mathbf{x}}$ is the unit vector in the direction of flow. The perturbations in question are assumed to be longitudinal in nature, thus relating them to sound waves.

Combining equations (1.5) to (1.8) and linearising gives four perturbation equations, two for each component:

$$\partial_t \delta n_{\mathrm{n}} + v_0 \partial_x \delta n_{\mathrm{n}} + n_{\mathrm{n}} \partial_x \delta v_{\mathrm{n}} = 0, \tag{1.9}$$

$$\partial_t \delta n_{\mathrm{p}} + n_{\mathrm{p}} \partial_x \delta v_{\mathrm{p}} = 0, \tag{1.10}$$

$$\partial_t \delta v_{\mathrm{n}} + v_0 \partial_x \delta v_{\mathrm{n}} + \partial_x \delta \tilde{\mu}^{\mathrm{n}} = 0 \tag{1.11}$$

and

$$\partial_t \delta v_{\mathrm{p}} + \partial_x \delta \tilde{\mu}^{\mathrm{p}} = 0. \tag{1.12}$$

It is then assumed that the perturbations are plane waves, that is, they harmonically dependent on both time, t, and position, x. It is further assumed that these perturbations are of fixed amplitude. This gives

$$\delta v_{\mathrm{x}}\left(t, x\right) = \bar{v_{\mathrm{x}}} \exp\left[i\left(\omega t - kx\right)\right], \tag{1.13}$$

where ω and k are the frequency and wave number respectively.

It would be more realistic, at this stage to consider obtaining solutions through use of a full Laplace/Fourier transform. However, we are, at this stage, only searching for a proof

of principle and, therefore, it is convenient to make as many simplifying assumptions as possible while still preserving the key features of our model.

The above assumption, combined with the four perturbation equations gives the following four equations:

$$i\left(\omega - kv_0\right)\bar{n_{\rm n}} - ikn_{\rm n}\bar{v_{\rm n}} = 0, \tag{1.14}$$

$$i\omega\bar{n_{\rm p}} - ikn_{\rm p}\bar{v_{\rm p}} = 0, \tag{1.15}$$

$$i\left(\omega - kv_0\right)\bar{v_{\rm n}} - i\bar{\tilde{\mu}}^{\rm n} = 0 \tag{1.16}$$

and

$$i\omega\bar{v_{\rm p}} - ik\bar{\tilde{\mu}}^{\rm p} = 0. \tag{1.17}$$

The other two equations to enable this system in six variable to be solved can be obtained from the equation (1.4), where it was assumed that the energy functional, ε, is a function of $n_{\rm p}$ and $n_{\rm n}$ only. From this, the following are obtained:

$$\begin{aligned}\delta\tilde{\mu}^{\rm n} &= \left(\frac{\partial\tilde{\mu}^{\rm n}}{\partial n_{\rm n}}\right)_{n_{\rm p}}\delta n_{\rm n} + \left(\frac{\partial\tilde{\mu}^{\rm n}}{\partial n_{\rm p}}\right)_{n_{\rm n}}\delta n_{\rm p} \\ &= \frac{\partial^2\varepsilon}{\partial n_{\rm n}^2}\delta n_{\rm n} + \frac{\partial^2\varepsilon}{\partial n_{\rm p}\partial n_{\rm n}}\delta n_{\rm p},\end{aligned} \tag{1.18}$$

and similarly

$$\begin{aligned}\delta\tilde{\mu}^{\rm p} &= \left(\frac{\partial\tilde{\mu}^{\rm p}}{\partial n_{\rm n}}\right)_{n_{\rm p}}\delta n_{\rm n} + \left(\frac{\partial\tilde{\mu}^{\rm p}}{\partial n_{\rm p}}\right)_{n_{\rm n}}\delta n_{\rm p} \\ &= \frac{\partial^2\varepsilon}{\partial n_{\rm p}\partial n_{\rm n}}\delta n_{\rm n} + \frac{\partial^2\varepsilon}{\partial n_{\rm p}^2}\delta n_{\rm p}.\end{aligned} \tag{1.19}$$

At this point three new constants for the two component fluid are defined. The sound speed for each individual fluid component, $c_{\rm x}$, is given by:

$$c_{\mathrm{n}}^2 = n_{\mathrm{n}} \left(\frac{\partial \tilde{\mu}^{\mathrm{n}}}{\partial n_{\mathrm{n}}} \right)_{n_{\mathrm{p}}} = n_{\mathrm{n}} \left(\frac{\partial^2 \varepsilon}{\partial n_{\mathrm{n}}^2} \right), \tag{1.20}$$

$$c_{\mathrm{p}}^2 = n_{\mathrm{p}} \left(\frac{\partial \tilde{\mu}^{\mathrm{p}}}{\partial n_{\mathrm{p}}} \right)_{n_{\mathrm{n}}} = n_{\mathrm{p}} \left(\frac{\partial^2 \varepsilon}{\partial n_{\mathrm{p}}^2} \right), \tag{1.21}$$

and a coupling parameter, C, given by,

$$C = n_{\mathrm{n}} \left(\frac{\partial \tilde{\mu}^{\mathrm{n}}}{\partial n_{\mathrm{p}}} \right)_{n_{\mathrm{n}}} = n_{\mathrm{p}} \left(\frac{\partial \tilde{\mu}^{\mathrm{p}}}{\partial n_{\mathrm{n}}} \right)_{n_{\mathrm{p}}} = n_{\mathrm{n}} \left(\frac{\partial^2 \varepsilon}{\partial n_{\mathrm{p}} \partial n_{\mathrm{n}}} \right). \tag{1.22}$$

It is worth pausing here to consider the physical significance of the parameter C. If we consider the energy, ε, as a function of both particle densities then we have

$$\varepsilon = \varepsilon n_{\mathrm{p}}, n_{\mathrm{n}}. \tag{1.23}$$

The first derivative of this gives us the chemical potential of each component by

$$\frac{\partial \varepsilon}{\partial n_{\mathrm{p}}} = \mu_{\mathrm{p}} \tag{1.24}$$

$$\frac{\partial \varepsilon}{\partial n_{\mathrm{n}}} = \mu_{\mathrm{n}} \tag{1.25}$$

So the individual chemical potentials apparently have no dependence upon the presence of the other component. But when we take the second derivative we arrive at equations (1.18) and (1.19). These equations have some term that relates to the sound speed plus some cross term, which couples the changes in chemical potential of one component to the particle density of the other.

This coupling parameter represents the mixed derivatives of the energy functional and it can be seen that it also has units of velocity squared.

Removal of this term, in the absence of entrainment, removes all coupling between the two components so the energy, ε, of the mixed fluid could be written as

$$\varepsilon = F\left(n_{\mathrm{n}}\right) + G\left(n_{\mathrm{p}}\right). \tag{1.26}$$

From the above definitions it is possible to obtain the chemical potentials in terms of the other variables:

$$n_{\mathrm{n}}\delta\tilde{\mu}^{\mathrm{n}} = c_{\mathrm{n}}^2\delta n_{\mathrm{n}} + C\delta n_{\mathrm{p}}, \tag{1.27}$$

$$n_{\mathrm{p}}\delta\tilde{\mu}^{\mathrm{p}} = c_{\mathrm{p}}^2\delta n_{\mathrm{p}} + \frac{n_{\mathrm{p}}}{n_{\mathrm{n}}}C\delta n_{\mathrm{n}}. \tag{1.28}$$

Combining these with the plane wave perturbation equations above (1.14) to (1.17), leads to a relatively simple dispersion relation,

$$\left[\left(\frac{\omega}{k} - v_0\right)^2 - c_{\mathrm{n}}^2\right]\left[\left(\frac{\omega}{k}\right)^2 - c_{\mathrm{p}}^2\right] = \frac{n_{\mathrm{p}}}{n_{\mathrm{n}}}C^2. \tag{1.29}$$

This dispersion relation can be simplified further by the introduction of the phase velocity, $\sigma = \omega/k$, for the harmonic perturbations. In this case, assuming k is real, σ will be real or complex identically with ω. The presence of complex roots for equation (1.29) indicates a dynamical instability. As a result of this substitution equation (1.29) becomes

$$\left[(\sigma - v_0)^2 - c_{\mathrm{n}}^2\right]\left(\sigma^2 - c_{\mathrm{p}}^2\right) = \frac{n_{\mathrm{p}}}{n_{\mathrm{n}}}C^2. \tag{1.30}$$

At this point, for completeness only, the case with zero chemical coupling is considered. In the case of a totally uncoupled system, that is $C = 0$, the roots of this equation are

$$\sigma = \pm c_{\mathrm{p}}, \qquad \sigma = v_0 \pm c_{\mathrm{n}}. \tag{1.31}$$

This demonstrates that our model is consistent with sound speed in Galilean relativity. At this stage it would be simple to produce numerical solutions for our problem, but we wish to continue analytically as far as possible to give us greater understanding of the physics underlying the model.

To solve analytically for a more general case, where $C \neq 0$, is a little more involved. To this end, two new dimensionless variables are introduced, $x = \sigma/c_{\mathrm{n}}$ and $y = v_0/c_{\mathrm{n}}$. The problem is further simplified by combining some of the parameters to produce the constants a and b, given by

$$a^2 \equiv \frac{n_{\rm p}}{n_{\rm n}} \frac{C^2}{c_{\rm n}^4} \quad \text{and} \quad b^2 \equiv \frac{c_{\rm p}^2}{c_{\rm n}^2}. \tag{1.32}$$

So equation (1.30) becomes

$$\frac{1}{a^2}\left[(x-y)^2 - 1\right]\left(x^2 - b^2\right) = 1. \tag{1.33}$$

To demonstrate the existence of unstable solutions, we need to find complex roots for this equation. This occurs when two real modes merge to give a conjugate pair of complex modes, one of which will be a growing solution, whilst the other will be a damped solution. Of particular concern is whether such a mode merger occurs at differential velocity between the two fluid components which is likely to be achieved in real life situations. It would also be useful to consider whether linear flow is likely to cease at the relative velocities of these mergers.

As this work is chiefly motivated by astrophysical applications, particularly those relevant to neutron star dynamics, it is sensible to investigate this instability in this situation. To this end, the PAL equation of state was chosen, as it allowed analytic solutions for the required parameters. The key feature of this equation of state, as it relates to our problem, is the assumption of incompressibility [62]. Other features of the equation of state, such as energy per baryon are also somewhat germane to our problem. Based upon this equation of state [63], values for the sound speeds, chemical coupling parameter and proton fraction were derived. These then led to the values $a^2 = 0.0249$ and $b^2 = 0.0379$. A full analysis of how these values were arrived at is not really material to our discussion and full details may be obtained from [2]. Plots of the real and imaginary parts of the four roots of the dispersion relation (1.33) are shown in Figure 1.6.

The values of y which yield complex roots illustrated in Figure 1.6 are then substituted to give v_0 and ω. This shows that this type of dynamical instability can occur at velocities between $v_0 \sim 0.6c_{\rm n}$ and $v_0 \sim 1.5c_{\rm n}$. It should be noted that when v_0 nears $c_{\rm n}$, one would expect to have exceeded the critical velocity beyond which frictionless flow between the two fluid components can not occur. It is also found that the corresponding frequency of the unstable perturbation is given by $\omega = 0.1kc_{\rm n}$.

The values given in the previous paragraph are those for the onset of the two-stream instability and, naturally, are dependent upon our choice of the equation of state. It should be noted that, after this onset and up to relative flow associated with the failure of superfluidity, there exists a continuous spectrum of unstable waves. The full Laplace/-Fourier analysis would have revealed this in detail and such work is ongoing for our more

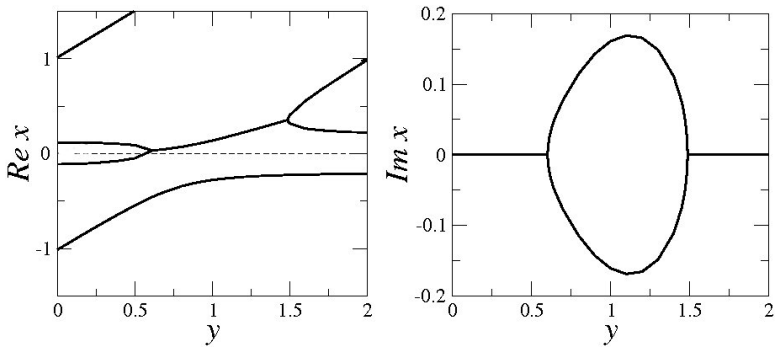

Figure 1.6: *Real and imaginary parts of the four roots of the dispersion relation* (1.33). *Complex roots, indicating the presence of the two-stream instability, can be seen to begin at* $y \sim 0.6$ *and end at* $y \sim 1.5$*, well beyond the superfluid limit. (Whilst we place no definite upper limit on superfluidity we would certainly expect such behaviour to be destroyed for supersonic flows [2]. We note that the two routes not shown in the right plot are always real.* Images from Andersson et al [2]

.

realistic model discussed in Chapter 4 [64]. At this stage of our investigation, we were merely interested in establishing the principle.

Of course, it is useful to describe the resulting instability in more detail. Unfortunately, a full time evolution of this unstable behaviour is beyond the scope of this thesis. However, a few salient points can be made. Firstly, the instability leads to the breakdown of laminar flow in both components. How this manifests as the instability grows is unclear because of the absence of said time evolution. But we can be reasonably certain that, owing to the vorticity imparted by the instability, vortices form in both fluids. Again, since our analysis covers only the onset of the instability, the future behaviour of these vortices is uncertain.

The example we have discussed in this section of the report establishes in principle the two-stream superfluid instability as existent. It further gives the conditions under which a two component superfluid becomes vulnerable to such instabilities. Once this has been done it is becomes possible to expand the relatively simple linear model to include more detailed models of physical phenomena. For instance, the initial model excludes such features as entrainment between the fluids and any external forces applied to the fluid body [2]. The forces that we may wish to consider include gravity and internal friction. In a more realistic neutron star model, it may also prove desirable to examine, for example, the effects of magnetic fields and the elasticity of the crust. It also is predicated upon only the most simple form of relative motion between the two fluids.

Here, the principle of the superfluid two-stream instability has been established. It has further been demonstrated that this instability has applications in neutron star dynamics. This application has been the subject of further investigations [65][66] and many others. This study has also been extended beyond a simple linear flow into the realms of rotating two component fluids; where the differential velocity is replaced by a differential bulk rotation of the fluids [67][68]. Applications of this instability have also been considered beyond the sphere of astrophysics; for example in superfluid Helium [8].

1.5 The Kelvin-Helmholtz Instability

As has been mentioned, the two stream instability is somewhat analogous to the Kelvin-Helmholtz (KH) instability. To this end there follows a brief derivation of the KH instability, with some discussion of its salient features. It should be emphasised that there is a major difference between the two instabilities. The KH instability occurs at the interface between two fluids, whereas the two-stream instability is manifest in two fluids essentially occupying the same space. But we note there are also similarities between the two.

Let us consider two fluids with some clearly defined interface between them as shown in Figure 1.7. Purely for convenience it is assumed that the background velocity of the lower layer is zero. We further assume that the background densities of the two fluids are each constant. So for the upper fluid we have:

$$\boldsymbol{u} = U_0, \tag{1.34}$$

$$\rho\left(z\right) = \rho_1, \tag{1.35}$$

$$p\left(z\right) = p_0 - g\rho_1 z. \tag{1.36}$$

Here g is the acceleration due to gravity. Similarly for the lower fluid we have:

$$\boldsymbol{u} = 0, \tag{1.37}$$

$$\rho\left(z\right) = \rho_2, \tag{1.38}$$

$$p\left(z\right) = p_0 - g\rho_2 z. \tag{1.39}$$

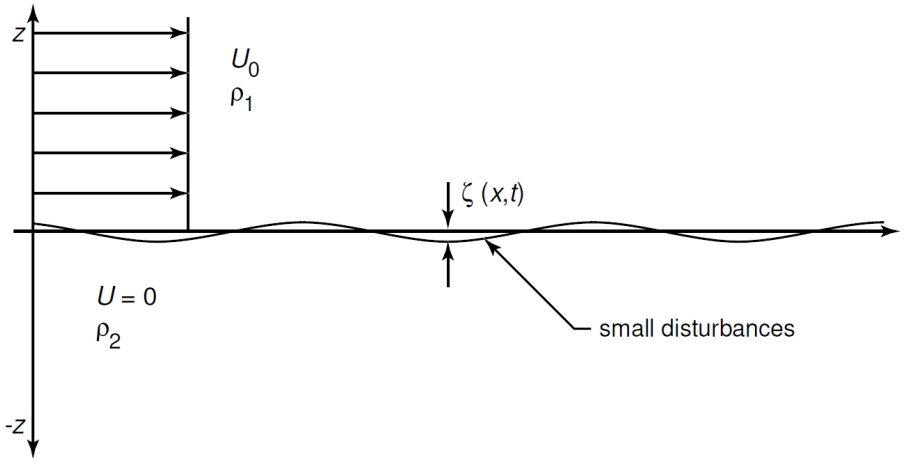

Figure 1.7: *Definition sketch for Kelvin-Helmholtz theoretical stability analysis.* University of Karlsruhe

.

Next we impose small disturbances on the background laminar flow. Without yet specifying their form, we define the velocity disturbances in the upper and lower layers as $\boldsymbol{q_1}$ and $\boldsymbol{q_2}$ respectively. Thus the disturbed velocity profiles become

$$\boldsymbol{u_1} = U_0 + \boldsymbol{q_1}, \tag{1.40}$$

and

$$\boldsymbol{u_2} = \boldsymbol{q_2}. \tag{1.41}$$

Substituting the disturbances into the conservation of mass and the inviscid Navier-Stokes equations and linearising in the convective terms, we obtain the following set of governing equations:

$$\boldsymbol{\nabla} \cdot \boldsymbol{q}_1 = \boldsymbol{\nabla} \cdot \boldsymbol{q}_2 = 0, \tag{1.42}$$

$$\frac{\partial \boldsymbol{q}_1}{\partial t} + U_0 \frac{\partial \boldsymbol{q}_2}{\partial x} = \frac{\boldsymbol{\nabla} p_1}{\rho_1}, \tag{1.43}$$

$$\frac{\partial \boldsymbol{q}_2}{\partial t} = \frac{\boldsymbol{\nabla} p_2}{\rho_2}. \tag{1.44}$$

Here p_1 and p_2 are the dynamic pressures of the disturbances.

To complete this step, it is necessary to specify boundary conditions. Firstly the kinematic boundary condition is specified: fluid particles can only move tangentially to the fluid interface. The interface location is defined by the function

$$F = z_i - \zeta(x,t) = 0, \tag{1.45}$$

where $\zeta(x,t)$ is the interface disturbance (refer to Figure 1.7). The normal velocity, $\boldsymbol{q}_s$, at the interface is given by the material derivative of F:

$$\frac{\partial F}{\partial t} + \boldsymbol{q}_s \cdot \nabla F = 0 \tag{1.46}$$

After linearising for the top and bottom layers respectively, we obtain

$$\frac{\partial \zeta}{\partial t} + U_0 \frac{\partial \zeta}{\partial x} = w_1, \tag{1.47}$$

$$\frac{\partial \zeta}{\partial t} = w_2 \tag{1.48}$$

taken at $z = 0$, where w_1 and w_2 are the vertical velocities of the upper and lower layers respectively.

The second boundary condition is a dynamic one: the normal stress of the fluid is continuous at the interface. For an inviscid fluid, this means that the pressure is continuous at the interface. For irrotational flow, the total pressure at the interface has a dynamic and a gravitational component, giving

$$p_1 - \rho_1 g\zeta = p_2 - \rho_2 g\zeta \tag{1.49}$$

applied at the linearised interface, $z = 0$.

The final boundary condition is simply that the disturbances only exist close to the interface and die away far from it.

We next assume that our disturbances are sinusoidal in nature, taking the forms

$$\begin{pmatrix} p_1 \\ w_1 \end{pmatrix} = \begin{pmatrix} P_1 \\ W_1 \end{pmatrix} e^{kz} e^{i(kx-\omega t)} \tag{1.50}$$

for the lower layer and

$$\begin{pmatrix} p_2 \\ w_2 \end{pmatrix} = \begin{pmatrix} P_2 \\ W_2 \end{pmatrix} e^{-kz} e^{i(kx-\omega t)} \tag{1.51}$$

for the upper layer. Here k and ω are the wave number and the wave frequency of the disturbances. P and W are the constant coefficients of the sinusoidal functions. For the interface we have

$$\zeta = Z e^{i(kx-\omega t)}, \tag{1.52}$$

where Z is the constant coefficient.

Combining the disturbances with the governing equations and boundary conditions gives the following matrix:

$$\begin{pmatrix} i\left(kU_0-\omega\right) & -1 & 0 & 0 & 0 \\ -i\omega & 0 & -1 & 0 & 0 \\ g\left(\rho_2-\rho_1\right) & 0 & 0 & 1 & -1 \\ 0 & 0 & -i\omega & 0 & k/\rho_2 \\ 0 & i\left(kU_0-\omega\right) & 0 & -k/\rho_1 & 0 \end{pmatrix} \begin{pmatrix} Z \\ W_1 \\ W_2 \\ P_1 \\ P_2 \end{pmatrix} = \begin{pmatrix} 0 \\ 0 \\ 0 \\ 0 \\ 0 \end{pmatrix} \tag{1.53}$$

This a classical eigenvalue problem for ω and k. To have a non-trivial solution the determinant of the coefficient matrix must be zero, which leads to

$$\left(\rho_1+\rho_2\right)\omega^2 - 2kU_0\rho_1 + k^2U_0^2\rho_1 - kg\left(\rho_2-\rho_1\right) = 0. \tag{1.54}$$

This dispersion relation leads us to a solution in ω of

$$\omega = \frac{kU_0\rho_1 \pm i\sqrt{k^2U_0^2\rho_1\rho_2 - kg\left(\rho_2-\rho_1\right)\left(\rho_1+\rho_2\right)}}{\left(\rho_1+\rho_2\right)}. \tag{1.55}$$

We, at this point, assume k to be real leading us to unstable behaviour if

$$k^2U_0^2\rho_1\rho_2 - kg\left(\rho_2-\rho_1\right)\left(\rho_1+\rho_2\right) > 0. \tag{1.56}$$

When we compare this to the solution for the two stream instability above we note that in both cases there is some critical value of background velocity, above which there is a range of critical frequencies.

Chapter 2

Laboratory Analogues for Superfluid Neutron Star Cores

As discussed in Chapter 1, direct experimentation with neutron stars is not something we can undertake. Nor can the conditions present in the star be reproduced on earth. However, our observations indicate that there are characteristics of the star that are well understood in terrestrial laboratory systems. For instance, we have sufficient data to be confident of the superfluid nature of a neutron star's core. From this we can infer aspects of the nature of the star that we can then use to make predictions about its future behaviour. The development of a laboratory analogue for the physics of a neutron star would represent a significant advance and, to some degree, allow research to initiate, rather than observe and interpret, major aspects of neutron stars' behaviours.

So, continuing with the theme of superfluidity, can we model in the laboratory the key points relating to this feature of a neutron star? Let us quickly summarise these key points, whilst discussing whether and how these might be reproduced experimentally in some laboratory analogue.

Firstly, the superfluidity. This is straightforward. Superfluids are readily available for experimental use. Secondly, the two component nature of the outer core, neutrons and protons. Again, this should not present any difficulties in a laboratory. Depending on the nature of the analogue used, one might use two distinct components or, as in the previously discussed use of He II, a fluid which can be modelled as having two components. Thirdly, the vortices formed by a rotating neutron superfluid component. This is a feature that applies to all superfluids and, therefore, poses no problems in a laboratory analogue. Finally, the pinning of these vortices to the crust. This is the feature that seems to present the biggest issue in any analogue system. However, as we shall see,

these issues are by no means insurmountable.

In this chapter, we review progress towards possible analogues for the behaviour of neutron star cores. We describe two distinct sorts of materials and discuss literature that relates, either directly and indirectly, to building such analogues. We firstly consider the most obvious candidate, superfluid Helium. We then move on to Bose-Einstein Condensates and review the properties that might offer analogous behaviour to that of neutron star cores. Finally, we discuss turbulence in quantum vortices and how this might relate to neutron stars.

It is both interesting and surprising to note the paucity of research, particularly with respect to Bose-Einstein Condensates, into how these materials could be used to model neutron star behaviour. Even in the case of superfluid Helium, much of the most relevant research was conducted several decades ago in the former Soviet Union and has since been discontinued. When the opportunities offered by laboratory analogues to enhance understanding are considered, this pretermission appears even more remarkable.

2.1 Superfluid Helium Analogues

Although discovered experimentally by Kapitsa [49], much of our current understanding of superfluid Helium comes from the seminal works of Landau [53] and Tisza [69]. In these works, amongst many other features, the key characteristics of the "two-fluid" model are laid out. It is this model that is most significant in attempts to model facets of a neutron star core. In this model it is shown that superfluid Helium can be described as a two component fluid. The first is an ideal superfluid, where all of the atoms occupy the lowest possible energy level. The second is a "normal" fluid component governed by the rules of fluid dynamics. The ratio of these two components vary with temperature, as discussed in Chapter 5. Below about 1K the proportion of the normal component becomes insignificant [47] and we are left with essentially an ideal superfluid. It is the temperature range where the concentrations of the two components are of similar that is of greatest interest in modelling core behaviour. Here we can hope to mimic the presence in the neutron star of superfluid neutrons by the superfluid component of Helium and that of superconducting protons by the normal component. Ratios of the two can be fine tuned by changes in temperature.

In Chapter 5 we consider whether Helium might offer a laboratory analogue for the r-mode instabilities described in Chapter 4. We shall show that the mutual friction coefficients for Helium were not sufficiently close to those of the neutron star to allow

such instabilities to become manifest. As such, we see both some of the limitations in Helium as an analogue and a more general problem in the construction of other materials whose behaviour might initially appear similar to that of a neutron star core. Unfortunately for attempts to mirror the behaviour of a star, some features are significantly "parameter dependent", in that they are only observable in the star because of the extreme conditions of density etc. This suggests that we would like any analogue to be sufficiently tunable so as to allow for such extremes. It not expected that the conditions of a neutron star core be replicated, but that ratios between parameters (and other similar phenomenology) in an analogue system can be tuned so as to reproduce important features.

The discovery of pulsars [20] and the development of the ideas that these were neutron stars with a core composed predominantly of superfluid neutrons with an admixture of protons and electrons [70] led to an interest in the use of Helium as a model for these stars. The observation of glitches in neutron star spin [29] further inspired a series of Helium experiments in an attempt to discover the mechanisms underlying this phenomenon.

In considering how one might use Helium to model glitches, it is useful to briefly note the observed features of a glitch that one is attempting to realise. The first feature observed is the initial rapid increase in rotation rate. This is followed by a slowing of the rotation which is more rapid than the normal spin down rate, which over some time period returns to this normal rate [71]. This indicates the presence of relaxation processes in the acceleration of the star [72]. This time period varies significantly between different stars. Further, on rare occaisions, there are decaying oscillations of the rotation rate during this period of increased deceleration [73]. It has been stated that one can demonstrate all of these observed astrophysical phenomena in a low temperature laboratory [72].

Much of the early work on the properties of rotating Helium was carried out by the low temperature school of Georgian physicists in the 1960s [72][74]. Studies were made of the creation, decay and elastic properties of vortices [72]. It is interesting to note that long before their physical observation, the existence of stars with super-nuclear densities had been predicted [75]. Several predictions as to the nature of these dense stars were made through the study of Helium. For instance, Migdal [76] showed in 1959 that if neutron stars exist, the neutrons in them must form a superfluid with transition temperature to the superfluid state of between 10^{10}K and 10^{12}K. It was further shown that the superfluid neutrons in these stars must be penetrated by quantised vortices if the rotation exceeds some critical angular velocity [77].

This research played a fundamental part in the recognition of neutron stars. It was shown that only a superfluid required the long relaxation times observed in the return

to equilibrium after glitches. In a normal viscous fluid, this relaxation time would be much shorter than that observed (of the order of microseconds) and in a solid, shorter still [78]. So, through kinematic considerations one can arrive at the conclusion that a pulsar consists predominantly of a superfluid liquid.

The observations from neutron stars and the experimental work on superfluids led to some of the earliest attempts to directly model a neutron star. These were undertaken by Tsakadze and Tsakadze in the USSR. The primary aims were to produce and to measure the relaxation times after rapid spin ups [79][80][81].

It should be clearly emphasised that initially these experiments were concerned exclusively with the relaxation time associated with pulsar glitches. They were designed to demonstrate the presence of superfluid neutrons (and their vortices) within the core and did not concern themselves with the mechanisms that might instigate said glitches.

The model pulsar was a glass sphere, radius 3.4 cm, attached to a drive shaft (in some experiments a cylinder of similar size was used), which was suspended without support by a magnetic field. The sphere was filled with liquid Helium by immersion in a Helium bath and suspended in the vapour from this bath. The sphere was then set in motion by an electric motor, it's rotation being measured by a light spot on the shaft. Once a predetermined rate of rotation was reached, the motor was switched off and the sphere was allowed to spin freely. As the initially immobile liquid was accelerated by the walls of the rotating vessel, the rotary speed of the vessel decreased. At first there was an abrupt decrease which, after a period of a few seconds, evolved into an exponential decay with a small damping factor. To increase the angular momentum of the rotating parts, a brass disc was secured to the drive shaft. This led to a markedly slower decay in the rotary speed [79].

These experiments were conducted at a range of temperatures and modifications were made to the equipment to make the model more relevant to the conditions present in a pulsar core. For instance, impurities, in the form of Plexiglas crystals were added to bind the normal component of Helium; thus increasing friction between this component and the inner wall of the sphere. To pin the vortices to the moving surface of the sphere, Plexiglas crystals were glued to the inside of the sphere.

Whilst these improvements to the equipment made small quantitative changes to the results [82], particularly to the damping coefficient, there was one major result of the experiments. At the λ point of Helium there was a large jump in the relaxation time.

This time increases as temperature decreases and the ratio of superfluid to normal components increases. It was stated [79] that the value for relaxation time obtained by extrapolating the experimental results to pulsars agree "in order of magnitude with the observed relaxation times of the two pulsars (Vela and the Crab)".

One unexpected result appeared when the spin down of the sphere was observed over a longer period. The experimenters noted a spontaneous acceleration in the rotation rate. This is shown in Figure 2.1 [72]. Despite the poor quality of this figure, it seemed appropriate to reproduce the original image.

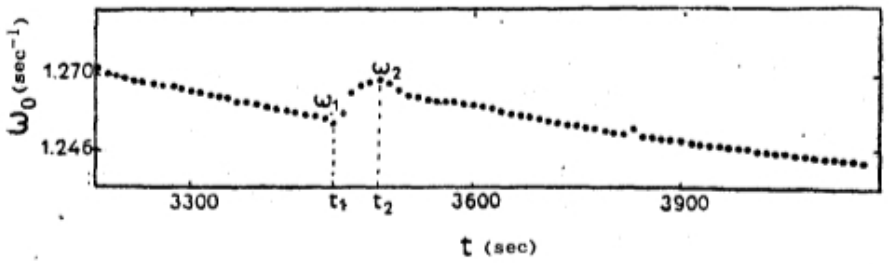

Figure 2.1: *This plot shows the time dependence for later time of the rotational velocity for the vessel containing pinned HeII. A relatively rapid spin up can be observed at about 3500 seconds, followed by a resumption of the spin down.*[3]

The observation of this increase reinforced some, at the time, novel ideas regarding glitches in neutron stars. Prior to this, it was largely assumed that such glitches were solely the result of star-quakes [33]. Clearly, no such phenomenon was present in the Helium experiments. It was hypothesised that this spin up was as a result of the decay of vortices as angular velocity decreased. The angular momentum of these vortices was then transferred to the normal component and subsequently to the vessel [72] in close agreement with the recent theoretical work [36]. An outline of how such a transfer should cause a sudden jump, rather than a slow steady transfer was given [81]. It was suggested that such a mechanism could also operate in neutron stars and shown that, in the case of the Vela pulsar, this matched well with the observed interval between the glitches.

Limited investigations were performed into the use of a rotating ^{3}He-^{4}He solution [83]. Here the ^{3}He acted as the normal component, whilst the ^{4}He was the superfluid. Results similar to those in pure ^{4}He were obtained but there was a notable increase in the critical rotation rate for vortex formation and in the observed relaxation times.

This was really the highpoint for the attempts to physically model neutron stars using superfluid Helium. It seems a shame that such experiments have not been repeated with

more modern laboratory equipment, as the advances made in the 1970s furthered our understanding in many ways.

2.2 Bose-Einstein Condensates

"*If the condensed atoms in a BEC were to attract each other, then the whole condensate can collapse. People have actually predicted that the physics is the same as that of a collapsing neutron star. So it's one way, maybe, to realise a tiny neutron star in a small vacuum chamber*"
Wolfgang Ketterle - NASA Science 2002.

A Bose-Einstein Condensate (BEC) is a state of matter of weakly interacting bosons confined in an external potential and cooled to temperatures very near absolute zero. In such a state a sizeable fraction of bosons occupy the lowest quantum state of the external potential. Under these conditions quantum effects become apparent on the macroscopic scale [84].

Such a state of matter was first hypothesised in 1924-25 following collaboration between Einstein and Bose. It was demonstrated that, if they were cooled to very low temperatures, bosonic atoms would condense into the lowest accessible quantum state. Such a state of matter was first realised experimentally in 1995 with a diffuse gas of rubidium atoms [85].

After this physical realisation of the previously theorised state of matter, there followed a series of experiments to test and confirm the predicted properties of such a material. Here we mention only those that are pertinent to the use of BEC's as possible analogues for neutron star cores.

Most obviously for any physical analogue of a neutron star core using Bose-Einstein Condensates is the existence of a binary mixture of condensates to simulate the two component nature of said core. This was first observed, almost accidentally, in 1997 [86]. In this example the binary condensate consisted of a condensate of two differing spin states of ^{87}Rb, rather than distinct elements. Even so, differences in the behaviour of the two condensates were observed. It was also noted that, in this particular mixture, there was a repulsive interaction between them.

Another feature that we would like to see is the presence of collective excitations, which we can describe as coherent fluctuations in the density distribution. The motivation for such experiments can be considered as two fold [87]. Firstly, if, as was expected,

BEC's exhibited superfluidity, then this is defined by their dynamical behaviour. The study of excitations is an initial step toward understanding this. Secondly, the observed frequency of standing wave excitations is a precise test of understanding of the effect of interactions [87]. These excitations were observed within months of the first realisation of a BEC [88]. Further to this, and also of interest in our search for analogues, the damping rates of such modes were also studied and found to show a roughly linear dependence on temperature [89][90].

These excitations in BEC's also offer the prospect of modelling some aspects of the seismology of neutron stars. By studying the oscillations of neutron stars, we are able, through analysis of their modes, to draw conclusions regarding density and composition [91]. The ability to model various density profiles in a laboratory might further enhance our understanding, particularly of the inner core.

Of crucial importance in mimicking the behaviour of the neutron star core is the presence of quantised vortices within the BEC's. These were first observed in 1999 in a binary condensate [92]. Using an interference technique, the phase of the vortex state was mapped, confirming that it possessed angular momentum. It was also demonstrated that vortices could be created independently in each condensate, with observed differences in the dynamics and stability.

In the accepted model for a neutron star core, the vortices within the core extend into the inner crust. These vortices are pinned energetically to the crust [93] and it is suggested that their unpinning and re-pinning might be a mechanism for neutron star glitches [94]. The pinning of the vortices in BEC's might appear to present a problem, since it is difficult in the extreme to pin them to any physical material. However, this problem is overcome by pinning using an optical lattice [95] and such a technique may be extended to cover two component BEC's [96]. Again the vortices are pinned by energy considerations and so mirror the pinning of those in a neutron star.

In order to investigate the superfluid two-stream instability in BEC's, in Chapter 3 we apply the hydrodynamic equations for two component BEC's. Naturally, this approach to BEC instabilities is only justified if there is evidence of superfluid condensate flow. This flow was observed as recently as 2011 [97]. The experiments conducted also showed a critical velocity for the onset of a pressure gradient, as a function of density of the BEC, indicating the beginning of dissipation and the break down of superfluidity. This led to further studies on the details of drag forces and their dependence on size and density of the condensate.

In Chapter 4 we discuss r-mode instabilities of a neutron star, which are dependent upon the relative motion of the neutrons and protons. In the simpler case of linear flow, we observe some critical relative velocity between the two components at which the flow becomes unstable to plane wave perturbations [2]. It is important that a similar instability should be present in BEC's, if we are to model most neutron star phenomena that depend upon, for example, differential rotation. The existence of a critical relative velocity was shown in 2001 for a binary mixture of moving BEC's [6]. This is reviewed in more detail in Chapter 3, but we can see immediately the relevance of such an instability to neutron star analogues. A natural extension of this is the investigation of two component BEC's in rotating traps. The physics of such a system has been shown to be very rich, with four classes of instability appearing in the mixture [98]. Whether the two types of 'centre of mass' instability (classical and intra-species) are of great interest in neutron star physics seems debatable. However, the other two classes, ripple and catastrophic instabilities, suggest turbulence in the BEC's and, at first impression, appear more closely related to previously observed instability phenomena previously observed in superfluid Helium.

The effects of differential velocity (and counterflow) between the two components of binary BEC's has been further explored, at times with direct reference to the similarities (and differences, particularly with reference to Helium) when compared with astrophysical applications and Helium [99]. The advantages of studying these phenomena in BEC's are that they are easily controlled and that the dynamics of topological defects can be easily visualised. Such counterflow instabilities in a quasi one dimensional system has been observed [100][101].

Further work in comparing BEC's with Helium includes the calculations regarding the first sound and second sound of two component condensates [102]. The approach adopted is similar to that used in Chapter 3 of this thesis. The hydrodynamic approximations are used to show these phenomena are present in BEC's and they are calculated in terms of the scattering lengths of the condensates. The problem with these calculations, when compared to higher density superfluids, is that they do not take into account the entrainment effect between the two components. The absence of entrainment is a non-trivial problem when it comes to the use of BEC's as an analogue for neutron star cores.

It is worthwhile at this point to emphasise the key feature that distinguishes entrainment from friction, with which it, at first glance, appears closely related. Whilst friction is a dissipative process, entrainment is entirely non-dissipative. There is no loss of energy associated with entrainment making it almost impossible to model using either linear or non-linear frictional processes. This issue is key when we consider any attempt to model

a neutron star core with diffuse condensates.

The observation of differing types of dynamical instabilities in two component BEC's should give pause for thought. In modelling neutron star cores we are looking to model a particular mechanism and there appear to be many varying mechanisms that manifest instabilities in binary BEC's. As a relatively simple example, there are energetic considerations that, under the correct circumstances, induce phase separation in two component BEC's [103][104]. It has been shown that in the regime of strong mutual repulsion between the two components, an inhomogeneous state (complete phase separation) is the most stable. This suggests that some caution needs to be applied in selection of the particular combination of condensates used in any analogue. A pair of condensates free from any such effects would be necessary to simulate the homogeneity of the neutron star core components, where phase separation of this type is not expected.

Having sounded a slightly pessimistic cautionary note, we move on to consider a major advantage that BEC's possess over superfluid liquids in constructing analogues of other physical systems. This is the ability to manipulate the physical characteristics of a two component condensate through environmental means. Density profiles can be arranged almost at will by the use of external potentials and motion of the two components can be similarly induced [87]. This allows construction of almost any physical configuration that might be desired.

Of as great a significance in the use of BEC's as analogues is the ability to fine-tune some parameters of a two component BEC, so as to match those of the core components of a neutron star. This can be achieved due to the existence of Feshbach resonance. It was calculated, even before the physical realisation of BEC's, that there was some dependence in the collisions between atoms upon the presence of a magnetic field [105]. It was shown that there were dramatic resonances in all cross sections as a function of magnetic field. These became known as Feshbach resonances because they are similar in nature to scattering resonances in nuclear collisions described by Herman Feshbach [87]. It was calculated that the presence of these resonances would allow the tuning of the s-wave scattering length of the atoms in a condensate. By varying the magnetic field over a few gauss in the vicinity of a Feshbach resonance these scattering lengths could be readily adjusted [106]. These resonances were first observed experimentally in 1998 in various different condensates [107][108][109].

Further experimentation in Feshbach resonances led to a most interesting observation [110][111]. Although not really pertinent to our subject, it is included as the observed phenomenon is, superficially, similar to the birth of a neutron star. When the magnetic

field interacting with a condensate was suddenly switched so that the self interaction became strongly attractive, the condensate became unstable and collapsed. The dynamics of this collapse were remarkable. The condensate was seen to shrink slightly, before undergoing an explosion. A substantial fraction of the atoms were simply blown off, leaving a small cold stable remnant. Because of its resemblance to a core collapse supernova, this became known as a Bosenova [87]. This brings us full circle to the quotation with which we begin this section.

One other aspect of BEC research that appears to have implications for neutron star physics is that of topological defects. This suggest that we may be able to model, to some degree, the interfaces between the differing layers of a star. Of particular interest is the investigation of the behaviour of vortices at interfaces between two condensates with differing spins [112][113]. It has been established that vortices are continuous across these boundaries. This may help in understanding how neutron star vortices behave at the interface between the inner crust and the outer core. This research may have further implications for how vortices penetrate the problematic inner core. Naturally this research is only relevant to neutron star physics if the inner core retains the property of superfluidity.

In conclusion, we see that BEC's offer the hope of qualitatively simulating the behaviour of neutron star cores. They offer all of the key characteristics desired, with one notable exception, and are tunable in many respects to offer the desired responses. The major issue that remains is that of entrainment. This problem does not seem likely to be insurmountable and recently there has been theoretical work on superfluid drag (entrainment) in two component BEC's and the effect of optical lattices on this phenomena [114].

As a final consideration of possible analogues, we mention that research in low temperature physics has expanded into the realm of ultracold atomic Fermi gases. These gases share many of the observed features of BEC's: superfluidity; quantised vortices; fine tuning of interactions [115]. However, unlike BEC's, Fermi gases are generally more strongly interacting and are not so diffuse. This raises the possibility of modelling neutron star cores where the difficulties with the absence of entrainment do not occur. Most research thus far has been related to determining the fundamental properties of these gases. More recently the qualitative similarities between Fermi gases and neutron matter has been explored [116]. It can be seen that there is a chance that analogues might be produced in Fermi gases, but this is a relatively new science and there remains much to be learned.

2.3 Vortex Instability and Turbulence

Phenomena exhibited by superfluids that are of particular interest in the study of neutron stars are those of instabilities in vortices and turbulence in fluid flow. The study of these phenomena in superfluids may offer an insight into, amongst others, irregularities in the precession of the star, as well as post glitch behaviour [54].

Before proceeding with a discussion of these phenomena, it should be made clear that, unless otherwise stated, the text refers to the behaviour of superfluid ^{4}He. Whilst there are other materials that exhibit superfluidity, their characteristics result in noticeably different behaviour in the superfluid phase. For instance, ^{3}He atoms are fermions and, as such, superfluidity requires the condensation of pairs of atoms through Cooper pairing. Whilst the superfluid is similar to that of ^{4}He, there are important differences. For instance, the viscosity of the normal fluid component of ^{3}He is many orders of magnitude higher than that of ^{4}He. Further, the nature of the vortices differs, being much larger and enclosing a high density of bound quasi particle states within the core [117].

2.3.1 Vortex Instabilities

An early theoretical prediction was that of a relatively simple hydrodynamic instability involving vortex lines [118][119]. It was shown that in the presence of counterflow along the vortex lines an instability is manifest through the mutual friction force in the two component model. This form of instability is important in the differential rotation discussed in Chapter 3. This analysis was extended to include impurities (^{3}He) into the superfluid and this was shown to cause major changes in the critical velocity for the onset of this instability [119].

This work was largely motivated by previous experimental work [120]. Here it was shown that the trapping of ions by quantised vortex lines was inhibited by a small thermal counterflow parallel to the axis of rotation. It was hypothesised that this was due to a vortex array instability [54]. Direct observation of this instability was later obtained [121], where the attenuation of the second sound was measured in a direction perpendicular to an array of rotation induced vortices. A large increase in attenuation was observed at critical counterflow velocities.

Also of interest was theoretical work regarding the properties of vortex waves [4]. Here the effects of the mutual friction and the Magnus force upon waves propagating through a vortex array are considered. It is demonstrated that these forces produce, along with

attenuation of the waves, a shift in frequency.

2.3.2 Superfluid Turbulence in ^{4}He

'Turbulence is widespread, indeed almost the rule, in the flow of classical fluids. It is a complex non-linear phenomenon, for which the development of a satisfactory theoretical framework has long been a challenge. That framework remains incomplete, but it is crucial to our understanding of many natural phenomena and a wide range of technical applications.' W.F. Vinen, Quantum Turbulence - 2002.

We see that, even in classical fluid mechanics, turbulence is a complex matter, where investigations into the associated phenomena are still active. Turbulence is also found in superfluid flow and an understanding of this is an important feature in describing the observed behaviour of ^{4}He. Much of the early motivation for the study of this turbulence came from the use of ^{4}He as a coolant for superconducting devices [117]. However, the previously discussed analogies between superfluid Helium and the outer core of a neutron star suggest strongly that this has applications in astrophysics.

As discussed in numerous texts [47][50][48][51] and others, superfluid flow is strongly influenced by quantum effects. As such, it is appropriate to refer to the resulting turbulence as '*quantum turbulence*'. It is noted that superfluid flow differs from that of a classical fluid in three important respects, all related to quantum effects: the superfluid exhibits two-fluid behaviour; the superfluid component can flow without viscous dissipation; and the flow of the superfluid component is subject to quantum restrictions [117]. In this section we review progress in the phenomena of quantum turbulence, both theoretical and experimental. Where appropriate, similarities to and differences from the observations of classical turbulence are included.

Before considering research into quantum turbulence, it is useful to review turbulence in classical fluids. In an interview with *USA Today* in 2006, Richard Feynman described turbulence as 'the most important unsolved problem of classical physics.' The behaviour of a classical fluid is described by the Navier Stokes equations. At low velocity the flow is laminar and can be accurately predicted using a linear model. However, at higher velocities (and Reynolds number) this laminar flow breaks down and is replaced by highly non-linear dynamics. It becomes impossible and increasingly meaningless to follow the change of fluid velocity in a turbulent flow.

However, it has been known since the 1940s that turbulent flow exhibits some characteristic behaviour that is statistical in nature [122][123]. It was shown that, for some volume of a fluid away from a boundary, a region of an incompressible classical fluid is locally approximately both homogeneous and isotropic. This leads to the statistics of the energy spectrum defined by what has become known as Kolmogorov's Law, which gives the energy per unit mass as a spectrum of wavenumbers from the Fourier transform of the velocity field [124]. These results were later demonstrated experimentally [125]. These early musings are particularly interesting in that they demonstrated the need for probabilistic description of what is, in essence a deterministic system. This was an early step in the description of many non-linear systems and was a key component in Chaos Theory [125]

Most research into classical turbulence, both experimental and theoretical, has been guided by this probabilistic approach [125]. Researchers have relied heavily on the assumptions of local homogeneity and isotropy. In the experimental community the problem of achieving these conditions was solved by the relatively simple expedient of placing a grid into a near laminar flow. This is shown in Figure 2.2, where we see turbulence generated as the interaction of the flows having passed through the grid.

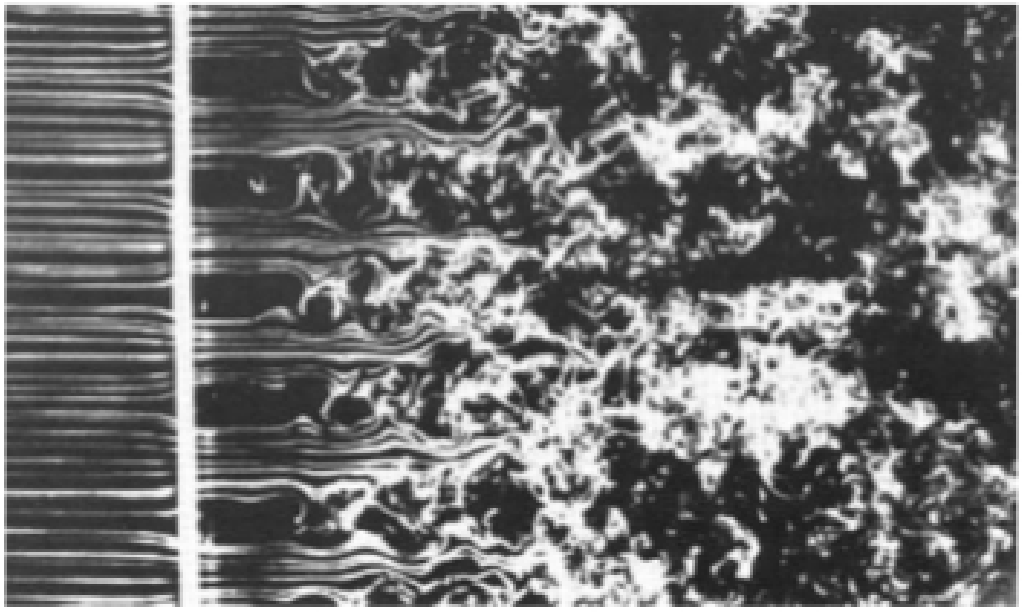

Figure 2.2: *Turbulence produced by inserting a grid into a laminar flow.* [4]

Another key area of investigation is the turbulence of classical fluids associated with flow around blunt objects. An example of this is shown in Figure 2.3. This is an excellent example of how, as the Reynolds number (or velocity) increases, the flow passes from laminar, through instability and into turbulence. This area of research has wide ranging

engineering applications, particularly in aeronautics and naval architecture.

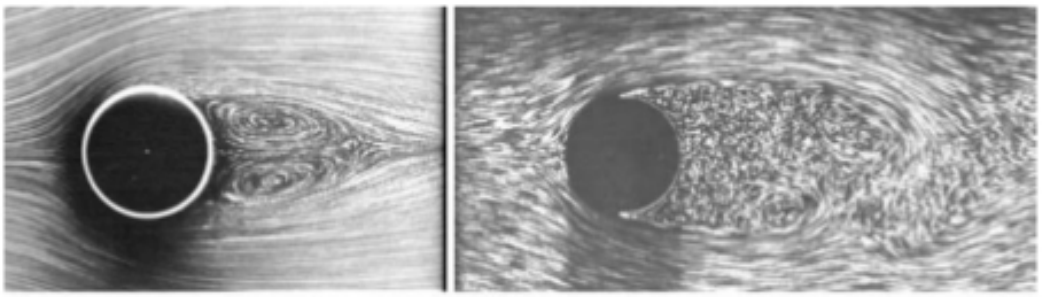

Figure 2.3: *The flow of a classical fluid past a circular cylinder. The left hand figure shows the flow for a Reynolds number of 26, whilst that on the right has a Reynolds number of 2000.* [4]

Some more recent experiments have focussed upon the flow of cryogenic He I (that is liquid helium at temperatures close to but above the λ point) in a small pipe. This is significant in that it enables the generation and study of extremely high Reynolds numbers [126]. Such experiments are at an early stage but offer the hope of significant advances by studying classical turbulence in its most extreme circumstances.

Having briefly discussed research in classical turbulence, we move on to consider superfluid ^{4}He. Unlike the classical fluid, the superfluid is described by a two fluid model. This would imply that it is likely to display, along with some of the more familiar phenomena, causes of turbulence that are not present in the classical fluid. As we shall see, this is indeed the case.

By its nature, turbulence in classical fluids must involve rotational motion [117], which is eventually dissipated by viscosity. We can regard the normal component of superfluid ^{4}He as a classical viscous fluid, so it would be expected that it can support a turbulent velocity field as described above. Any such field may be modified by the existence of mutual friction resulting from the presence of quantised vortex lines in the superfluid component. Such rotational motion in the superfluid component, whilst not prohibited, is restricted to these quantised line vortices and is free from viscous dissipation. Assuming that turbulence in the superfluid component can be established, the absence of viscosity implies that this should differ in general from that present in classical fluids [117].

This leads to a considerably more complex set of possibilities for turbulence in superfluid ^{4}He than in a classical fluid. Summarising, as well as the turbulent behaviour of the normal component, it is necessary to consider the following: interaction between the

two components; mutual friction; quantum restrictions; and the inviscid nature of the superfluid component.

In fact, aspects of quantum turbulence can be observed that are similar to those in the classical case. But there are also important differences. These similarities and differences appear generally to depend upon the length scale involved, with longer length scales exhibiting features that are closer to classical behaviour [124][117].

Most early experimental studies on superfluid turbulence focussed on thermal counterflow, clearly a phenomenon that can not be observed in a single component classical fluid. This is the phenomenon described in the previous section when discussing vortex instabilities. The flow is driven by an injected heat current which leads to a differential velocity between the two components [124]. It was observed that, above some critical relative velocity, the superflow becomes dissipative [127][122][123]. It was later proposed that this demonstrates a superfluid turbulent state and that this state consists of a tangle of quantised vortices [128]. This is illustrated in Figure 2.4. This view was confirmed experimentally by demonstrating that the dissipation is a product of mutual friction between the vortices and the normal flow [5][129][130]. This type of instability is of particular interest in neutron star physics, where the two fluid model is often applied to the physics of the core [39].

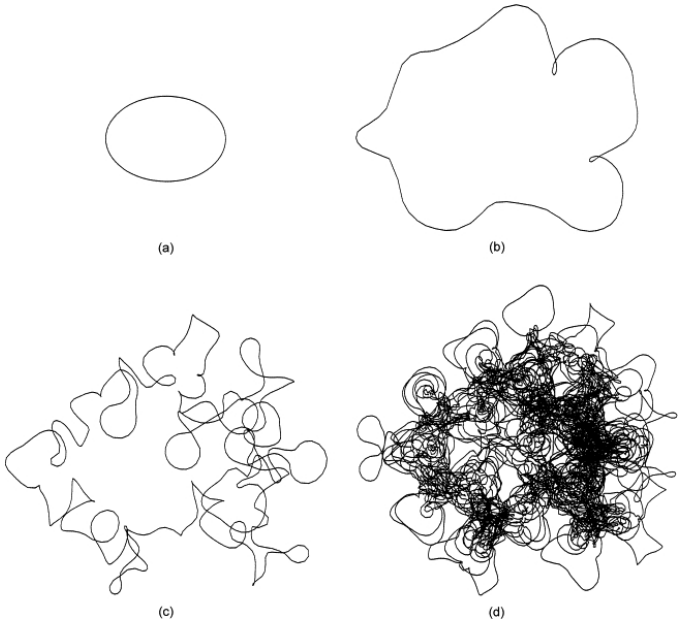

Figure 2.4: *A vortex line illustrating the onset of quantum turbulence from: (a) stability; through (b) instability; to (c) and (d) turbulence and a vortex tangle.* [5]

Whilst these counterflow experiments were useful in furthering our understanding of superfluid behaviour, there is no classical analogue. As such it does little to contribute to the understanding of the relation between quantum turbulence and its classical cousin.

However, from the mid 1990s a series of experimental studies were undertaken involving ^{4}He that did not feature thermal counterflow [124]. One of the earliest significant contributions was made at the Ecole Normale Supériere in Paris [131]. Here, in a series of experiments, a turbulent flow was induced in a cylinder containing two counter rotating disks. These experiments were conducted at temperatures both above and below the λ point, so as to compare results for classical and superfluid flows. By observation of the local pressure fluctuations the energy spectrum was obtained. This revealed the first experimental confirmation of the Kolmogorov spectrum.

This was followed by significant advances made at the University of Oregon. Here, there was (these are still ongoing [54]) a series of experiments investigating grid turbulence [132][133][134][135]. This uses a method to produce turbulence similar to that used in earlier investigations into classical turbulence. However, in this case, rather than the placement a grid in a laminar flow, the grid is dragged through a fluid at rest. This has the advantage in that the relative velocity of the grid and fluid can be much higher, so creating the equivalent of higher Reynolds numbers in the normal component. It was shown that the coupling between the superfluid and normal fluid components through mutual friction produced a quasi-classical flow at length scales greater than the mean spacing between the vortices. This causes the fluid to behave as though it had only one component. Further observations of the decay of turbulence showed that this was consistent with the classical Kolmogorov spectrum.

One other significant observation made by the Oregon group was that of four distinct regimes of decaying grid turbulence [135]. The timescales of the decay were demonstrated to switch between these regimes with varying Reynolds number.

Further ongoing research includes the comparison of the decay of grid turbulence with that of counterflow turbulence. These have been shown to be distinct and several research teams are investigations these differences and their underlying physics [126][136]. Research also continues that aims to account for the critical velocity in counterflow instability and its temperature dependence [126]. In the past, the study of superfluid turbulence in relation to flow around blunt objects has been largely neglected [126]. However, there has been relatively recent study of turbulence generated by high Reynolds number flows over a sphere [137]. The proposed development of 'wind tunnels' (at the University of Oregon) capable of operating in the superfluid regime offers the chance of

further experimentation in this area [126].

2.3.3 Further Examples of Quantum Vortices and Turbulence

The realisation of Bose-Einstein condensation in trapped atomic gases opened new avenues for the investigation of quantum turbulence [124]. BEC's have several advantages over superfluid helium in this area of study. Most obviously, quantised vortices in BEC's can be directly visualised[1]. Also, owing to the weakly interacting nature of these condensates, their behaviour can be mathematically described by the Gross-Pitaevski equations. Theoretical work has shown that quantum turbulence can be generated in trapped BEC's and, importantly, that the energy spectrum obeys Kolmogorov's law [139][140]. Whilst not wishing to reiterate all of the features of BEC's, it is clear that their relative ease of manipulation and ideal superfluidity make them prime candidates for the investigation of quantum turbulence.

Until relatively recently, the use of superfluid Helium-3 to investigate quantum turbulence has been restricted because of the difficulty of production at the low temperatures required. There is also a major issue with the paucity of this isotope in naturally occurring Helium, where it constitutes only one part in a million [141]. The quantities required for experimentation are only available through the nuclear reactions resulting from bombarding Lithium-6 with neutrons. Such were the issues associated with the production that the first condensation of Helium-3, which occurs at approximately 3.2 K, was not achieved until 1949 [142].

Larger quantities of Helium-3 did not become readily available until the 1960's [141] . With the increased quantities at their disposal, researchers undertook numerous experiments, many of which mirrored those previously performed with Helium-4. There was also great interest in the realisation of the predicted superfluid phase. Owing to the fermionic nature of Helium-3 atoms, their behaviour is governed by the predictions of Bardeen-Cooper-Shcrieffer (BCS) theory and superfluidity was predicted to occur at temperatures well below that for Helium-4. This predicted superfluid behaviour, analogous to that previously observed for electrons in superconducting metals [143], was first observed in 1971 [141].

Soon after the realisation of superfluidity, it was shown that Helium-3 undergoes at least two phase transitions close to the critical temperature [144][145]. As such it exhibits

[1] In recent years, advances in experimental techniques have allowed direct vortex visualisation in superfluid Helium-4. In some aspects this exceeds that available in BEC's. For example, reconnection of individual vortices have been observed in Helium but not in BEC's [138].

more than one superfluid phase, with different properties for each. Initially only two phases were observed, which became known simply as Helium-3A and Helium-3B. The existence of these two superfluid phases offered scope for a new range of experimental works that are not available with the single superfluid phase of Helium-4.

Of particular interest to neutron star physics are experiments relating to the behaviour of quantised vortices where an interface exists between volumes of the two phases [146]. Here the two superfluid phases are held in a cylindrical container, a distinct junction between the two being magnetically maintained. The two fluids are spun up until a condition exists where a steady array of vortices, perpendicular to the plane of the interface, but passing through it can be observed. We note that one of the superfluids has these vortices pinned to its end of the container, whilst the other has no such restriction. Once a satisfactory condition, where the two fluids are rotating at the same rate, is achieved, the system is allowed to spin down. Owing to the differing properties of the two phases, along with the pinning of one end of the vortices, the unpinned phase slows more rapidly. As this happens the vortices in the unpinned phase drift to the outside of the container causing those in the pinned phase to bend outwards close to the interface. This eventually leads to a vortex plane at the interface and subsequently, turbulent behaviour in both phases. It is hoped that further study of this phenomenon will enhance understanding of the behaviour of vortices within neutron stars. This is of greatest relevance at the interface between the outer core, where the vortices are free to drift, and the inner crust, where they are generally pinned to the lattice. The experiment mirrors the build up of differential rotation between the neutrons in the crust and those within the core, and may offer further insight into phenomena related to pulsar glitches.

2.3.4 Cosmic Strings

Moving beyond the terrestrial laboratory and into the realms of cosmology, we discover a very different application for the study of vortices, that of cosmic strings. Early in its evolution, as it grew and became less dense, the Universe underwent numerous phase changes. These were associated with many different phenomena, from the appearance of nuclear material to the separation of fundamental forces. It has been theorised that some of these phase changes may have produced effects that are still observable today. One such effect may be the existence of cosmic strings.

The search for cosmic strings began in the 1970's when it was theorised that phase changes in the early universe might produce symmetry breaking in a scalar field. It was conjectured that this might occur as a result of the separation of the strong nuclear force from the electro-weak force. A similar, although less significant, phenomenon was also

suggested for the separation of the weak and electromagnetic forces [147].

It is theorised that this symmetry breaking leads to topological defects which may have zero-dimension (monopoles), one dimension (strings) or two dimensions (domain walls) [148]. The existence of domain walls appears to be ruled out by gravitational considerations [149], whilst the topic of monopoles goes beyond the scope of this review. However, the nature of the hypothesised cosmic strings is of interest as these one dimensional defects can be viewed as analogous in some ways to vortices [147].

The nature of these strings suggests that they may have had great significance in the evolution of the Universe. They are believed to be stable over very long time scales, so it is expected that they would still be existent. They grow with time and so would be expected to now be of great length, almost certainly as large (or larger) as the diameter of our galaxy [147]. However, their radius would still be on the atomic scale. According to the theory underlying these strings, they would be under tension and, as such, they would have mass. It has been suggested that, if such an object existed, a cosmic string that was as long as the diameter of our sun would have a mass equal to the sun [149]. It has been proposed that the advent of these strings in the early Universe may have acted as 'seeds' for galaxy formation, since they would produce local gravity effects.

The most obvious method of detection of these strings is as a result of their mass. One would expect them to be a source of observable gravitational lensing [147]. Whilst the current lack of such observations might appear discouraging, it is thought that there are likely to be very few strings within the observable Universe. Efforts continue to detect the effects of strings on signals reaching the earth and, if they are ever found, the analogous natures of these one dimensional defects to quantum vortices would open new areas of research in cosmology and low temperature physics.

In the spirit of this chapter, where we are discussing laboratory analogues, it is encouraging to note the development of experimental models for cosmic strings. These experiments, conducted at Lancaster University, use superfluid ^{3}He to study the formation and decay of cosmic strings [150]. In recent years the experiments have been extended to consider how brane collisions and annihilations in the early universe may have created topological defects that persist to the current time [151][152]. It has been suggested that this work may enhance our understanding of inflationary epochs in the early Universe, which may have been initiated and terminated by such brane collisions [151]. These experiments show clearly how advances in one field of physics may have unforeseen applications in other fields, which is the major argument put forward in this

chapter.

The scope of quantum turbulence encompasses the physics of many different fields of studies. Research into its causes and effects stretches from traditional superfluid helium through BEC's to compact stars. With the advent of cosmic strings in the early universe, quantum turbulence could also be stretched to truly cosmological scales [153]. Whilst this section is by no means an all encompassing review of the field, it includes many of the salient features when considering applications in neutron star physics.

Chapter 3

Binary Bose-Einstein Condensates as Analogues for Two Component Superfluids.

3.1 The two-stream Instability in Binary BEC's without Entrainment

In this chapter we explore the nature of a class of dynamical instabilities in binary Bose-Einstein Condensates (BEC's) and the two stream instabilities described in chapter 2. To assist in our endeavour we make use of material from both the fluid dynamics and condensate communities. Our aim in investigating the analogous nature of the two classes of instabilities is to understand to what extent the BEC instability is related to those expected to be present in the superfluid cores of neutron stars.

If we are to consider the two instabilities as in some way analogous, then it would be advantageous that BEC's exhibit attributes similar to those seen in superfluids. For instance, it would be seem to be of paramount importance that BEC's manifest a superfluid flow so that their behaviour might, to some degree, mirror that of the superfluid neutrons in a neutron star. Such a flow was observed by Onofrio [97] in 2011 and this was followed by the observation of several other related phenomena. One such example which is of particular importance in considering analogous behaviour was the observation of a critical velocity for such a flow [154]. These observations lend credence to the possibility of analogous behaviour of binary BEC's and two component superfluids. However, even before these phenomena had been established, it was muted that BEC's might have some use in modelling some aspects of ultra low temperature fluid behaviour.

An early discussion as to how BEC's might be used to model some features of superfluid behaviour appeared in a paper by Ho & and Shenoy [155] in 1996. In this case the authors discussed how coexisting regions in a binary BEC are an analogue for ^{3}He-^{4}He interpenetrating superfluids. In the paper, they consider various possible compositions of binary condensates, which fall into three categories. The first is a mixture of two different alkalis; in the analysis presented they consider ^{87}Rb-^{23}Na. The second is a mixture of different isotopes of the same alkali, the example being ^{87}Rb-^{85}Rb. Finally they consider a mixture of different hyperfine states of ^{87}Rb. By hyperfine states, they are referring to a difference in spin between the two samples. It is discussed how, by varying the trap potentials for the two 'species' of condensates, it is possible to produce configurations of coexistence that mirror almost any required density profile for interpenetrating superfluids. Although the paper does not extend the analysis to dynamical analogues of two component superfluids, when considered alongside some of the aforementioned work of Onofrio et al [97] and Raman et al [154], it appears that such analogues are, at the very least, worthy of investigation.

3.2 Instability in a Binary Mixture of Moving Bose-Einstein Condensates

The existence of an instability in binary BEC's analogous to the superfluid two-stream instability is reinforced by the work of Law et al [6]. Here, the dynamic stability of two interacting BEC's moving through each other with some fixed relative velocity, v_r, is investigated. The details of inducing relative motion between the two components is not of great importance at this stage. The method suggested involves "stirring" the condensates by a moving laser potential barrier. It is shown that there exists some critical relative velocity, $\boldsymbol{v}_r^{(c)}$, such that relative flows with $\boldsymbol{v}_r > \boldsymbol{v}_r^{(c)}$ cause the condensate mixture to become unstable. Further an analytic expression is constructed for the unstable collective modes. Since this forms an important part of our investigations, the relevant material is reproduced (and, where this facilitates understanding, expanded upon) here.

To remain consistent with [6], we retain the notation used by the author in discussions specific to this work.

Initially, two interacting BEC's, labelled by species 1 and species 2 are considered. A frame co-moving with species 1 is used and species 2 is assumed to be moving in this frame with velocity, $\boldsymbol{v}_r$. According to the mean-field description, the condensate wave

functions, $\psi_j(\boldsymbol{x},t)\,(j=1,2)$, are governed by the coupled non-linear Schrödinger equation, giving

$$i\hbar\frac{\partial\psi_1}{\partial t}=\left(-\frac{\hbar^2}{2m_1}\boldsymbol{\nabla}^2+\frac{4\pi\hbar^2a_{11}}{m_1}\left|\psi_1\right|^2+\frac{2\pi\hbar^2a_{12}}{m_{12}}\left|\psi_2\right|^2-\mu_1\right)\psi_1 \tag{3.1}$$

and

$$i\hbar\frac{\partial\psi_2}{\partial t}=\left(-\frac{\hbar^2}{2m_2}\boldsymbol{\nabla}^2+\frac{4\pi\hbar^2a_{22}}{m_2}\left|\psi_2\right|^2+\frac{2\pi\hbar^2a_{21}}{m_{21}}\left|\psi_1\right|^2-\mu_2\right)\psi_2. \tag{3.2}$$

Here, m_j and μ_j are respectively the atomic masses and the chemical potential associated with the two species. The m_{12} term refers to the reduced mass for interspecies interaction, such that $m_{12}=(m_1m_2)/(m_1+m_2)$. The intra-species and interspecies $s-$wave scattering lengths are denoted by a_{jj} and a_{12} respectively. We note that $a_{12}=a_{21}$.

Using the hydrodynamic equations, it can be seen that, since species 2 has a velocity $\boldsymbol{v}_r$, a solution of the wave functions is given by $\psi_1=\sqrt{\rho_1}$ and $\psi_2=\sqrt{\rho_2}\mathrm{e}^{i\boldsymbol{k}\cdot\boldsymbol{x}}$, where $\boldsymbol{k}=m_2\boldsymbol{v}_r/\hbar$ and $\rho_j\,(=N_j/V)$ are the particle densities.

Next the evolution of the described condensate system is examined, assuming that ψ_1 and ψ_2 deviate slightly from the above solution. This is expressed by:

$$\psi_1(\boldsymbol{x},t)=\sqrt{\rho_1}+\phi_1(\boldsymbol{x},t), \tag{3.3}$$

$$\psi_2(\boldsymbol{x},t)=\sqrt{\rho_2}\mathrm{e}^{i\boldsymbol{k}\cdot\boldsymbol{x}}.+\phi_2(\boldsymbol{x},t) \tag{3.4}$$

Here ϕ_1 and ϕ_2 are small perturbations to the wave functions, ψ_1 and ψ_2, of the non-linear Schrödinger equations, (3.1) and (3.2). In a manner analogous with the superfluid two-stream instabiliy, it is assumed that the condensate mixture is stable if $\phi(\boldsymbol{x},t)$ remains small at all times. To this end, the linearised forms of (3.1) and (3.2) are considered:

$$\begin{aligned}i\hbar\frac{\partial\phi_1}{\partial t}=&\left(\frac{-\hbar^2}{2m_1}\nabla^2-\mu_1+2g_{11}+g_{12}\sqrt{\frac{\rho_2}{\rho_1}}\right)\phi_1+g_{11}\phi_1^*\\&+\left(g_{12}\mathrm{e}^{-i\boldsymbol{k}\cdot\boldsymbol{x}}\phi_2+g_{12}\mathrm{e}^{-i\boldsymbol{k}\cdot\boldsymbol{x}}\phi_2^*\right),\end{aligned} \tag{3.5}$$

$$i\hbar\frac{\partial\phi_2}{\partial t} = \left(\frac{-\hbar^2}{2m_2}\nabla^2 - \mu_2 + 2g_{22} + g_{12}\sqrt{\frac{\rho_1}{\rho_2}}\right)\phi_2 + g_{22}\mathrm{e}^{2i\boldsymbol{k}\cdot\boldsymbol{x}}\phi_2^* + \left(g_{12}\mathrm{e}^{i\boldsymbol{k}\cdot\boldsymbol{x}}\phi_1 + g_{12}\mathrm{e}^{i\boldsymbol{k}\cdot\boldsymbol{x}}\phi_1^*\right), \tag{3.6}$$

where $g_{jj} = 4\pi\hbar^2 a_{jj}\rho_j/m_j$ and $g_{12} = 2\pi\hbar^2 a_{12}\sqrt{\rho_1\rho_2}/m_{12}$. An assumption that $g_{12}^2 \ll g_{11}g_{12}$ is made, as this is a condition of the stability of the stationary ($\boldsymbol{v}_r = 0$) case with no phase separation.

Using a form explained in [156], expansions in terms of ϕ_1 and ϕ_2 are obtained,

$$\phi_1 = \sum_{\mathbf{q}}\left(u_{\mathbf{q}}^{(1)}\mathrm{e}^{i\mathbf{q}\cdot\mathbf{x}}c_{\mathbf{q}}\mathrm{e}^{-i\omega_{\mathbf{q}}t} + v_{\mathbf{q}}^{(1)}\mathrm{e}^{-i\mathbf{q}\cdot\mathbf{x}}c_{\mathbf{q}}^*\mathrm{e}^{i\omega_{\mathbf{q}}t},\right) \tag{3.7}$$

$$\phi_2 = \mathrm{e}^{i\mathbf{k}\cdot\mathbf{x}}\sum_{\mathbf{q}}\left(u_{\mathbf{q}}^{(2)}\mathrm{e}^{i\mathbf{q}\cdot\mathbf{x}}c_{\mathbf{q}}\mathrm{e}^{-i\omega_{\mathbf{q}}t} + v_{\mathbf{q}}^{(2)}\mathrm{e}^{-i\mathbf{q}\cdot\mathbf{x}}c_{\mathbf{q}}^*\mathrm{e}^{i\omega_{\mathbf{q}}t},\right) \tag{3.8}$$

where $c_{\mathbf{q}}$ are the amplitudes associated with the collective excitation modes formed by the condensate mixture. In equations (3.7) and (3.8), the terms containing $u_{\mathbf{q}}$ and $v_{\mathbf{q}}$ are the left and right moving waves respectively. The normal modes of each condensate component are defined, as in [157] and others, as a two component object by

$$\phi_{\mathbf{q}}^{(i)} = \begin{pmatrix} u_{\mathbf{q}}^{(i)} \\ v_{\mathbf{q}}^{(i)}. \end{pmatrix} \tag{3.9}$$

Then, by substituting equations (3.7) and (3.8) into equations (3.5) and (3.6) and using the notation from [157],

$$\mathbf{W}_{\mathbf{q}} \equiv \left(u_{\mathbf{q}}^{(1)}, u_{\mathbf{q}}^{(2)}, v_{\mathbf{q}}^{(1)}, v_{\mathbf{q}}^{(2)}\right), \tag{3.10}$$

we arrive at the eigenequation,

$$M_{\mathbf{q}}\mathbf{W}_{\mathbf{q}} = \omega_{\mathbf{q}}\mathbf{W}_{\mathbf{q}}, \tag{3.11}$$

where

$$M_{\mathbf{q}} = g_{11} \begin{pmatrix} \gamma_m \tilde{q}^2 + 1 & \gamma_{12} & 1 & \gamma_{12} \\ \gamma_{12} & \tilde{q}^2 + 2\tilde{k}\tilde{q}\cos\theta + \gamma_2 & \gamma_{12} & \gamma_2 \\ -1 & -\gamma_{12} & -\gamma_m \tilde{q}^2 - 1 & -\gamma_{12} \\ -\gamma_{12} & -\gamma_2 & -\gamma_{12} & -\tilde{q}^2 - 2\tilde{k}\tilde{q}\cos\theta - \gamma_2. \end{pmatrix} \tag{3.12}$$

Equation (3.12) introduces the following variables. The angle θ is defined by $\theta = \cos^{-1}(\mathbf{k}\cdot\mathbf{q})/kq$. Two dimensionless momenta are introduced; $\tilde{k} = \hbar k/\sqrt{2m_2 g_{11}}$ and $\tilde{q} = \hbar q/\sqrt{2m_2 g_{11}}$. The following ratios are also defined; $\gamma_2 = g_{22}/g_{11}$, $\gamma_{12} = g_{12}/g_{11}$ and $\gamma_m = m_2/m_1$.

Equation (3.11) determines collective excitation frequencies, $\omega_{\mathbf{q}}$, of the condensate mixture [158]. Using essentially the same reasoning as that for demonstrating dynamical instability in a two component superfluid, the condensate mixture is assumed to be dynamically stable when all $\omega_{\mathbf{q}}$ are real and dynamically unstable when there exist modes with complex $\omega_{\mathbf{q}}$.

By a simple rearrangement, the relative velocity, $\boldsymbol{v}_r$, can be expressed as $\boldsymbol{v}_r = \hbar\mathbf{k}/m_2$. Given such an expression it is possible to examine all collective excitation frequencies, $\omega_{\mathbf{q}}$, for all $\mathbf{q}$. Before discussion of analytical results, a range of typical stability phase diagrams are produced in Figure 3.1 for a range of parameters. In each case the shaded area corresponds to an unstable region in which $\omega_{\mathbf{q}}$ are complex. There are two main features of these diagrams. Firstly, they show that for each set of parameters there exists a critical $\tilde{k}_c$, such that for all $\tilde{k} < \tilde{k}_c$, all $\omega_{\mathbf{q}}$ are real. This indicates the existence of a critical velocity, $v_r^{(c)} = \tilde{k}_c\sqrt{2g_{11}/m_2}$ below which the condensate mixture is stable. Secondly, there is only a finite range of values for $\tilde{k}_c$ for which $\omega_{\mathbf{q}}$ take complex value for some given $\tilde{q}$. This indicates a finite range of relative velocities that manifest the instability being considered. When compared with Figure 1.6 from Chapter 2 of this thesis, we see that these results add further credence to the analogous behaviour of the condensate mixture and the two component superfluid with relation to this class of dynamical instability.

It is also interesting to note that the shaded bands in these graphs become narrower as the interspecies interactions are weakened. Whether this is in some way analogous to decreasing the chemical coupling in the two component superfluid case, as discussed in Chapter 2, may prove an interesting question for the future.

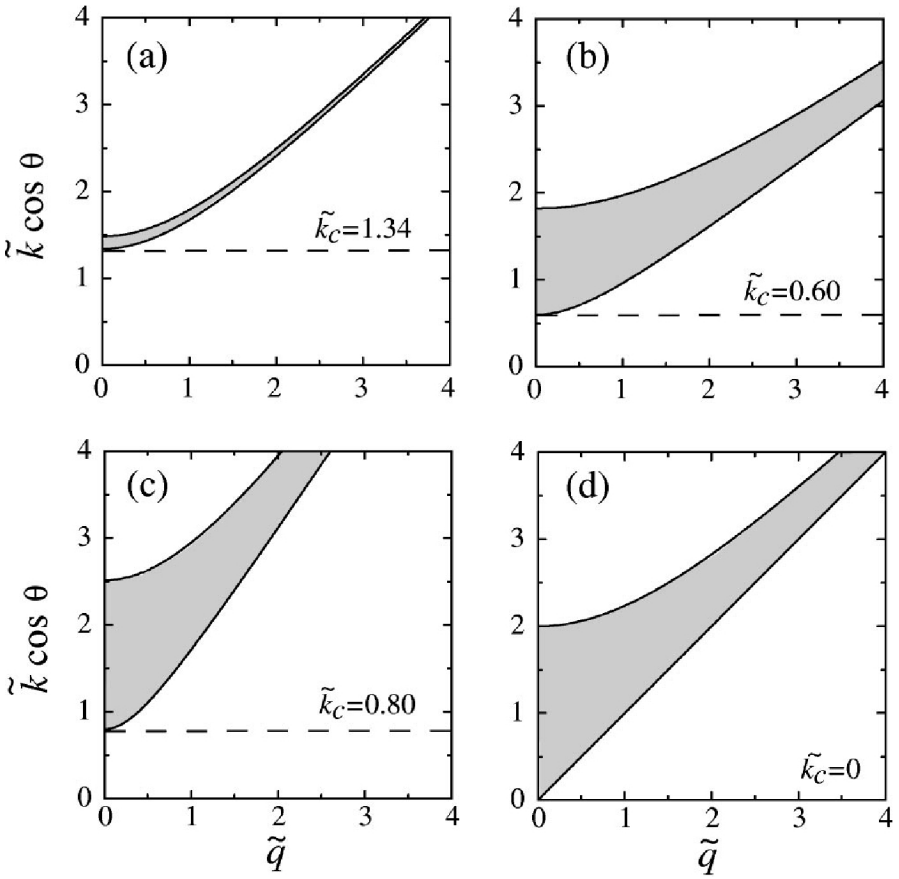

Figure 3.1: *Stability phase diagrams of the system with different dimensionless parameters. The collective excitation frequencies, $\omega_{\mathbf{q}}$, are complex inside the shaded region. The dashed lines show the value of $\tilde{k}_c$. Both $\tilde{k}$ and $\tilde{q}$ are dimensionless, being defined after equation (3.12). The interaction parameters are (a) $\gamma_2 = 1$, $\gamma_{12} = 0.1$ and $\gamma_m = 1$; (b) $\gamma_2 = 1.5$, $\gamma_{12} = 1$ and $\gamma_m = 0.5$; (c) $\gamma_2 = 1.5$, $\gamma_{12} = 1$ and $\gamma_m = 2$; (d) $\gamma_2 = 1$, $\gamma_{12} = 1$ and $\gamma_m = 1$. Note that only the region with positive $\cos\theta$ is shown. The negative $\cos\theta$ region is simply a reflection in the horizontal axis.* Figure reproduced from [6]

In considering a full analytic solution to the problem, it is noted that Equation (3.11) yields a quartic in $\omega_{\mathbf{q}}$ when expanded using $\det\left[M_{\mathbf{q}} - \omega_{\mathbf{q}} I\right] = 0$. So if the mode $\mathbf{q}$ is stable, the above equation in $\omega_{\mathbf{q}}$ has four real roots. Whilst this may appear difficult here, it is essentially the same problem as that presented by equation (1.33) from chapter 2, the onset of instability occurring when a pair of these real roots merge and become complex. Whilst a full analytic solution can be found for this quartic, the number of terms in the matrix, $M_{\mathbf{q}}$, suggest that this will be too complicated to easily yield useful information about the nature of such a solution. It may be that a numerical treatment of the problem will be necessary to yield full results. However, some insight on $\tilde{k}_c$ can be gained by considering the weak and strong interspecies coupling limits.

Firstly, consider the weak-coupling regime. In this case we have $g_{12} \ll \sqrt{g_{11} g_{22}}$, which leads to

$$\tilde{k}_c^2 = \frac{\left(\sqrt{\gamma_m}+\sqrt{\gamma_2}\right)^2}{2} - (\gamma_m\gamma_2)^{1/4}\left(\sqrt{\gamma_m}+\sqrt{\gamma_2}\right)\frac{\gamma_{12}}{\sqrt{\gamma_2}} + \mathcal{O}\left(\frac{\gamma_{12}}{\sqrt{\gamma_2}}\right)^2. \tag{3.13}$$

Whilst in the strong coupling regime, we have $g_{12} \approx \sqrt{g_{11}g_{22}}$, which gives

$$\tilde{k}_c^2 = \frac{\left(\sqrt{\gamma_m}+\sqrt{\gamma_2}\right)}{\sqrt{\gamma_m}}\left(\sqrt{\gamma_2-\gamma_{12}}\right) - \frac{(\gamma_m-\gamma_2)^2}{2\gamma_2\left(\gamma_m+\gamma_2\right)}\left(\sqrt{\gamma_2-\gamma_{12}}\right)^2 + \mathcal{O}\left(1-\frac{\gamma_{12}}{\sqrt{\gamma_2}}\right)^3. \tag{3.14}$$

Using the two limiting cases from equations (3.13) and (3.14), an approximate solution for $\tilde{k}_c$ is constructed, which approximates the solution for the entire parameter ranges;

$$2\tilde{k}_c^2 \approx (\sqrt{\gamma_m}+\sqrt{\gamma_2})^2\left(1-\frac{\gamma_{12}}{\sqrt{\gamma_2}}\right) + \alpha\gamma_{12}\left(\sqrt{\gamma_2-\gamma_{12}}\right)^2\beta\gamma_{12}^2\left(\sqrt{\gamma_2-\gamma_{12}}\right), \tag{3.15}$$

where

$$\alpha = \left(\sqrt{\gamma_2}+\sqrt{\gamma_m}\right)\left(\sqrt{\gamma_2}-2\gamma_m^{1/4}\gamma_2^{1/4}+\sqrt{\gamma_m}\right)\gamma_2^{-3/2} \tag{3.16}$$

and

$$\beta = \left(\gamma_m - 2\sqrt{\gamma_2\gamma_m}+\gamma_2\right)\gamma_2^{-3/2}. \tag{3.17}$$

Whilst the approximate formula, equation (3.15), is not an exact solution to the quartic obtained from equation (3.11), it is constructed so that it matches the values of $\tilde{k}_c^2$ and their first derivatives with respect to γ_{12} in the limits of equations (3.13) and (3.14). The approximate formula was also tested against numerical solutions for exact values for $\tilde{k}_c$ and found to be in reasonable agreement over a wide range of parameters. This formula is sufficiently tractable to allow information with regard to how the dimensionless

parameters affect $\tilde{k}_c$. This is shown in Figure 3.2. The approximations used show that the instability is present in both the strong and weak coupling limits. From this it is reasonable to infer that it is manifest across the full range of coupling parameters, as is the case with the approximate general solution, (3.15).

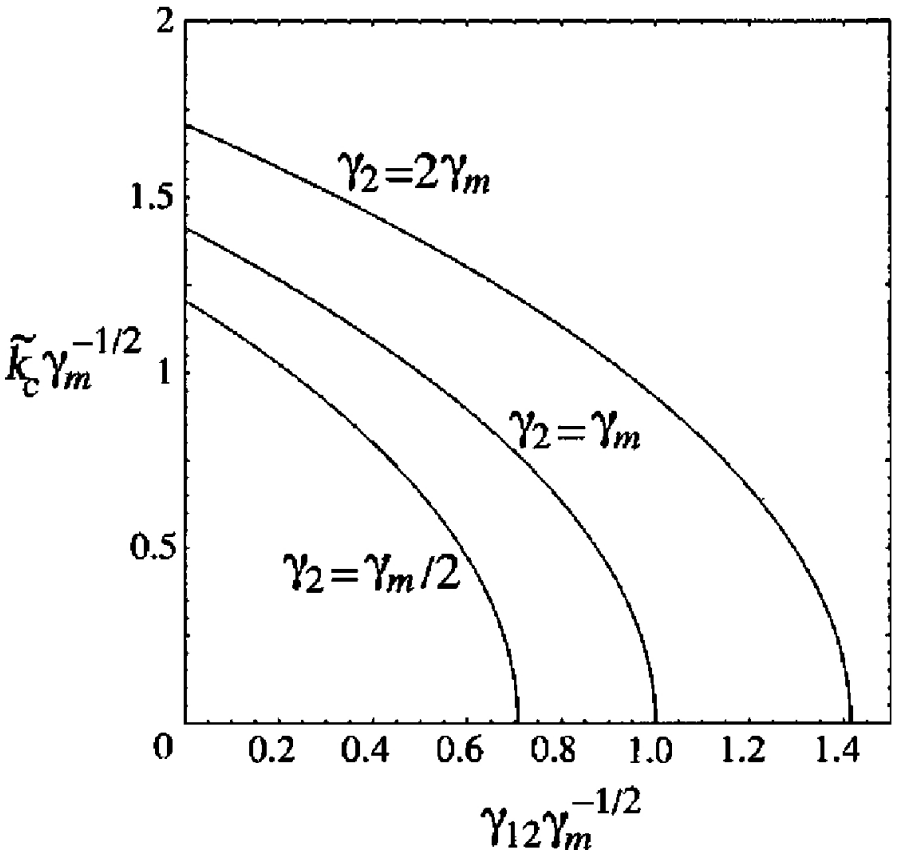

Figure 3.2: $\tilde{k}_c$ *as a function of the dimensionless interaction parameters.* Figure reproduced from [6]

In common with the superfluid two-stream instability, the BEC instability associated with $\tilde{k}_c$ depends only on the relative velocity of the two components. It is present for relative velocities well below the speed of sound. This result tells us that the instability represents an analogue for the two-stream instability discussed in Chapter 2. Mathematically modelling this instability in more complex situations, such as rotating bodies, requires considerable further work.

3.3 The Hydrodynamic Approximation

In further considering the analogous nature of the instability in a condensate mixture and the superfluid two-stream instability [2], it is useful to apply the hydrodynamic approximation from Pethick and Smith [84] to the problem posed by Law et al [6]. At this juncture we return to the use of the more standard notation used throughout the rest of this thesis, rather than that used in [6], although to simplify comparison with the original text, we make use of some of the notation from [84]. The hydrodynamic equations are derived from the single component, time-dependent Gross-Pitaevskii (GP) equation (which is also referred to as the non-linear Schrödinger equation). If we define $\psi(\mathbf{r},t)$ as the wave function (or order parameter) associated with a single species BEC, where $\mathbf{r}$ is the vector representing position in three dimensions, then the time dependent behaviour given by the GP equation,

$$-\frac{\hbar^2}{2m}\nabla^2\psi(\mathbf{r},t)+V(\mathbf{r})\psi(\mathbf{r},t)+U_0\left|\psi(\mathbf{r},t)\right|^2\psi(\mathbf{r},t)=i\hbar\frac{\partial\psi(\mathbf{r},t)}{\partial t}. \tag{3.18}$$

Here V is the external potential. U_0 is the effective (long range) interaction between two particles in the condensate. This is obtained from the Born approximation [159] and is related to the s-wave scattering length by

$$U_0=\frac{4\pi\hbar^2 a}{m}, \tag{3.19}$$

where m is the particle mass.

Firstly, we note that this equation is identical to equations (3.1) and (3.2), with one exception. The earlier equations include a term for the chemical potential. With relation to the application we are considering here, this does not really need to concern us. In the analysis that follows, terms relating to potentials will cancel and will not appear in the final result.

Without loss of generality, we consider only equation (3.1), which we reproduce here for convenience.

$$i\hbar\frac{\partial\psi_1}{\partial t}=\left(-\frac{\hbar^2}{2m_1}\boldsymbol{\nabla}^2+\frac{4\pi\hbar^2 a_{11}}{m_1}\left|\psi_1\right|^2+\frac{2\pi\hbar^2 a_{12}}{m_{12}}\left|\psi_2\right|^2-\mu_1\right)\psi_1. \tag{3.20}$$

In order to obtain the conservation and Euler equations from equation (3.20), we firstly rearrange and multiply this by the complex conjugate of ψ_1, which we denote ψ_1^*. This yields

$$-i\hbar\psi_1^*\frac{\partial\psi_1}{\partial t}-\frac{\hbar^2}{2m_1}\psi_1^*\boldsymbol{\nabla}^2\psi_1+\left(\frac{4\pi\hbar^2a_{11}}{m_1}\left|\psi_1\right|^2+\frac{2\pi\hbar^2a_{12}}{m_{12}}\left|\psi_2\right|^2-\mu_1\right)\left|\psi_1\right|^2=0. \quad (3.21)$$

We then subtract equation (3.21) from its own complex conjugate. The bracketed terms, being wholly real, disappear (including the 'extra' chemical potential term) and we are left with

$$\partial_t\left|\psi_1\right|^2+\nabla_i\cdot\left[\frac{\hbar}{2m_1i}\left(\psi_1^*\nabla^i\psi_1-\psi_1\nabla^i\psi_1^*\right)\right]=0. \quad (3.22)$$

We associate the order parameter, ψ_1, with the particle density, n, by

$$\psi_1=\sqrt{n_1}\mathrm{e}^{iS_1}, \quad (3.23)$$

where S_1 represents the phase of ψ_1. This leads to

$$n_1=\left|\psi_1\right|^2. \quad (3.24)$$

We further recall that, in quantum mechanics, the momentum operator is defined [160] by

$$p_1^i=\frac{\hbar}{2i}\frac{1}{\left|\psi_1\right|^2}\left(\psi_1^*\nabla^i\psi_1-\psi_1\nabla^i\psi_1\right). \quad (3.25)$$

Assuming that the equation, $p_i=mv_i$, holds in this case, then we can express the velocity as

$$v_1^i=\frac{1}{\left|\psi_1\right|^2}\left[\frac{\hbar}{2m_1i}\left(\psi_1^*\nabla^i\psi_1-\psi_1\nabla^i\psi_1^*\right)\right]. \quad (3.26)$$

It can now be seen that, by combining equations (3.24) and (3.26), equation (3.22) can be expressed in the form

$$\partial_t n_1+\nabla_i\left(n_1v_1^i\right)=0. \quad (3.27)$$

This is the particle number conservation equation from fluid mechanics.

We now allow our second degree of freedom to be represented by the phase of ψ_1. We express this by

$$\psi_1 = \sqrt{n_1}\mathrm{e}^{\mathrm{i}S_1}. \tag{3.28}$$

This allows us to express the velocity by

$$v_1^i = \frac{\hbar}{m_1}\nabla^i S_1. \tag{3.29}$$

This further allows us to rewrite the real part of the Gross-Pitaevskii equation, (3.18) as

$$-\hbar\partial_t S_1 = U_0 n_1 + V_{\text{ext}} + \frac{m_1 v_1^2}{2} - \frac{\hbar^2}{2m_1}\frac{1}{\sqrt{n_1}}\nabla^2\sqrt{n_1}. \tag{3.30}$$

By combining equations (3.29) and (3.26) we obtain

$$\frac{\hbar^2}{2m_1}\left(\nabla_i S_1\right)\left(\nabla^i S_1\right) = \frac{m_1 v_1^2}{2}. \tag{3.31}$$

By taking the gradient of equation (3.30) and using the irrotational nature of the flow, we arrive at

$$m_1\left(\partial_t + v_1^j\nabla_j\right)v_i^1 + \nabla_i\left(U_0 n_1 + V_{\text{ext}}\right) - \nabla_i\left(\frac{\hbar^2}{2m_1}\frac{1}{\sqrt{n_1}}\nabla^2\sqrt{n_1}\right) = 0. \tag{3.32}$$

This is similar to the standard fluid result with only the last term differing. This term retains the quantum origin of the model through the presence of Planck's constant. We can, however, take our calculations a little further. If we assume that the density is spatially uniform then

$$\nabla^2\sqrt{n_1} = 0, \tag{3.33}$$

and the last term disappears. It may appear that this assumption is rather arbitrary but we can justify this if we consider the lengthscales with which we are working. If we assume that the order parameter varies on some length scale, L, it follows that

$$\nabla\mu \sim \frac{nU_0}{L} \tag{3.34}$$

and

$$\nabla\left(\frac{\hbar^2}{2m}\frac{1}{\sqrt{n}}\nabla^2\sqrt{n}\right) \sim \frac{\hbar^2}{mL^3}. \tag{3.35}$$

So our assumption is simplification is justified if

$$\frac{\hbar^2}{mnL^2U_0} \ll 1. \tag{3.36}$$

To give this relation some physical meaning, we introduce the 'coherence length', ξ, which is roughly the length scale on which kinetic energy balances the pressure. This leads to

$$\frac{\hbar^2}{2m\xi^2} \approx nU_0. \tag{3.37}$$

So we need

$$\left(\frac{\xi}{L}\right) \ll 1. \tag{3.38}$$

Then, if we consider sufficiently large scale variations, this becomes a valid assumption and we are left with classical hydrodynamics.

To make this problem as close as possible to that posed in the basic two-stream instability analysis from Chapter 2, we assume there is no external potential present. This condition is equivalent, to some degree, to the exclusion of gravitational potential from the two-stream instability calculation. This leads us to

$$-m_1\partial_t v_1^i = \nabla^i\left(\frac{1}{2}m_1 v_1^2\right) + \nabla^i\left(U_0 n_1\right). \tag{3.39}$$

We make use of the vector identity, expressed here in index form,

$$v^j\nabla_j v^i = \frac{1}{2}\nabla^i\left(v^k v_k\right) - \epsilon^{ijk}v_j\epsilon_{klm}\nabla^l v^m, \tag{3.40}$$

along with the definition of irrotational flow, that tells us that

$$\epsilon^{ijk}v_j\epsilon_{klm}\nabla^l v^m = 0. \tag{3.41}$$

Substituting equations (3.40) and (3.41) into equation (3.39) gives the much simpler

$$\partial_t v_1^i + v_1^j\nabla_j v_1^i + \frac{1}{m_1}\nabla^i\left(U_0 n_1\right) = 0. \tag{3.42}$$

This is the Euler equation and is identical in structure to equation (1.6) from Chapter 2. The chemical potential term has simply been replaced with a term that includes the interaction terms as well as the chemical potential.

As the above exercise did not rely on properties peculiar to any one BEC, it can equally be applied to the second species in our condensate mixture, as described by equation (3.2). So we have shown that, by using the hydrodynamic approximation, we can produce a description of the behaviour of the two individual condensates in the mixture. This suggests that we may use the two-stream instability as an analogue to a class of dynamical instabilities in a binary BEC.

It is, however, necessary to sound a note of caution at this stage. Firstly, in using the hydrodynamic approximation, we have made several assumptions that may not be fully applicable to the condensates in all cases. In particular, the approximations are reasonable only if we have a sufficiently large number of particles in our condensates. Further, we have made assumptions dependent on the lengthscales of variations in the wave functions. Such may not be fully valid in practice.

Possibly of greater concern is the existence, in the neutron star, of entrainment between the two fluid components and its absence in BEC's. In our analysis this has been totally ignored, which, in any attempt at using BEC's as a physical model for multi component superfluids, will introduce major discrepancies. In our analysis in Chapter 4, we show that the exclusion introduces large quantitative changes in the unstable modes of differentially rotating superfluids. In the next section, we discuss the inclusion of entrainment and how this would impact on the governing equations, (3.1) and (3.2) for a two component BEC.

One further issue is that, although they are governed by the same equations, we do not yet know if the physical characteristics of the BEC's allow these instabilities to be exhibited in our simple two-stream model. (Although the generic nature of the two-stream instability suggests very strongly that such instabilities will occur.) To this end we consider two condensates of known characteristics and assume them to be co-existing. By substituting the scattering lengths (the only property that influences the instabilities in our model) into our hydrodynamic approximation equations, (3.27) and (3.42), we are able to calculate where the BEC analogue exhibits unstable tendencies.

In our example we choose two different hyper-states of Rubidium-87 (^{87}Rb); the first, designated species 1, having spin 1, the other, designated species 2, having spin 2. The scattering length for species 1 is given by $a_{11} = 5.315$nm, that for species 2 by

$a_{22} = 5.052$nm, and the inter-species scattering length by $a_{12} = a_{21} = 5.191$nm. Since we are considering two species of Rubidium-87 condensates [161], $m_1 = m_2$. For convenience, we assume the particle density has been arranged to be the same for each BEC. By substituting the scattering lengths into equations (3.1) and (3.2) we are able to calculate the a and b in equation (1.32) from Chapter 1. This leads to the constants $a^2 = 0.905$ and $b^2 = 0.9539$, which we now substitute into the two-stream dispersion relation equation (1.33).

It should be noted at this point, that the sound speed calculations are made using the hydrodynamic approximation. In this calculation there are some issues that may introduce minor errors when applying the hydrodynamic limit directly to real BEC's. It has been shown in one dimension by integration of the Gross-Pitaevskii equation that a disorder potential present in a BEC leads to a marginally lower actual speed of sound, depending on the level of disorder, than that calculated using the hydrodynamic approximation [162]. This produces only small variations in the speed of sound and will not affect our model in a significant way. There also exists a relationship between the speed of sound and the trap potential. However, this is actually a rather complex subject and, for now at least, we shall not attempt to include it in our analysis. (In our simple model, we assume no trap potential is in place and so this does not apply here.)

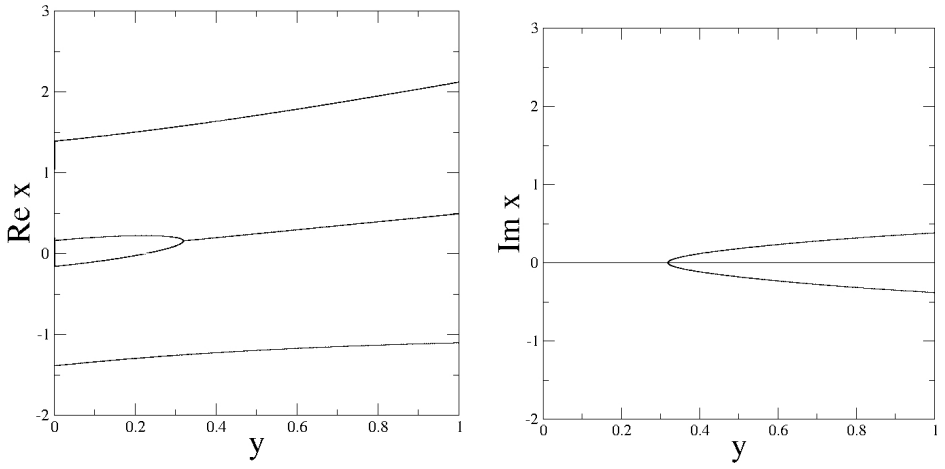

Figure 3.3: *Real and imaginary parts of the two roots of the dispersion relation, equation (1.33), for the binary BEC. Complex roots, mirroring the two-stream instability of the two component superfluid, exist at approximately* 30% *of the speed of sound and continue beyond the speed of sound.*

With this in mind, the above values are substituted into equation (1.33) and we obtain the results shown in Figure 3.3. It can be seen that these graphs exhibit essentially the same characteristics as those seen in the two component superfluid case. Most importantly there exists a critical relative velocity in the background, above which the binary BEC exhibits dynamical instabilities. In this particular case the instabilities are existent

at a much lower percentage of the speed of sound than was obtained in the example given for the two-stream instability in Chapter 2. Of course, we are discussing an analogue here, rather than an identity, so the important fact is that the two models display the same phenomenon but do not need to be quantitatively identical. These results suggest that experimental work with such a condensate mixture could offer insight into non linear behaviour of multi component superfluids and shed further light on mechanisms associated with neutron star glitches.

We note that, in the example shown here, we have the strong interaction case ($g_{12} \approx \sqrt{g_{11}g_{22}}$) from [6]. We note that, as in Figure 3.1, the range of unstable relative velocities in our example is wide, extending well beyond the speed of sound (and, ipso facto, beyond the speed where super fluidity breaks down and our model ceases to be valid). It might be interesting to explore the results of the weak coupling case and compare this with the figures in [6]. However, we have in essence already produced results equivalent to weaker interaction. It can be seen that the effect of such weaker interaction is to produce values for a^2 and b^2 in equation (1.33) that are further from being equal than those in the two Rubidium species example we have chosen here. Such 'less equal' values have already been used in the calculation for the two-stream instability in Chapter 2. So it is not unreasonable to use these results as an example of a more weakly interacting condensate mixture. (The $g_{12} \ll \sqrt{g_{11}g_{22}}$ case.)

If we compare the results shown in Figure 1.6 and Figure 3.3, we can see that they conform with those shown in Figure 3.1. Firstly we have a much narrower range of relative velocities for the instability in the case of the weaker interaction. This is consistent with [6]. Secondly, we note that the instabilities are present at a lower percentage of the speed of sound in the strongly interacting case. Again this is consistent with [6]. These two features show that the hydrodynamic approximation shares key characteristics in common with the BEC's behaviour. It appears by varying the interaction between the two condensates we can model with increased accuracy the superfluid behaviour.

Of course, we should bear in mind that we have, as yet, only produced a proof of principle for the analogous behaviour of the two instabilities. In considering our simple linear model, we should recall that examples in nature (in our case, neutron stars) are neither simple nor linear. This is, however, a significant first step. We should note that through the use of external potentials, we can manipulate the condensate mixture into almost any configuration we may desire. For example, of more practical use, rotating binary condensates can be produced [163]. With such an arrangement it should be possible to extend the model to include the r-mode instabilities in differentially rotating neutron stars as discussed in Chapter 4.

Another advance of recent years is the observation of vortex pinning in BEC's [164]. Since the unpinning and re-pinning of vortices is central to some existing models of neutron star glitches, [37, 165] and many others, this may offer an opportunity to model these features. Whether the analogue we have demonstrated here can be expanded to encompass this last feature has not yet (as far as we are aware) been considered. However, it certainly warrants investigation.

In summary, we have shown in this section that the dynamical instability of a condensate mixture is sufficiently analogous to that of a two component superfluid, that the former offers the prospect of "neutron star physics in a laboratory". There still remains much work to be done to extend this model so that it more completely mirrors the features of a neutron star core.

3.4 Binary BEC's with Entrainment

We have shown that the superfluid two-stream instability can be observed in a purely chemically coupled binary BEC, using the hydrodynamic equations. This is, at least, a start along the path to modelling this class of instability within a neutron star core. It should be noted that, as described in Chapter 1, the original mathematical demonstration of this new instability [2] assumed that the two component fluids were themselves coupled chemically. However, for a more complete model of the super-dense neutron-proton conglomerate at the core of these stars, we need to include some means of modelling the entrainment between the components.

Before proceeding, it is useful to consider what entrainment is and why it is present in a neutron star core, yet absent from a diffuse condensate. Put very simply, entrainment, in this context, is an effect whereby the strong nuclear interaction causes one component to be endowed with a virtual cloud of particles from the other. There is a symmetry to this effect so that the second component is similarly endowed by particles from the first [61]. This, in turn alters the individual momenta of the two components, with each possessing a term dependent upon the strength of this effect and the relative velocity of the two components.

The explanation of the absence of such an effect in binary BEC's is, therefore, relatively easily explained. The particle density of a typical BEC is of the order of $10^{-13} - 10^{-15}$ cm^{-3} [84], giving an average particle separation of approximately 10^{-7}m. Given that the range of the strong interaction is of the order of 10^{-15}m, it is clear that it plays no significant role in the dynamical behaviour of BEC's. In the case of neutron stars, we

are considering nuclear densities, approximately 10^{38} particles cm^{-3}, and greater. This gives us average separations comfortably within the range of the strong interaction.

Here we explore how this effect might be reproduced in a BEC. Previously we showed that, given the Gross-Pitaevskii (GP) equations, we could obtain the hydrodynamic equations for an entrainment free two-component fluid. Here we start with the hydrodynamic equations for a two component fluid and see how these might alter the standard GP equations.

We start with a two component fluid whose components are represented by the constituent indices x and y. It is assumed that each of these components is both incompressible and irrotational. As such we can describe their dynamics by the standard Euler equations:

$$\partial_t p_i^{\mathrm{x}} + \nabla_i \left(\mu_{\mathrm{x}} - \frac{m_{\mathrm{x}}}{2} v_{\mathrm{x}}^2 + v_{\mathrm{x}}^j p_j^{\mathrm{x}} \right) = 0 \tag{3.43}$$

and

$$\partial_t p_i^{\mathrm{y}} + \nabla_i \left(\mu_{\mathrm{y}} - \frac{m_{\mathrm{y}}}{2} v_{\mathrm{y}}^2 + v_{\mathrm{y}}^j p_j^{\mathrm{y}} \right) = 0. \tag{3.44}$$

Owing to the symmetry of these fluid equations, we need only consider the x component. The inclusion of entrainment means that the momentum term, p_i^{x}, can be expressed by

$$p_i^{\mathrm{x}} = m_{\mathrm{x}} \left(v_i^{\mathrm{x}} + \varepsilon_{\mathrm{x}} w_i^{\mathrm{yx}} \right), \tag{3.45}$$

where ε_{x} is the entrainment parameter for x, and w_i^{yx} $(= v_i^{\mathrm{y}} - v_i^{\mathrm{x}})$ is the relative velocity of the two components.

We assume that we are dealing with some local region of the condensate where the particle density, n_{x}, is constant (implying a uniform condensate [84]), as is the entrainment and the velocity. So

$$n_{\mathrm{x}} = const, \tag{3.46}$$

$$\varepsilon_{\mathrm{x}} = const, \tag{3.47}$$

$$\nabla_i v_{\mathrm{x}}^i = 0. \tag{3.48}$$

Using the method followed previously, we now express our fluid parameters in terms of the condensate parameters. From [84] we have

$$\psi_{\mathrm{x}} = \sqrt{n_{\mathrm{x}}}\mathrm{e}^{iS_{\mathrm{x}}}, \tag{3.49}$$

where S_{x} is real.

We also make use of the standard momentum operator,

$$p_i^{\mathrm{x}} = \frac{\hbar}{2}\frac{1}{|\psi_{\mathrm{x}}|^2}\left(\psi_{\mathrm{x}}^*\nabla_i\psi_{\mathrm{x}} - \psi_{\mathrm{x}}\nabla_i\psi_{\mathrm{x}}^*\right). \tag{3.50}$$

When combined with equation (3.49), this gives

$$p_i^{\mathrm{x}} = \hbar\nabla_i S_{\mathrm{x}}. \tag{3.51}$$

From our previous assumption, equation (3.48), we have

$$\nabla^i p_i^{\mathrm{x}} = 0 \qquad \Rightarrow \nabla^2 S_{\mathrm{x}} = 0. \tag{3.52}$$

It is convenient to express the entrainment parameters, ε_{x}, in terms of a single coefficient. Since the change in momentum of the two fluid components as a result of entrainment must be equal and opposite, we have

$$m_{\mathrm{x}}\varepsilon_{\mathrm{x}} = m_{\mathrm{y}}\varepsilon_{\mathrm{y}} \tag{3.53}$$

This allows us to use a single coefficient, α, to describe the entrainment, where

$$\alpha = \frac{\varepsilon_{\mathrm{x}}\rho_{\mathrm{x}}}{2}, \tag{3.54}$$

where ρ_{x} $(= m_{\mathrm{x}}n_{\mathrm{x}})$ is the fluid density.

So we can express the entrainment parameter in terms of this entrainment coefficient as

$$\varepsilon_{\mathrm{x}} = \frac{2\alpha}{m_{\mathrm{x}}n_{\mathrm{x}}}. \tag{3.55}$$

We can now rewrite the momentum, equation (3.45), as

$$
\begin{aligned}
p_i^{\mathrm{x}} &= m_{\mathrm{x}} \left(v_i^{\mathrm{x}} + \frac{2\alpha}{m_{\mathrm{x}} n_{\mathrm{x}}} w_i^{\mathrm{xy}} \right) \\
&= \frac{\rho_{\mathrm{x}}}{n_x} \left(v_i^{\mathrm{x}} + \frac{2\alpha}{m_{\mathrm{x}} n_{\mathrm{x}}} v_i^{\mathrm{y}} - \frac{2\alpha}{m_{\mathrm{x}} n_{\mathrm{x}}} v_i^{\mathrm{x}} \right) \\
&= \frac{1}{n_{\mathrm{x}}} \{ (\rho_{\mathrm{x}} - 2\alpha)\, v_i^{\mathrm{x}} + 2\alpha v_i^{\mathrm{y}} \}.
\end{aligned} \tag{3.56}
$$

This enables us to express the momentum density for the two components as,

$$
n_{\mathrm{x}} p_i^{\mathrm{x}} = (\rho_{\mathrm{x}} - 2\alpha)\, v_i^{\mathrm{x}} + 2\alpha v_i^{\mathrm{y}} \tag{3.57}
$$

and

$$
n_{\mathrm{y}} p_i^{\mathrm{y}} = 2\alpha v_i^{\mathrm{x}} + (\rho_{\mathrm{y}} - 2\alpha)\, v_i^{\mathrm{y}}. \tag{3.58}
$$

It would be helpful if we could express the individual velocities in terms of the momenta. We do this via

$$
\begin{pmatrix} v_{\mathrm{x}}^i \\ v_{\mathrm{y}}^i \end{pmatrix} = \frac{1}{D} \begin{pmatrix} \rho_{\mathrm{y}} - 2\alpha & -2\alpha \\ -2\alpha & \rho_{\mathrm{x}} - 2\alpha \end{pmatrix} \begin{pmatrix} n_{\mathrm{x}} p_{\mathrm{x}}^i \\ n_{\mathrm{y}} p_{\mathrm{y}}^i, \end{pmatrix} \tag{3.59}
$$

where D is the determinant such that

$$
D = (\rho_{\mathrm{x}} - 2\alpha)\,(\rho_{\mathrm{y}} - 2\alpha) - 4\alpha^2 = \rho_{\mathrm{x}}\rho_{\mathrm{y}} - 2\alpha\,(\rho_{\mathrm{x}} + \rho_{\mathrm{y}})\,. \tag{3.60}
$$

This gives us the two components velocities as

$$
v_{\mathrm{x}}^i = \frac{1}{D} \{ (\rho_{\mathrm{y}} - 2\alpha)\, n_{\mathrm{x}} p_{\mathrm{x}}^i - 2\alpha n_{\mathrm{y}} p_y^i \}, \tag{3.61}
$$

$$
v_{\mathrm{y}}^i = \frac{1}{D} \{ -2\alpha n_{\mathrm{x}} p_{\mathrm{x}}^i + (\rho_{\mathrm{x}} - 2\alpha)\, n_{\mathrm{y}} p_{\mathrm{y}}^i \}. \tag{3.62}
$$

So having calculated the individual velocities in terms of the component momenta, we return to our Euler equations, (3.43) and (3.44). We would like to eliminate the velocity terms from these equations. This can be most conveniently achieved by first considering the

$$-\frac{m_{\mathrm{x}}}{2}v_{\mathrm{x}}^2+v_{\mathrm{x}}^j p_j^{\mathrm{x}} \tag{3.63}$$

term. For convenience we express this using vector notation,

$$\begin{aligned}-\frac{m_{\mathrm{x}}}{2}\left|\boldsymbol{v}_{\mathrm{x}}\right|^2+\boldsymbol{v}_{\mathrm{x}}\cdot\boldsymbol{p}_{\mathrm{x}}&=\frac{m_{\mathrm{x}}}{2}\left|\boldsymbol{v}_{\mathrm{x}}\right|^2+m_{\mathrm{x}}\boldsymbol{v}_{\mathbf{x}}\cdot\left\{\boldsymbol{v}_{\mathrm{x}}+\varepsilon\left(\boldsymbol{v}_{\mathrm{y}}-\boldsymbol{v}_{\mathrm{x}}\right)\right\}\\&=\frac{m_{\mathrm{x}}}{2\rho_{\mathrm{x}}}\left(\left|\boldsymbol{v}_{\mathrm{x}}\right|^2\rho_{\mathrm{x}}+4\alpha\boldsymbol{v}_{\mathrm{x}}\cdot\boldsymbol{v}_{\mathrm{y}}-4\alpha\left|\boldsymbol{v}_{\mathrm{x}}\right|^2\right).\end{aligned} \tag{3.64}$$

Substituting the expressions for velocity, (3.61) and (3.62), into equation (3.64) gives us, after some manipulation

$$\begin{aligned}&-\frac{m_{\mathrm{x}}}{2}\left|\boldsymbol{v}_{\mathrm{x}}\right|^2+\boldsymbol{v}_{\mathrm{x}}\cdot\boldsymbol{p}_{\mathrm{x}}\\=&\frac{1}{2n_{\mathrm{x}}D^2}\{\left(\rho_{\mathrm{x}}\rho_{\mathrm{y}}^2-4\alpha\rho_{\mathrm{x}}\rho_{\mathrm{y}}+4\alpha^2\rho_{\mathrm{x}}-4\alpha\rho_{\mathrm{y}}^2+8\alpha^2\rho_{\mathrm{y}}\right)\left(n_{\mathrm{x}}^2\left|\boldsymbol{p}_{\mathrm{x}}\right|^2\right)\\&-4\alpha^2\rho_{\mathrm{x}}n_{\mathrm{x}}^2\left|\boldsymbol{p}_{\mathrm{y}}\right|^2\\&+8\alpha^2\rho_2 n_{\mathrm{x}}n_{\mathrm{y}}\boldsymbol{p}_{\mathrm{x}}\cdot\boldsymbol{p}_{\mathrm{y}}\}.\end{aligned} \tag{3.65}$$

For expedience sake we write this as

$$\begin{aligned}&-\frac{m_{\mathrm{x}}}{2}\left|\boldsymbol{v}_{\mathrm{x}}\right|^2+\boldsymbol{v}_{\mathrm{x}}\cdot\boldsymbol{p}_{\mathrm{x}}\\=&\frac{1}{2n_{\mathrm{x}}D^2}\left(A_{\mathrm{x}}n_{\mathrm{x}}^2\left|\boldsymbol{p}_{\mathrm{x}}\right|^2+B_{\mathrm{x}}n_{\mathrm{x}}^2\left|\boldsymbol{p}_{\mathrm{y}}\right|^2+C_{\mathrm{x}}n_{\mathrm{x}}n_{\mathrm{y}}\boldsymbol{p}_{\mathrm{x}}\cdot\boldsymbol{p}_{\mathrm{y}}\right),\end{aligned} \tag{3.66}$$

where

$$\begin{aligned}A_{\mathrm{x}}&=m_{\mathrm{x}}m_{\mathrm{y}}^2n_{\mathrm{x}}n_y^2-4\alpha m_{\mathrm{x}}m_{\mathrm{y}}n_{\mathrm{x}}n_{\mathrm{y}}+4\alpha^2m_{\mathrm{x}}n_x-4\alpha m_{\mathrm{y}}^2n_{\mathrm{y}}^2+8\alpha^2m_{\mathrm{y}}n_{\mathrm{y}},\\B_{\mathrm{x}}&=-4\alpha^2m_{\mathrm{x}}n_{\mathrm{x}},\\C_{\mathrm{x}}&=8\alpha^2m_{\mathrm{y}}n_{\mathrm{y}}.\end{aligned} \tag{3.67}$$

Note that these factors are expressed in terms of the particle density as this is more customary in the BEC community. Similarly, we can express the factor D in this manner as

$$D = m_{\mathrm{x}} m_{\mathrm{y}} n_{\mathrm{x}} n_{\mathrm{y}} - 2\alpha \left(m_{\mathrm{x}} n_{\mathrm{x}} + m_{\mathrm{y}} n_{\mathrm{y}} \right). \tag{3.68}$$

We can now make the substitution from equation (3.51) into equation (3.66) giving

$$\begin{aligned} &- \frac{m_{\mathrm{x}}}{2} \left| \boldsymbol{v}_{\mathrm{x}} \right|^2 + \boldsymbol{v}_{\mathrm{x}} \cdot \boldsymbol{p}_{\mathrm{x}} \\ =&\frac{\hbar^2}{2 n_{\mathrm{x}} D^2} \{ A_{\mathrm{x}} n_{\mathrm{x}}^2 \left(\nabla_i S_{\mathrm{x}} \right) \left(\nabla^i S_{\mathrm{x}} \right) + B_{\mathrm{x}} n_{\mathrm{y}}^2 \left(\nabla_i S_{\mathrm{y}} \right) \left(\nabla^i S_{\mathrm{y}} \right) + C_{\mathrm{x}} n_{\mathrm{x}} n_{\mathrm{y}} \left(\nabla_i S_{\mathrm{x}} \right) \left(\nabla^i S_{\mathrm{y}} \right) \}. \end{aligned} \tag{3.69}$$

We now consider how we might express this in terms of the wave function, ψ_{x}. To this end we use

$$\begin{aligned} \psi_{\mathrm{x}}^* \nabla^2 \psi_{\mathrm{x}} &= \sqrt{n_{\mathrm{x}}} \mathrm{e}^{-iS_{\mathrm{x}}} \nabla^2 \left(\sqrt{n_{\mathrm{x}}} \mathrm{e}^{iS_{\mathrm{x}}} \right) \\ &= n_{\mathrm{x}} \mathrm{e}^{-iS_{\mathrm{x}}} \nabla_i \{ \mathrm{e}^{iS_{\mathrm{x}}} \left(i \nabla^i S_{\mathrm{x}} \right) \} \\ &= n_{\mathrm{x}} \{ - \left(\nabla_i S_{\mathrm{x}} \right) \left(\nabla^i S_{\mathrm{x}} \right) + i \nabla^2 S_{\mathrm{x}} \}. \end{aligned} \tag{3.70}$$

But we recall from our condition of incompressibility that

$$\nabla^2 S_{\mathrm{x}} = 0. \tag{3.71}$$

So we can rewrite equation (3.70) as

$$\left(\nabla_i S_{\mathrm{x}} \right) \left(\nabla^i S_{\mathrm{x}} \right) = - \frac{1}{n_{\mathrm{x}}} \psi_{\mathrm{x}}^* \nabla^2 \psi_{\mathrm{x}}. \tag{3.72}$$

We also need to consider mixed terms using

$$\left(\psi_{\mathrm{x}}^* \nabla_i \psi_{\mathrm{x}} \right) \left(\psi_{\mathrm{y}}^* \nabla^i \psi_{\mathrm{y}} \right) = - n_{\mathrm{x}} n_{\mathrm{y}} \left(\nabla_i S_{\mathrm{x}} \right) \left(\nabla^i S_{\mathrm{y}} \right). \tag{3.73}$$

or

$$\left(\nabla_i S_{\mathrm{x}} \right) \left(\nabla^i S_{\mathrm{y}} \right) = - \frac{1}{n_{\mathrm{x}} n_{\mathrm{y}}} \left(\psi_{\mathrm{x}}^* \nabla_i \psi_{\mathrm{x}} \right) \left(\psi_{\mathrm{y}}^* \nabla^i \psi_{\mathrm{y}} \right). \tag{3.74}$$

To fully express the Euler equation, (3.43), in terms of the wave function we still to to address $\partial_t p_i^{\mathrm{x}}$.

$$\partial_t p_i^{\mathrm{x}} = \hbar \partial_t \left(\nabla_i S_{\mathrm{x}} \right) = \hbar \nabla_i \left(\partial_t S_{\mathrm{x}} \right). \tag{3.75}$$

But

$$\psi_{\mathrm{x}}^* \partial_t \psi_{\mathrm{x}} = n_x \left(i \partial_t S_x \right), \tag{3.76}$$

which leads to

$$\partial_t p_i^{\mathrm{x}} = -\frac{i\hbar}{n_{\mathrm{x}}} \nabla_i \left(\psi_{\mathrm{x}}^* \partial_t \psi_{\mathrm{x}} \right). \tag{3.77}$$

By combining equations (3.72), (3.74) and (3.77) with the Euler equation, (3.43), we have

$$\begin{aligned} 0 = &- \nabla_i \left\{ \frac{i\hbar}{n_{\mathrm{x}}} \psi_{\mathrm{x}}^* \partial_t \psi_{\mathrm{x}} \right\} + \nabla_i \mu_{\mathrm{x}} \\ &+ \nabla_i \left\{ \frac{1}{2 n_{\mathrm{x}} D^2} \left(-\frac{\hbar^2}{n_x} A_{\mathrm{x}} n_{\mathrm{x}}^2 \psi_{\mathrm{x}}^* \nabla^2 \psi_{\mathrm{x}} \right) \right\} \\ &+ \nabla_i \left\{ \frac{1}{2 n_{\mathrm{x}} D^2} \left(-\frac{\hbar^2}{n_{\mathrm{y}}^2} B_{\mathrm{x}} n_{\mathrm{y}}^2 \psi_{\mathrm{y}}^* \nabla^2 \psi_{\mathrm{y}} \right) \right\} \\ &+ \nabla_i \left\{ \frac{1}{2 n_{\mathrm{x}} D^2} \left(-\frac{\hbar^2}{n_{\mathrm{x}} n_{\mathrm{y}}} \right) \left(\psi_{\mathrm{x}}^* \nabla_i \psi_{\mathrm{x}} \right) \left(\psi_{\mathrm{y}}^* \nabla^i \psi_{\mathrm{y}} \right) \right\}. \end{aligned} \tag{3.78}$$

By integrating this total derivative, we arrive at

$$\begin{aligned} 0 = &- i\hbar \psi_{\mathrm{x}}^* \partial_t \psi_{\mathrm{x}} + n_{\mathrm{x}} \mu_{\mathrm{x}} \\ &+ \frac{\hbar^2}{2D^2} \left\{ - \frac{A_{\mathrm{x}}}{n_{\mathrm{x}}} n_{\mathrm{x}}^2 \psi_{\mathrm{x}}^* \nabla^2 \psi_{\mathrm{x}} - \frac{B_{\mathrm{x}}}{n_{\mathrm{y}}} n_{\mathrm{y}}^2 \psi_{\mathrm{y}}^* \nabla^2 \psi_{\mathrm{y}} - \frac{C_{\mathrm{x}}}{n_{\mathrm{x}} n_{\mathrm{y}}} n_{\mathrm{x}} n_{\mathrm{y}} \left(\psi_{\mathrm{x}}^* \nabla_i \psi_{\mathrm{x}} \right) \left(\psi_{\mathrm{y}}^* \nabla^i \psi_{\mathrm{y}} \right) \right\}. \end{aligned} \tag{3.79}$$

We can now factor out ψ_{x}^* and simplify to give

$$\begin{aligned} 0 = &- i\hbar \partial_t \psi_{\mathrm{x}} + \mu_{\mathrm{x}} \psi_{\mathrm{x}} \\ &+ \frac{\hbar^2}{2D^2} \left\{ - A_{\mathrm{x}} n_{\mathrm{x}} \nabla^2 \psi_{\mathrm{x}} - B_{\mathrm{x}} \frac{n_{\mathrm{y}}}{n_{\mathrm{x}}} \psi_{\mathrm{x}} \left(\psi_{\mathrm{y}}^* \nabla^2 \psi_{\mathrm{y}} \right) - C_{\mathrm{x}} \nabla_i \psi_{\mathrm{x}} \left(\psi_{\mathrm{y}}^* \nabla^i \psi_{\mathrm{y}} \right) \right\}. \end{aligned} \tag{3.80}$$

Similarly for the second component we have

$$\begin{aligned} 0 = &- i\hbar\partial_t\psi_{\mathrm{y}} + \mu_{\mathrm{y}}\psi_{\mathrm{y}} \\ &+ \frac{\hbar^2}{2D^2}\Bigg\{ - A_{\mathrm{y}} n_{\mathrm{y}} \nabla^2\psi_{\mathrm{y}} - B_{\mathrm{y}} \frac{n_{\mathrm{x}}}{n_{\mathrm{y}}}\psi_{\mathrm{y}} \left(\psi_{\mathrm{x}}^* \nabla^2 \psi_{\mathrm{x}}\right) - C_{\mathrm{y}} \nabla_i \psi_{\mathrm{y}} \left(\psi_{\mathrm{x}}^* \nabla^i \psi_{\mathrm{x}}\right) \Bigg\}, \end{aligned} \tag{3.81}$$

where

$$\begin{aligned} A_{\mathrm{y}} &= m_{\mathrm{y}} m_{\mathrm{x}}^2 n_{\mathrm{y}} n_x^2 - 4\alpha m_{\mathrm{y}} m_{\mathrm{x}} n_{\mathrm{y}} n_{\mathrm{x}} + 4\alpha^2 m_{\mathrm{y}} n_{\mathrm{y}} - 4\alpha m_{\mathrm{x}}^2 n_{\mathrm{x}}^2 + 8\alpha^2 m_{\mathrm{x}} n_{\mathrm{x}}, \\ B_{\mathrm{y}} &= -4\alpha^2 m_{\mathrm{y}} n_{\mathrm{y}}, \\ C_{\mathrm{y}} &= 8\alpha^2 m_{\mathrm{x}} n_{\mathrm{x}}. \end{aligned} \tag{3.82}$$

At this point it is profitable to reproduce the non linear Schrödinger equations for a two component BEC [6]:

$$0 = -i\hbar\partial_t\psi_{\mathrm{x}} + \left(-\frac{\hbar^2}{2m_{\mathrm{x}}}\nabla^2 + \frac{4\pi\hbar^2 a_{\mathrm{xx}}}{m_x} |\psi_x|^2 + \frac{2\pi\hbar^2 a_{\mathrm{xy}}}{m_{\mathrm{xy}}} |\psi_{\mathrm{y}}|^2 - \mu_{\mathrm{x}} \right) \psi_x, \tag{3.83}$$

and

$$0 = -i\hbar\partial_t\psi_{\mathrm{y}} + \left(-\frac{\hbar^2}{2m_{\mathrm{y}}}\nabla^2 + \frac{4\pi\hbar^2 a_{\mathrm{yy}}}{m_y} |\psi_y|^2 + \frac{2\pi\hbar^2 a_{\mathrm{xy}}}{m_{\mathrm{xy}}} |\psi_{\mathrm{x}}|^2 - \mu_{\mathrm{y}} \right) \psi_y. \tag{3.84}$$

To show the proposed effect of entrainment that we would like to realise in a composite BEC, we can compare equations (3.80) and (3.83). An obvious disparity is the omission of the terms that relate to the scattering length. This is a potential term that in a uniform condensate, as we have assumed, is equal to the product of the chemical potential and the particle density [84]. As such, we can treat this as being included in any chemical potential term in our solution.

We also have the terms including B_{x} and C_{x}. These terms each include $\psi_{\mathrm{y}}^* \nabla^i \psi_{\mathrm{y}}$ and indicate some additional interaction (the entrainment) between the two components.

Finally, we have the term

$$-\frac{\hbar^2}{2D^2} A_{\mathrm{x}} n_{\mathrm{x}} \nabla^2 \psi_{\mathrm{x}} \left(\neq -\frac{\hbar^2}{2m_{\mathrm{x}}}\nabla^2\psi_{\mathrm{x}} \right). \tag{3.85}$$

To extract the part of this term that has been introduced as a result of the entrainment effect, we introduce a new term, $A_{\mathrm{x}}^{\mathrm{Diff}}$, which we define as

$$A_{\mathrm{x}}^{\mathrm{Diff}} = \frac{1}{2D^2} A_{\mathrm{x}} n_{\mathrm{x}} - \frac{1}{2m_{\mathrm{x}}}. \tag{3.86}$$

This leads to

$$A_{\mathrm{x}}^{\mathrm{Diff}} = -\frac{1}{2D^2} \frac{4\alpha^2 m_{\mathrm{y}}^2 n_{\mathrm{y}}^2}{m_{\mathrm{x}}}. \tag{3.87}$$

This gives us a final equation that includes the original non-linear Schrödinger equation with additional terms indicating the effects of entrainment.

$$\begin{aligned} 0 = &- i\hbar\partial_t \psi_{\mathrm{x}} - \left(\frac{\hbar^2}{2m_{\mathrm{x}}} \nabla^2 + \mu_{\mathrm{x}} \right) \psi_{\mathrm{x}} \\ &+ \frac{\hbar^2}{2D^2} \left\{ \frac{4\alpha^2 m_{\mathrm{y}}^2 n_{\mathrm{y}}^2}{m_{\mathrm{x}}} \nabla^2 + 4 \frac{n_{\mathrm{y}}}{n_{\mathrm{x}}} \alpha^2 m_{\mathrm{y}} n_{\mathrm{y}} \left(\psi_{\mathrm{y}}^* \nabla^2 \psi_{\mathrm{y}} \right) - 8\alpha^2 m_{\mathrm{x}} n_{\mathrm{x}} \left(\psi_{\mathrm{y}}^* \nabla^2 \psi_{\mathrm{y}} \right) \right\} \psi_{\mathrm{x}}. \end{aligned} \tag{3.88}$$

This simplifies slightly to

$$\begin{aligned} 0 = &- i\hbar\partial_t \psi_{\mathrm{x}} - \left(\frac{\hbar^2}{2m_{\mathrm{x}}} \nabla^2 + \mu_{\mathrm{x}} \right) \psi_{\mathrm{x}} \\ &+ \frac{\hbar^2}{2D^2} \left\{ \frac{4\alpha^2 m_{\mathrm{y}}^2 n_{\mathrm{y}}^2}{m_{\mathrm{x}}} \nabla^2 + 4\alpha^2 \left(\frac{n_{\mathrm{y}}^2 m_{\mathrm{y}}}{n_{\mathrm{x}}} - 2m_{\mathrm{x}} n_{\mathrm{x}} \right) \left(\psi_{\mathrm{y}}^* \nabla^2 \psi_{\mathrm{y}} \right) \right\} \psi_{\mathrm{x}}. \end{aligned} \tag{3.89}$$

It can be seen that we have cross terms in equation (3.89) indicating some additional coupling between the two condensates. This is what we would intuitively expect if we add entrainment that couples our two components in the fluid model.

Having arrived at the governing non-linear Schrödinger equations for a two component BEC with entrainment, the next step is to calculate the Hamiltonian for this system. This, in turn, would lead to a physical realisation. However, the next step is not so obvious. The inclusion of the $\left(\psi_{\mathrm{y}}^* \nabla^2 \psi_{\mathrm{y}} \right) \psi_{\mathrm{x}}$ term in equation (3.89) tells us that the fine tuning of any interspecies interaction needs to be position sensitive. Experimental configurations of this nature are currently being considered but this is new physics [166].

The multi-fluid equations are derived directly from a Lagrangian using the variational principle [167]. Here the problem is similar, in that we are endeavouring to find a Hamiltonian (and the experimental set up) that will produce the governing equations for a two-component BEC. This problem is far from trivial and is not persued further at this time.

It is interesting to note that recently a small number of cold atom physicists have begun research on modelling entrainment in BEC's [114]. Others have been considering the effects of significant quantities of the normal diffuse gas (from which condensates were formed) on the dynamics of BEC's [168]. This includes the consideration of entrainment effects between the superfluid and the BEC. Whilst these experiments are starting from the "other end" of the problem, in that they are working directly with BEC's; they may offer insights into our own research.

The next step would seem to be to include entrainment in the two stream instability and compare the results with the BEC case. Unfortunately, since we did not proceed any further with the BEC case, it was decided to pursue other areas of research.

Chapter 4

Instabilities in a Differentially Rotating Neutron Star Core

Having established the phenomenon of the two-stream instability in a simple linear model and shown that this is analogous to the behaviour of binary Bose-Einstein condensates, we now apply it the more mathematically complex environment of rotating a two component fluid. In this configuration we are able to model some of the key features of the neutron star outer core and explore instabilities, as discussed in our introduction, that may act as a trigger for vortex unpinning. Such action is considered a promising mechanism for the glitches in neutron star spin down rates.

4.1 Neutron Star Glitches as a Result of Vortex Pinning/Unpinning

Before proceeding to the analysis of our model, it is relevant to touch upon glitches in neutron star spin down in a little more detail than in the introduction to this thesis; the mechanisms with which physicists endeavour to explain them and their importance to gravitational physics.

Radio pulsars were first discovered in 1968 [20] and were quickly identified as rotating, strongly magnetic neutron stars [21]. It was also observed that the rotational period of these bodies increased slowly and monotonically with time [91]. This was believed to be as a result of magnetic breaking. However, in early 1969 it was noticed that the Vela pulsar showed a significant and sudden increase in its rotational frequency [29]. Since this first observation, these sudden increases, given the cognomen glitch, have been observed to occur regularly in the Vela and Crab pulsars, as well as less frequently in

other pulsars [31, 30]. Owing to the large number of observations, it is against the data obtained from the two named stars that any physical theory to explain the mechanism (or mechanisms) underlying these glitches will most likely be measured [34].

In fact there have been several competing, or possibly complimentary, mechanisms suggested for these glitches. Today the two most widely accepted candidates to explain the observed glitch phenomena are the 'star-quake' model and that of 'vortex unpinning'. There exists the possibility that both may be correct, either as mechanisms that can both happen at any time or that the prevalent cause depends on the age and spin rate of the star [37].

The first of these mechanisms, the star-quake model [32, 37], postulates that in a newly formed, rapidly rotating neutron star a small equatorial oblateness in the crust may develop. As the star slows under magnetic breaking and the centrifugal pressure from the core is reduced, the crust can no longer support this. The core may then crack under gravity and reform into a more spherical configuration. As the star resumes its spin down, this process may recur until there is no energetic advantage to any further repetition. This suggests that the star-quake model is most prevalent in younger neutron stars [38].

The second model involves the unpinning of the vortices in the core from the inner crust and their subsequent re-pinning. The transfer of angular momentum from the core to the crust during this process results in a rapid, but short lived acceleration in the spin speed of the crust [44, 34, 36]. To explain this mechanism is more than lambent detail, it is necessary to give a somewhat more detailed description of the structure of a neutron star than that provided in the introduction to this thesis.

The description of the outer core as coexisting superfluid neutrons and superconducting protons, where the neutrons form large numbers of vortices parallel to the axis of rotation of the star is sufficiently detailed for our purpose. An explanation of vortex formation in highly rotational superfluids is given in many standard text books, for example, Landau & Lifshitz [169].

It is regarding the structure of the crust that our description requires elucidation. As previously stated, the outer crust consists of a crystalline structure of heavy, neutron rich nuclei. As we move inward toward the centre, the pressure increases. Once the pressure exceeds the 'neutron drip pressure' (approximately $4.3 \times 10^{14}\mathrm{kgm}^{-3}$), it becomes energetically favourable for the neutrons to 'drip' out of the nuclei [93]. It is the zone where the density reaches this level that we define as the transition from the outer to

inner crust. As we continue inwards, the density continues to increase until we reach a density at which the nuclei dissolve (approximately $2 \times 10^{17}\text{kgm}^{-3}$). This marks the end of the inner crust and the start of the outer core.

Throughout much of the inner crust, the neutrons pair, as in the core, to produce a superfluid. This superfluid is, in some manner, coupled to the vortices in the outer core and enables them to effectively extend into the inner crust. These vortices then interact with the nuclei in the crust. Depending on the local density, such interaction may be either attractive or repulsive [93]. Regardless of the sense of the interaction, the vortex line 'strives' to follow a path that minimises its energy. This essentially pins the vortex to the crust.

The vast majority of the angular momentum possessed by the superfluid is a consequence of the vortices. If we assume that all vortices are pinned to the crust, then the neutron superfluid has its angular momentum, to all intents, fixed. As the surface of the star undergoes magnetic braking, the vortices act as a 'momentum reservoir', since this braking cannot impact upon the pinned vortices, and the neutron fluid maintains its angular momentum. This leads to a growing velocity difference between the superfluid in the core and the crustal lattice.

We note at this juncture that the superconducting particles in the core are also slowed by the magnetic damping. The resulting difference in velocity between the two components of the core suggests that we can apply some variant of the two-stream model to the core in the search for a related class of instabilities in the interpenetrating fluids.

Returning to the pinned vortices in the crust, not only can the magnetic breaking have only a minor effect upon them, but they are, in this state, unable to transfer momentum to the crust. As such, both the momentum reservoir and the difference between charged and uncharged particles in the core increase in size. To allow the vortices to be displaced and, as a consequence, transfer angular momentum to the crust, we require some mechanism that is able temporarily to break their pinning. It is here that the differential velocities mentioned in the preceding paragraph offer the beginnings of a credible explanation and forms the basis of this chapter. We demonstrate, in a somewhat simplified case, that the two-stream instability can apply to the differentially rotating fluids in the neutron star core. We show that this instability depends upon the difference in rotational velocity between the two components. We suggest that such instabilities may account for the unpinning and the associated transfer of angular momentum from the core to the crust. This transfer of momentum evinces itself to the observer as the glitch

in spin down.

Taking this explanation one step further, it can be seen that once any disturbances to the normal state of affairs have been smoothed out, the vortices will seek the lowest energy state and become pinned again. Once this occurs the differences in angular momentum between crust and superfluid, as well as the differences in angular velocity between charged and uncharged particles within the core, will start to increase again. This suggests that the unpinning will occur at fairly regular intervals and may account for the behaviour of such stars as the Vela pulsar, which has been observed to glitch many times [34].

4.2 Superfluid Instability as a Trigger for Neutron Star Glitches - The Strongly Coupled Case

As previously discussed, one of the more prominent theories to explain the glitches in neutron star spin down is that of vortex unpinning. Whilst the physics underlying the transfer of angular momentum from the core to the crust has been well documented, as yet very little has been published regarding possible triggers for such an event.

Here we consider the basic mechanism of such a possible trigger as discussed by Andersson and Glampedakis [7], namely a superfluid instability in a system of two interpenetrating components with differing angular velocities. They argue that unstable r-modes may be generated by the differential rotation of the two fluid components and demonstrate that such modes exist in a strongly coupled system. They further show that viscosity does not fully suppress these instabilities. We include the main points of the paper here as it is a logical precursor to the work that follows.

To set up the problem, a standard two-fluid model for superfluid neutron stars is used [170]. In this case it is assumed that the two components are the neutron superfluid, indexed n, and a conglomerate of all off the charged particles, indexed p. It is assumed that both fluids rotate rigidly with differing angular velocities. These velocities are given by

$$v_{\mathrm{x}}^{i} = \epsilon^{ijk}\Omega_{j}^{\mathrm{x}}x_{k}. \tag{4.1}$$

Here Ω_{x}^{i} is the angular velocity of the indexed fluid, where, as a consequence of the differential velocity,

$$|\Omega_{\rm n}| \neq |\Omega_{\rm p}|. \tag{4.2}$$

It is assumed that the background is perturbed by small linear oscillations with time dependency of the form $\exp(i\omega t)$, where ω is simply the perturbation frequency. The linear perturbations of the system are, in the inertial frame, described by the pair of coupled Euler equations,

$$\left(i\omega + v^j_{\rm n}\nabla_j\right)\delta v^i_{\rm n} + \delta v^j_{\rm n}\nabla_j v^i_{\rm n} + \nabla^i\delta\psi_{\rm n} = \delta f^i_{\rm mf} \tag{4.3}$$

and

$$\left(i\omega + v^j_{\rm p}\nabla_j\right)\delta v^i_{\rm p} + \delta v^j_{\rm p}\nabla_j v^i_{\rm p} + \nabla^i\delta\psi_{\rm p} = -\frac{\delta f^i_{\rm mf}}{x_{\rm p}}. \tag{4.4}$$

In the above equations

$$\delta\psi_{\rm x} = \delta\tilde{\mu}_{\rm x} + \delta\Phi, \tag{4.5}$$

where $\tilde{\mu}_{\rm x}$ and Φ represent the specific chemical potential and the gravitational potential respectively. The term $x_{\rm p}$ represents the proton fraction by

$$x_{\rm p} = \frac{\rho_{\rm p}}{\rho_{\rm n}}. \tag{4.6}$$

We note that $\rho_{\rm p} \ll \rho_{\rm n}$.

To simplify the problem at this early stage, a few basic assumptions are made. Firstly it is assumed that both fluids are incompressible, so

$$\nabla_i\delta v^i_{\rm x} = 0. \tag{4.7}$$

Secondly the effects of entrainment are ignored. This means that the two components are coupled chemically, gravitationally and by the vortex mediated mutual friction, which is denoted in equations (4.3) and (4.4) by $f^i_{\rm mf}$. When considering inertial modes, this mutual friction force is the major mechanism for coupling the two components. The general expression for such a force is given by [171],

$$f^{\rm mf}_i = \mathcal{B}\epsilon_{ijk}\epsilon^{kml}\hat{\omega}^j_{\rm n}\omega^{\rm n}_m w^{\rm np}_l + \mathcal{B}'\epsilon_{ijk}\omega^j_{\rm n}w^k_{\rm np}. \tag{4.8}$$

In equation (4.8) $w^i_{\rm np} = v^i_{\rm n} - v^i_{\rm p}$, $\omega^i_n = \epsilon^{ijk}\nabla_j v^n_k$ and $\hat{\omega}^j_{\rm n}$ is the unit vector. It is shown that if the interaction between the vortices and the charged fluid, henceforth referred to as the drag force, is represented by some dimensionless parameter $\mathcal{R}$, then,

$$\mathcal{B}' = \mathcal{R}\mathcal{B} = \mathcal{R}^2/\left(1+\mathcal{R}^2\right). \tag{4.9}$$

Referring back to some older papers on the subject of r-modes in superfluid neutron stars [172][173][174], we are told that, when expressed in terms of spherical harmonics, the r-mode velocity fields can be expressed in the form

$$\delta v^i_{\rm x} = \left(-\frac{imU^{\rm x}_l Y^m_l}{r^2 sin^2\theta}\hat{e}^i_\theta + \frac{U^{\rm x}_l \partial_\theta Y^m_l}{r^2 sin^2\theta}\hat{e}^i_\varphi\right) e^{i\omega t}. \tag{4.10}$$

We discuss the meaning of this equation in more detail later, but essentially this is reducing the problem to a one dimensional problem with angular dependencies expressed in terms of the spherical harmonics, $Y^m_l(\theta,\varphi)$. Because of the symmetry of the problem, the m-contributions decouple and can be considered separately. $U^{\rm x}_l$ represent the perturbed velocity of each component associated with the different l multipoles.

Obtaining solutions for all values of $\mathcal{R}$ may prove difficult. But we are given a solution where the problem simplifies in the strong coupling limit, that is where $\mathcal{R} \gg 1$, which gives $\mathcal{B} = 0$ and $\mathcal{B}' = 1$. The solution is expressed in terms of dimensionless parameters κ, where

$$\kappa = \frac{\omega + m\Omega_{\rm p}}{\Omega_{\rm p}}, \tag{4.11}$$

and Δ, where

$$\Delta = \frac{\Omega_{\rm n} - \Omega_{\rm p}}{\Omega_{\rm p}}. \tag{4.12}$$

There are two frequency solutions obtained for κ,

$$\kappa_{1,2} = -\frac{1}{(m+1)\,x_{\rm p}}\left[1 - x_{\rm p} + \Delta \pm \mathcal{D}^{1/2}\right], \tag{4.13}$$

where

$$\mathcal{D} = (1+x_{\rm p})^2 + 2\Delta\left[1 + x_{\rm p}\{3 - m\,(m+1)\}\right] + \mathcal{O}\left(\Delta^2\right). \tag{4.14}$$

The amplitudes of the perturbations of the two components are related by

$$\frac{A_{\mathrm{n}}}{A_{\mathrm{p}}} = \frac{2\left(1+\Delta\right)}{\left(m+1\right)\kappa}, \tag{4.15}$$

where

$$U_m^{\mathrm{x}} = A_{\mathrm{x}} r^{m+1}. \tag{4.16}$$

Focusing on the short length scale modes, $m \gg 1$, it is shown that there is some critical mode, m_{c}, for which $\mathrm{Im}\left(\kappa\right)$ changes from positive to negative, indicating instability. By assuming both Δ and x_{p} are small with, in general, $\Delta \ll x_{\mathrm{p}}$, an approximate value for m_{c} is given by

$$m_{\mathrm{c}} \approx \frac{1}{\sqrt{2x_{\mathrm{p}}\Delta}}. \tag{4.17}$$

The growth scale of unstable modes are approximated, where $m \gg m_{\mathrm{c}}$, as

$$\tau_{\mathrm{grow}} \approx \frac{P}{2\pi}\sqrt{\frac{x_{\mathrm{p}}}{2\Delta}}, \tag{4.18}$$

where P is the observed spin frequency. This tells us that the instability can grow rapidly on the timescale of the rotation period of the neutron star.

The next consideration is that of viscous damping, which, depending on relative time scales, may suppress the instability. Using the canonical values for a typical neutron star and applying the method from [175] the shear viscosity is calculated, since it is this force that dominates the dissipation. For the instabilities to withstand being suppressed by this damping, their growth timescale needs to be less than that of the shear viscosity. This produces a range of m modes that remain unstable in the presence of viscous damping and a critical lag between the two components above which the system becomes unstable.

As a reality check, the model's predictions are compared with observational glitch data. It is noted that the observational estimate for the rotational difference for large glitches is close to that predicted by the model for the onset of the superfluid r-mode instability. A note of caution is sounded when it is stated that, even though these instabilities grow on a timescale of a few rotations, it is uncertain as to their characteristics beyond linear amplitudes.

The model is then compared with other observed traits of neutron star glitches and is found to be consistent with several of these idiosyncrasies. These include the prediction of small but frequent glitches in young, hot, rapidly spinning stars; with the magnitude of, and time between, glitches increasing with age. Since the rotational velocity decreases with age, the build up of lag between the two components takes an increasingly long time. This implies that, as the star ages, it will eventually cease to glitch.

Finally, it is also noted that since no magnetic field has been included in the model, except as an initial mechanism to account for the differential rotation, then it is really impossible to confidently apply the model to magnetars. Whether it can reasonably be extended to allow for the strong magnetic fields associated with these bodies is left as an open question.

4.3 Beyond the High Drag Limit - A More General Case

We consider a more general case of the r-mode instability, where we extend the analysis beyond the high drag limit, although we still restrict ourselves to the Newtonian case. Some of the work presented in this section will duplicate the structure of the previous fragment but will be discussed with greater prolixity. As previously our aim is to explore r-mode instabilities in the core of a neutron star by considering linear perturbations of a two component fluid that exhibits rotational instability. Because of this set-up, it is natural to work in the inertial frame (rather than choosing one of the rotating frames). It is also natural, given the complex nature of the perturbed velocity fields et cetera to carry out the analysis in a coordinate basis. This means that vectors, like the velocity, are expressed in terms of their components, v^i (say), and a distinction is made between co- and contra-variant objects, with the former following from the latter as $v_i = g_{ij}v^j$ where g_{ij} is the flat three-dimensional metric. This description of the problem is also advantageous since it involves the use of the co-variant derivative ∇_i associated with the given metric, which automatically encodes the scale factors associated with the curvilinear coordinates that are appropriate for the problem we consider.

As previously, we consider a fluid consisting of two interpenetrating components, which we index n and p to represent the neutron superfluid and the conglomerate of charged particles respectively. The previously stated case for Cooper pairing of the neutrons and the subsequent superfluid behaviour is taken as read. We assume that these components are each rotating rigidly such that,

$$v^i_{\rm x} = \Omega_{\rm x}\hat{e}^i_\varphi \qquad , \qquad {\rm x} = {\rm n}, {\rm p}. \tag{4.19}$$

We further assume that the two components are free to rotate independently so introducing the differential rotation between them. It is assumed that the axes of the independent rotations are the same, as this simplifies the analysis considerably without, we feel, losing any of the key features of the model. We also continue to take no account of the complexities introduced by the star's magnetic field, with the exception of it acting to slow some components of the star more than others, leading to the differential rotation. In this case, if we assume the observed angular rotation frequency of the star to be Ω^i, then it is further assumed that the charged components in the core have undergone identical slowing and so

$$\Omega^i_{\rm p} = \Omega^i. \tag{4.20}$$

However, the uncharged neutron superfluid component has been less affected by the magnetic braking and so retains a higher angular rotation frequency. We express this by

$$\Omega^i_{\rm n} = (1 + \Delta)\Omega^i, \tag{4.21}$$

where Δ represents the fractional difference in spin down between the two components. We would expect Δ to be small even at the time of glitch, a figure of the order of 10^{-4} being the generally accepted value [165].

We reassert the statement from Glampedakis and Andersson [7] regarding the bulk rotation of the neutron superfluid being accounted for by the formation of quantised vortices. It is established [176] that the quantisation condition is imposed on the momentum, $p^{\rm n}_i$, that is conjugate to the velocity, $v^i_{\rm n}$, and this is given by

$$p^{\rm n}_i = m\left(v^{\rm n}_i + \varepsilon_{\rm n} w^{\rm pn}_i\right). \tag{4.22}$$

Here, m is the mass of the nucleon[1], $\varepsilon_{\rm n}$ is the entrainment with the protons and $w^{\rm pn}_i$ is the relative velocity between the two components. This is given by

$$w^i_{\rm pn} = v^i_{\rm p} - v^i_{\rm n}. \tag{4.23}$$

[1] We assume that the mass of neutrons and protons are identical. This is sufficiently accurate for our purposes.

We now introduce another assumption that has the effect of simplifying the problem. We assume the fluid components are each incompressible and this allows us, at least in the case of small Δ, to treat the entrainment coefficients as constants. Taking the quantisation conditions and combining with the above we arrive at a local vortex density per unit area expressed by

$$\begin{aligned} n_v \kappa^i &= \epsilon^{ijk} \nabla_j \left[v^{\mathrm{n}}_k + \varepsilon_{\mathrm{n}} w^{\mathrm{pn}}_k \right] \\ &= 2 \left[\Omega^i_{\mathrm{n}} + \varepsilon_{\mathrm{n}} \left(\Omega^i_{\mathrm{p}} - \Omega^i_{\mathrm{n}} \right) \right] \\ &= 2 \left[1 + (1 - \varepsilon_{\mathrm{n}}) \, \Delta \right] \Omega^i. \end{aligned} \tag{4.24}$$

Here n_v is the vortex density and κ^i is the vector aligned with the vortex array with magnitude $\kappa = h/2m_{\mathrm{p}}$ (h is Planck's constant).

Making use of our assumption of incompressibility, we consider linear perturbations of the configuration we have described. As a consequence of this assumption we have

$$\nabla_i \delta v^i_{\mathrm{x}} = 0. \tag{4.25}$$

Also the perturbed momenta satisfy

$$\delta p^{\mathrm{x}}_i = \delta v^{\mathrm{x}}_i + \varepsilon_{\mathrm{x}} \delta w^{\mathrm{yx}}_i, \tag{4.26}$$

and are governed by the Euler equations;

$$\mathcal{E}^{\mathrm{x}}_i = i\omega \delta p^{\mathrm{x}}_i + \delta v^j_{\mathrm{x}} \nabla_j p^{\mathrm{x}}_i + v^j_{\mathrm{x}} \nabla_j \delta p^{\mathrm{x}}_i + \varepsilon_{\mathrm{x}} (\delta w^{\mathrm{yx}}_j \nabla_i v^j_{\mathrm{x}} + w^{\mathrm{yx}}_j \nabla_i \delta v^j_{\mathrm{x}}) + \nabla_i \delta \Psi_{\mathrm{x}} = \delta f^{\mathrm{x}}_i. \tag{4.27}$$

As earlier Ψ_{x} is the sum of the gravitational potential Φ and the specific chemical potential $\tilde{\mu}_{\mathrm{x}} = \mu_{\mathrm{x}}/m$. Also in common with Glampedakis and Andersson we assume the time dependence of the perturbation equations is harmonic in nature $\sim \exp(i\omega t)$. The right hand side (after the second "equals" sign) of (4.27) describes any external forces acting on the fluid components.

At this point we introduce a new variable, $\mathcal{W}^i_{\mathrm{x}}$, for the perturbed "vorticity", defined by

$$\mathcal{W}^i_{\mathrm{x}} = \epsilon^{ijk} \nabla_j \mathcal{E}^{\mathrm{x}}_k. \tag{4.28}$$

Although, we have stated that f_i^{x} from (4.27) represents external forces, this also includes any forces that result from interactions between the components. As such, f_i^{x} is dominated by the mutual friction force arising from the quantised vortices [44][177]. This force is expressed as in (4.8) , although here we include n_v and κ^{x}, by

$$f_i^{\mathrm{x}} = \frac{\rho_{\mathrm{n}}}{\rho_{\mathrm{x}}}\mathcal{B}' n_v \epsilon_{ijk}\kappa^j w^k_{\mathrm{xy}} + \frac{\rho_{\mathrm{n}}}{\rho_{\mathrm{x}}}\mathcal{B} n_v \epsilon_{ijk}\hat{\kappa}^j \epsilon^{klm}\kappa_l w^{\mathrm{xy}}_m. \tag{4.29}$$

As previously we shall relate the coefficients $\mathcal{B}$ and $\mathcal{B}'$ to the dimensionless coefficient $\mathcal{R}$, which represents the drag force. A detailed explanation of these coefficients and how they are obtained appears in Hall and Vinen [171]. In equation (4.29) we introduce a term for mass density, $\rho_{\mathrm{x}} = mn_{\mathrm{x}}$, of the respective fluid components. Perturbing the force equation (4.29), we obtain

$$\begin{aligned}\delta f_i^{\mathrm{x}} = {} & \frac{\rho_{\mathrm{n}}}{\rho_{\mathrm{x}}}\mathcal{B}'\left[\delta(n_v\kappa^j)\epsilon_{ijk}w^k_{\mathrm{xy}} + n_v\kappa^j\epsilon_{ijk}\delta w^k_{\mathrm{xy}}\right] \\ & + \frac{\rho_{\mathrm{n}}}{\rho_{\mathrm{x}}}\mathcal{B}\epsilon_{ijk}\epsilon^{klm}\left[\delta(n_v\kappa_l)\hat{\kappa}^j w^{\mathrm{xy}}_m + n_v\kappa_l(w^{\mathrm{xy}}_m\delta\hat{\kappa}^j + \hat{\kappa}^j\delta w^{\mathrm{xy}}_m)\right].\end{aligned} \tag{4.30}$$

To evaluate this we need

$$\delta(n_v\kappa^i) = \epsilon^{ijk}\nabla_j\delta p^{\mathrm{n}}_k \tag{4.31}$$

and

$$\delta\hat{\kappa}^i = \frac{1}{n_v\kappa}\left(\delta^i_j - \hat{\kappa}^i\hat{\kappa}_j\right)\epsilon^{jlm}\nabla_l\delta p^{\mathrm{n}}_m, \tag{4.32}$$

where $\hat{\kappa}^i$ is a unit vector aligned with κ^i, together with the norm of (4.24),

$$n_v\kappa^i = 2[1 + (1-\varepsilon_{\mathrm{n}})\Delta]\Omega^i. \tag{4.33}$$

We wish now to isolate the two dynamical degrees of freedom. To this end, rather than use the momentum equations (4.27) per se, we use two combinations of the perturbed equations for each fluid; namely the sum and the difference of the two momentum equations. So we need the following:

$$\rho_{\mathrm{n}}\delta f_i^{\mathrm{n}} + \rho_{\mathrm{p}}\delta f_i^{\mathrm{p}} = 0 \tag{4.34}$$

and

$$\delta f_i^{\rm p} - \delta f_i^{\rm n} = -\frac{1}{x_{\rm p}}\delta f_i^{\rm n}. \tag{4.35}$$

As a consequence, only the second degree of freedom is explicitly affected by the mutual friction.

Rather than consider the full range of oscillatory modes associated with a neutron star, we restrict our analysis to the possibility of how the rotational lag might impact upon the r-modes of a star. In connection with the model we have adopted, particularly with respect to the assumed solid rotation of the component fluids, we would not really expect radial instabilities to occur. However, it is expected that any instabilities of the system would have major repercussions for any axial modes. This suggests that the purely axial r-modes would make an excellent candidate for our deliberations. It is also known that r-modes have a strong instability with respect to gravitational waves [172] [67] and that they are associated with simple velocity fields [94]. This leads us to perturbed velocities of the form

$$\delta v_{\rm x}^i = -\frac{im}{r^2\sin\theta}U_{\rm x}^l Y_l^m \hat{e}_\theta^i + \frac{1}{r^2\sin\theta}U_{\rm x}^l \partial_\theta Y_l^m \hat{e}_\varphi^i. \tag{4.36}$$

As discussed in the previous section, $Y_l^m(\theta,\varphi)$ are the standard spherical harmonics and $U_{\rm x}^l$ are the mode amplitudes. As a result of the symmetry, the problem is such that the m-multipoles decouple.

Also previously we stated that we would work with the sum and difference momentum equations, (4.34) and (4.35). As such we need to consider variables that are most easily accommodated in this and the choice of operating with the total momentum flux seems particularly favourable. This is given by

$$\rho U^l = \rho_{\rm n} U_{\rm n}^l + \rho_{\rm p} U_{\rm p}^l. \tag{4.37}$$

We also introduce a difference term, this time for the perturbed velocities only,

$$u^l = U_{\rm p}^l - U_{\rm n}^l. \tag{4.38}$$

In the calculations that follow we make use of several new simplifying variables in order to stop the equations becoming unmanageable. For convenience, we define all of these

variables here, rather than introduce them piecemeal during the analysis. We can achieve some simplification of the final perturbation equations if we express the frequency in a rotating frame. To this end we define $\tilde{\kappa}$ such that

$$\omega + m\Omega = \tilde{\kappa}\Omega, \tag{4.39}$$

We also introduce

$$L = l(l+1), \tag{4.40}$$

$$Z = 1 - x_{\rm p} - \varepsilon_{\rm p}, \tag{4.41}$$

and

$$\bar{Z} = \frac{x_{\rm p} Z}{1 - x_{\rm p}}. \tag{4.42}$$

Finally, we use the scaled mutual friction coefficients [178], again to reduce the number of terms in the equations that follow;

$$\bar{\mathcal{B}}' = \mathcal{B}'/x_{\rm p} \tag{4.43}$$

and

$$\bar{\mathcal{B}} = \mathcal{B}/x_{\rm p}. \tag{4.44}$$

Throughout the calculations that follow extensive use was made of MAPLE and GRtensorII.

We now obtain the perturbation equations by combining the expected velocity field, $\mathcal{W}^r_{\rm x}$ with the sum (4.37) and difference (4.38) equations above. Firstly, we consider the sum, where $\rho_{\rm n}\mathcal{W}^r_{\rm n} + \rho_{\rm p}\mathcal{W}^r_{\rm p}$ yields

$$[L\kappa - 2m]\, U^l Y^m_l = -m\Delta(L-2)[U^l - \bar{Z}u^l]Y^m_l. \tag{4.45}$$

The difference equation, $\mathcal{W}^r_{\rm p} - \mathcal{W}^r_{\rm n}$, gives us

$$
\begin{aligned}
&\left[\frac{L\kappa\bar{Z}}{x_{\rm p}} - 2m(1-\bar{\mathcal{B}}') - 2i\bar{\mathcal{B}}(L-m^2)\right] u^l Y_l^m \\
&= -m\Delta\left\{\frac{[(L-4)x_{\rm p}+2]\bar{Z}}{x_{\rm p}} - 2(1-x_{\rm p})\right\} u^l Y_l^m + m\Delta\left(L - \frac{2\bar{Z}}{x_{\rm p}}\right) U^l Y_l^m \\
&+ m\Delta L\bar{\mathcal{B}}'(\bar{Z}u^l - U^l)Y_l^m - 2m\bar{\mathcal{B}}'\Delta(\bar{Z}+1-x_{\rm p})u^l Y_l^m \\
&+ i\bar{\mathcal{B}}\Delta L[\bar{Z}(r\partial_r u^l - u^l) - r\partial_r U^l + U^l]Y_l^m + 2i\bar{\mathcal{B}}\Delta(L-m^2)(\bar{Z}+1-x_{\rm p})u^l Y_l^m \\
&+ i\bar{\mathcal{B}}L\Delta[r\partial_r U^l - 3U^l - \bar{Z}(r\partial_r u^l - 3u^l)]\cos^2\theta Y_l^m \\
&+ i\bar{\mathcal{B}}\Delta[2r\partial_r U^l - LU^l - \bar{Z}(2r\partial_r u^l - Lu^l)]\cos\theta\sin\theta\partial_\theta Y_l^m. \qquad (4.46)
\end{aligned}
$$

We also make use of the same sum and difference equations in the case of the radial Euler equations. The sum, $\rho_{\rm n}\mathcal{E}^r_{\rm n} + \rho_{\rm p}\mathcal{E}^r_{\rm p}$, giving us

$$
\begin{aligned}
&[x_{\rm p}r\partial_r\delta\Psi^l_{\rm p} + (1-x_{\rm p})r\partial_r\delta\Psi^l_{\rm n}]Y_l^m - 2\Omega U^l\sin\theta\partial_\theta Y_l^m \\
&= -\Delta\Omega(1-x_{\rm p})[(x_{\rm p}-\bar{Z})r\partial_r u^l + 2\bar{Z}u^l - 2U^l]\sin\theta\partial_\theta Y_l^m. \qquad (4.47)
\end{aligned}
$$

Whilst the difference equation, $\mathcal{E}^r_{\rm p} - \mathcal{E}^r_{\rm n}$, gives

$$
\begin{aligned}
&(r\partial_r\delta\Psi^l_{\rm p} - r\partial_r\delta\Psi^l_{\rm n})Y_l^m - 2\Omega(1-\bar{\mathcal{B}}')u^l\sin\theta\partial_\theta Y_l^m - 2im\bar{\mathcal{B}}\Omega u^l\cos\theta Y_l^m \\
&= -\Delta\Omega\Bigg\{\left(1-\frac{\bar{Z}}{x_{\rm p}}\right)r\partial_r U^l + \frac{2\bar{Z}}{x_{\rm p}}U^l + (1-2x_{\rm p})\left[\left(1-\frac{\bar{Z}}{x_{\rm p}}\right)r\partial_r u^l + \frac{2\bar{Z}}{x_{\rm p}}u^l\right] \\
&\quad - 2(1-x_{\rm p})u^l\Bigg\}\sin\theta\partial_\theta Y_l^m \\
&\quad + \bar{\mathcal{B}}'\Delta\Omega[r\partial_r U^l - \bar{Z}r\partial_r u^l - 2(1-x_{\rm p}+\bar{Z})u^l]\sin\theta\partial_\theta Y_l^m \\
&\quad + im\bar{\mathcal{B}}\Delta\Omega[r\partial_r U^l - \bar{Z}r\partial_r u^l + 2(1-x_{\rm p}+\bar{Z})u^l]\cos\theta Y_l^m. \qquad (4.48)
\end{aligned}
$$

Lastly we apply the same equations to the divergence equation. This yields, from the sum,

$$
\begin{aligned}
&\sin\theta\partial_\theta[\sin\theta(\rho_{\rm n}\mathcal{E}^\theta_{\rm n} + \rho_{\rm p}\mathcal{E}^\theta_{\rm p})] + \partial_\varphi[\rho_{\rm n}\mathcal{E}^\varphi_{\rm n} + \rho_{\rm p}\mathcal{E}^\varphi_{\rm p}] \\
&\quad \to -L[x_{\rm p}\delta\Psi^l_{\rm p} + (1-x_{\rm p})\delta\Psi^l_{\rm n}]Y_l^m + 2\Omega U^l[L\cos\theta Y_l^m + \sin\theta\partial_\theta Y_l^m] \\
&= -\Delta\Omega(1-x_{\rm p})\Big\{2U^l[L\cos\theta Y_l^m + \sin\theta\partial_\theta Y_l^m] \\
&\quad -Lx_{\rm p}u^l[2\cos\theta Y_l^m + \sin\theta\partial_\theta Y_l^m] + (L-2)\bar{Z}u^l\sin\theta\partial_\theta Y_l^m\Big\}. \qquad (4.49)
\end{aligned}
$$

Considering the difference gives us

$$
\begin{aligned}
&\sin\theta\partial_\theta[\sin\theta(\mathcal{E}^\theta_{\rm p}-\mathcal{E}^\theta_{\rm n})]+\partial_\varphi[\mathcal{E}^\varphi_{\rm p}-\mathcal{E}^\varphi_{\rm n}] \quad \longrightarrow\\
&L(\delta\Psi_{\rm n}-\delta\Psi_{\rm p})Y^m_l+2\Omega(1-\bar{\mathcal{B}}')u^l[L\cos\theta Y^m_l+\sin\theta\partial_\theta Y^m_l]\\
&+2im\Omega\bar{\mathcal{B}}u^l[2\cos\theta Y^m_l+\sin\theta\partial_\theta Y^m_l]\\
=&\Delta\Omega L(U^l-x_{\rm p}u^l)[2\cos\theta Y^m_l+\sin\theta\partial_\theta Y^m_l]\\
&-\Delta\Omega\left[\frac{(L-2)\bar{Z}}{x_{\rm p}}(U^l+u^l)-(L-2)(1-x_{\rm p}+2\bar{Z})u^l\right]\sin\theta\partial_\theta Y^m_l\\
&+\Delta\Omega\bar{\mathcal{B}}'\left\{-LU^l+[2(Z+x_{\rm p})-(1-x_{\rm p})]Lu^l\right\}[2\cos\theta Y^m_l+\sin\theta\partial_\theta Y^m_l]\\
&-\Delta\Omega\bar{\mathcal{B}}'(L-2)(Z+x_{\rm p})u^l\sin\theta\partial_\theta Y^m_l\\
&-2im\Omega\bar{\mathcal{B}}\Delta(x_{\rm p}+Z)u^l[2\cos\theta Y^m_l+\sin\theta\partial_\theta Y^m_l]\\
&-im\Omega\bar{\mathcal{B}}\Delta[2r\partial_rU^l+LU^l+(1-2x_{\rm p}-Z)(2r\partial_ru^l+Lu^l)]\cos\theta Y^m_l. \qquad (4.50)
\end{aligned}
$$

Our aim at this stage is to separate the m-multipoles. This we do by means of the standard recurrence relations,

$$\cos\theta Y^m_l=Q_{l+1}Y^m_{l+1}+Q_lY^m_{l-1} \qquad (4.51)$$

and

$$\sin\theta\partial_\theta Y^m_l=lQ_{l+1}Y^m_{l+1}-(l+1)Q_lY^m_{l-1}, \qquad (4.52)$$

where

$$Q^2_l=\frac{(l-m)(l+m)}{(2l-1)(2l+1)}. \qquad (4.53)$$

In the context of our problem we also need to have recurrence relations involving $\cos^2\theta Y^m_l$ and $\cos\theta\sin\theta\partial_\theta Y^m_l$. These we calculate as

$$\cos^2\theta Y^m_l=(Q^2_{l+1}+Q^2_l)Y^m_l+Q_{l+1}Q_{l+2}Y^m_{l+2}+Q_lQ_{l-1}Y^m_{l-1} \qquad (4.54)$$

and

$$\cos\theta\sin\theta\partial_\theta Y^m_l=[lQ^2_{l+1}-(l+1)Q^2_l]Y^m_l+lQ_{l+1}Q_{l+2}Y^m_{l+2}-(l+1)Q_lQ_{l-1}Y^m_{l-2}. \qquad (4.55)$$

Having laid the foundations for a very general problem, we simplify the problem by considering the only the purely axial r-modes. We make use of the fact that, in their simplest setting, the eigenfunctions of these modes cut off at $l \geq m$. This feature survives the transition to the two fluid co-rotating model [173]. We show here that, in the case involving rotational lag, the same type of relatively simple r-mode solutions exist.

We note that from equation (4.53) that $Q_m = 0$. We further assume that the perturbed velocity fields can be expressed as the co-rotating case [172]. This means

$$U^l_{\rm x} = \begin{cases} A_{\rm x} r^{m+1} & \text{for } l = m \\ 0 & \text{for } l \geq m \end{cases} \tag{4.56}$$

This assumption leads us to two much simpler expressions for the relation for the amplitudes. These are expressed in terms of the sum and difference velocities as

$$\begin{aligned} &[(m+1)\tilde{\kappa} - 2 + \Delta(1-x_{\rm p})(m-1)(m+2)]U^m \\ &-(1-x_{\rm p}-\varepsilon_{\rm p})\Delta x_{\rm p}(m-1)(m+2)u^m = 0 \end{aligned} \tag{4.57}$$

and

$$\begin{aligned} &-\left[(m-1)(m+2) + 2\bar{\varepsilon} - m(m+1)(\bar{\mathcal{B}}' + i\bar{\mathcal{B}})\right]\Delta U^m \\ &+\Big\{(1-\bar{\varepsilon})(m+1)\tilde{\kappa} - 2(1-\bar{\mathcal{B}}' + i\bar{\mathcal{B}}) + \Delta x_{\rm p}(m-1)(m+2) \\ &-\bar{\varepsilon}\Delta\left\{[m(m+1)-4]x_{\rm p} + 2\right\} - m(m+1)\Delta x_{\rm p}(1-\bar{\varepsilon})(\bar{\mathcal{B}}' + i\bar{\mathcal{B}}) \\ &+2(1-\varepsilon_{\rm n})(\bar{\mathcal{B}}' - i\bar{\mathcal{B}})\Delta\Big\}u^m = 0, \end{aligned} \tag{4.58}$$

where we have again simplified by defining

$$\bar{\varepsilon} = \varepsilon_{\rm n}/x_{\rm p} = \varepsilon_{\rm p}/(1-x_{\rm p}). \tag{4.59}$$

It is clear that if we assume all coefficients to be constant then the above equations will result in a quadratic in $\tilde{\kappa}$. However, the general solution to this contains too many terms to offer much elucidation regarding the behaviour of the modes in question. To obtain some insight into the problem we consider several 'special cases', where we examine the effects of constraining certain of the parameters.

As will become apparent, the instabilities found in our investigation fall into two categories, dynamical and secular. Whilst these were not necessarily found independently of each other, for convenience, we separate the analysis of the two categories.

4.3.1 Dynamical Instabilities

We first consider the case of vanishing entrainment, where $\bar{\varepsilon} = 0$, which appears to offer a suitable simplification. Whilst this simplifies the solution markedly, we still arrive at a rather long winded quadratic in $\tilde{\kappa}$ where

$$(m+1)^2\tilde{\kappa}^2 + P_1\tilde{\kappa} + P_0 = 0. \tag{4.60}$$

This looks quite straightforward until we express P_1 and P_0 fully as

$$\begin{aligned} P_0 =& 2(m-1)(m+2)\left(\bar{\mathcal{B}}' - i\bar{\mathcal{B}}\right)\Delta^2 + 4\left[1 - (1+x_{\rm p})\left(\bar{\mathcal{B}}' - i\bar{\mathcal{B}}\right)\right] \\ &+ 2\Delta\left[(m-1)(m+2)(x_{\rm p}\bar{\mathcal{B}}' - 1)\right. \\ &+ \left.\left(\bar{\mathcal{B}}' - i\bar{\mathcal{B}}\right)(m^2+m-4) + ix_{\rm p}\bar{\mathcal{B}}(m^2+m+2)\right] \end{aligned} \tag{4.61}$$

and

$$\begin{aligned} P_1 =& (m+1)\Big\{ -4 + 2\,(1+x_{\rm p})\left(\bar{\mathcal{B}}' - i\bar{\mathcal{B}}\right) \\ &+ \Delta\left[2\left(\bar{\mathcal{B}}' - i\bar{\mathcal{B}}\right) + (m-1)(m+2)(1 - x_{\rm p}\bar{\mathcal{B}}') - ix_{\rm p}\bar{\mathcal{B}}(m^2+m+2)\right]\Big\}. \end{aligned} \tag{4.62}$$

Whilst not as clear as we might wish, if we apply the limit of strong mutual friction coupling ($\mathcal{R} \to \infty$), such that $\mathcal{B} \approx 0,\ \mathcal{B}' \approx 1$, then our solution simplifies to

$$\tilde{\kappa} = -\frac{1}{(m+1)x_{\rm p}}\left[1 - x_{\rm p} + \Delta \pm \mathcal{D}^{1/2}\right], \tag{4.63}$$

where

$$\mathcal{D} = (1+x_{\rm p})^2 + 2\Delta\left\{1 + x_{\rm p}\left[3 - m(m+1)\right]\right\}. \tag{4.64}$$

If we consider the higher modes where $m \gg 1$, then we obtain

$$\mathcal{D} \approx (1 + x_{\rm p})^2 - 2x_{\rm p} m^2 \Delta. \tag{4.65}$$

This clearly means that we have, for sufficiently high m, complex roots for $\tilde{\kappa}$. Since these roots will form complex conjugates, one will have a negative imaginary part, the condition for a growing (unstable) solution. This is in agreement with the results of [7]. We can identify the value of m at which this instability sets in, which we denote as m_c, as

$$m_c = \frac{1 + x_{\rm p}}{\sqrt{2x_{\rm p}\Delta}}. \tag{4.66}$$

Using the same method as in [7] we can express the growth timescale, $\tau_{\rm grow}$, of the unstable modes in terms of the rotation period of the star, P, by

$$\tau_{\rm grow} \approx \frac{mP}{2\pi} \left(\frac{x_{\rm p}}{1 + x_{\rm p}} \right) \left(\frac{m^2}{m_c^2} - 1 \right)^{-1/2}. \tag{4.67}$$

If we consider multipoles well above this critical value, that is $m \gg m_c$, then this growth timescale can be reasonably approximated by

$$\tau_{\rm grow} \approx \frac{P}{2\pi} \left(\frac{x_{\rm p}}{2\Delta} \right)^{1/2}. \tag{4.68}$$

This can be more clearly expressed as

$$\tau_{\rm grow} \approx 3 \left(\frac{x_{\rm p}}{0.05} \right)^{1/2} \left(\frac{10^{-4}}{\Delta} \right)^{1/2} P. \tag{4.69}$$

As in [7], using the same scaling we can express m_c as

$$m_c \approx 300 \left(\frac{x_{\rm p}}{0.05} \right)^{-1/2} \left(\frac{\Delta}{10^{-4}} \right)^{-1/2}. \tag{4.70}$$

So we have a growth timescale that is directly proportional to the orbital period of the star and is also dependent upon the rotational lag and the proton fraction. The approximation for the critical multipole depends only upon the latter two parameters.

Equation (4.70) corresponds to length scales for the critical mode in a typical neutron star of a few tens of metres. As we increase m, the growth time of the unstable r-modes will decrease. We return to this point in our concluding paragraphs.

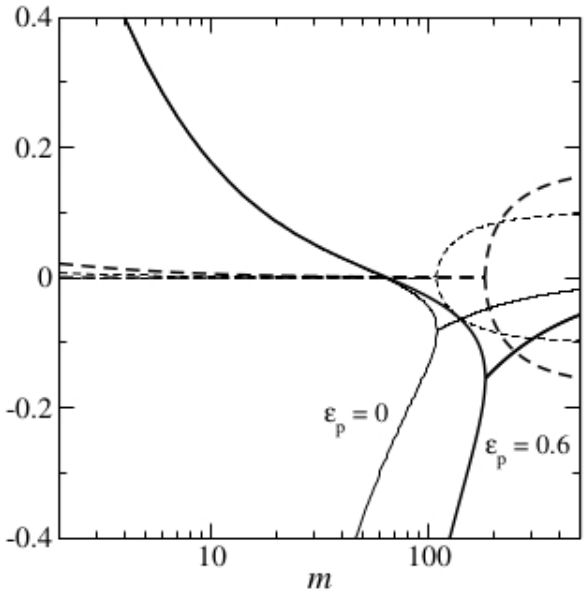

Figure 4.1: *Real and imaginary parts (solid and dashed lines respectively) of the roots of the dispersion relation in the strong coupling limit (with $\mathcal{R} = 10^3$). Plots without ($\varepsilon_{\rm p} = 0$) and with ($\varepsilon_{\rm p} = 0.6$) entrainment. In both cases $\Delta = 5 \times 10^{-4}$. We can see a critical value for m, m_c, where real roots merge, beyond which the modes are unstable. We see that the inclusion of entrainment shift m_c upwards.*

The results obtained thus far take no account of entrainment and its inclusion in our analysis further complicates this. However, in the strong coupling limit, $\mathcal{B} \approx 0,\ \mathcal{B}' \approx 1$, the issue remains tractable. In this case we obtain roots

$$\tilde{\kappa} = \frac{\gamma}{(m+1)\, x_{\rm p}} \left[-(1+\varepsilon_{\rm n}) + (1-\varepsilon_{\rm n})\,(x_{\rm p} - \Delta) \pm \mathcal{D}^{1/2} \right] \tag{4.71}$$

where

$$\gamma = (1 - \varepsilon_{\rm n} - \varepsilon_{\rm p})^{-1} \tag{4.72}$$

and

$$\begin{aligned} \mathcal{D} = {} & \left(1 + \frac{x_{\rm p}}{\gamma}\right)^2 + 2\,(1-\varepsilon_{\rm n}) \left[1 - \left(m^2 + m - 3\right) \frac{x_{\rm p}}{\gamma}\right] \Delta \\ & + (1-\varepsilon_{\rm n})^2 \left[1 - \frac{2x_{\rm p}}{\gamma}\,(m+2)\,(m-1)\right] \Delta^2. \end{aligned} \tag{4.73}$$

If we assume small scale modes ($m \gg 1$) and small differential rotation ($\Delta \ll 1$), then we have the approximation for equation (4.73)

$$\mathcal{D} \approx \frac{(\gamma + x_{\rm p})^2}{\gamma^2}\left(1 - \frac{m^2}{m_c^2}\right), \tag{4.74}$$

where

$$m_c = \frac{(\gamma + x_{\rm p})}{\sqrt{2x_{\rm p}\Delta\gamma\,(1-\varepsilon_{\rm n})}}. \tag{4.75}$$

This leads to a growth time for unstable modes expressed by

$$\tau_{grow} \approx \frac{mP}{2\pi}\left(\frac{x_{\rm p}}{\gamma + x_{\rm p}}\right)\left(\frac{m^2}{m_c^2} - 1\right)^{-1/2}. \tag{4.76}$$

If we consider the case where $m \gg m_c$, then equation (4.76) reduces to

$$\tau_{grow} \approx \frac{P}{2\pi}\left(\frac{x_{\rm p}}{2\Delta}\right)^{1/2}\epsilon_*^{1/2}. \tag{4.77}$$

Here we have introduced a new variable, ϵ_*, which is defined as

$$\epsilon_* = \frac{1 - \varepsilon_{\rm n} - \varepsilon_{\rm p}}{1 - \varepsilon_{\rm n}} \approx \frac{m_p^*}{m_p}, \tag{4.78}$$

where m_p^* is the effective proton mass [68]. Given that, in a neutron star core, we would expect this effective proton mass to be in the range of $0.5 - 0.9$ times that of the rest mass, we conclude that the inclusion of entrainment has a minor impact on the growth timescale. This is illustrated in Figure 4.1 where we show the imaginary and real roots with $\varepsilon_{\rm p} = 0$ and $\varepsilon_{\rm p} = 0.6$.

We can summarise these results as follows. For the typical magnitude of rotational lag inferred from radio pulsar glitches [30], we predict unstable modes with a characteristic horizontal length scale of some tens of metres. Smaller scale r-modes would also be unstable and these would have growth times that would be as short as a few rotation periods. These unstable modes grow very quickly when we compare with the evolutionary timescale of a star's cooling, spin-down etc. Therefore, it is not unreasonable to conclude that they will affect a star that develops sufficient lag, Δ.

4.3.2 Secular Instability

Having confirmed the results of [7], (the existence of an instability in the strong-coupling limit), and extended the analysis of this instability to include entrainment, we move away from this limit and consider a more general case. It is helpful, to get a 'feel' for the behaviour away from the strong coupling limit, to solve equation (4.60) for a range of fixed parameters. We consider the problem for fixed $\mathcal{R}$, leading to the mode frequencies depending on m. The results are shown in Figures 4.2, 4.3 and 4.4 , which show the behaviour of r-mode solutions for decreasing values of $\mathcal{R}$ (that is, as we move away from the strong coupling limit).

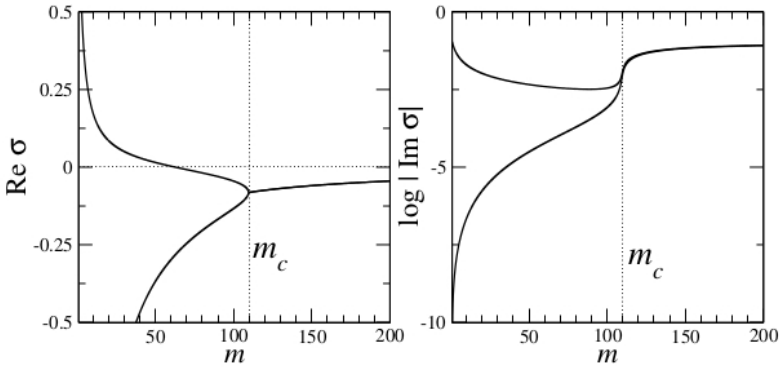

Figure 4.2: *Real (left hand panel) and imaginary (right hand panel) parts of r-modes for* $\mathcal{R} = 100$, $x_{\rm p} = 0.1$ *and* $\Delta = 5 \times 10^{-4}$. *Beyond the critical value,* m_c, *the modes are dynamically unstable. The onset of the dynamical instability is associated with the near merger of the of the real parts of the two frequencies. (Because of the scaling of the plot it is not obvious that these do not merge. This is more apparent in Figure 4.3 and Figure 4.4 where* $\mathcal{R}$ *takes lower values.) The absence of a sign change in either imaginary branch is indicative of a secular instability.*

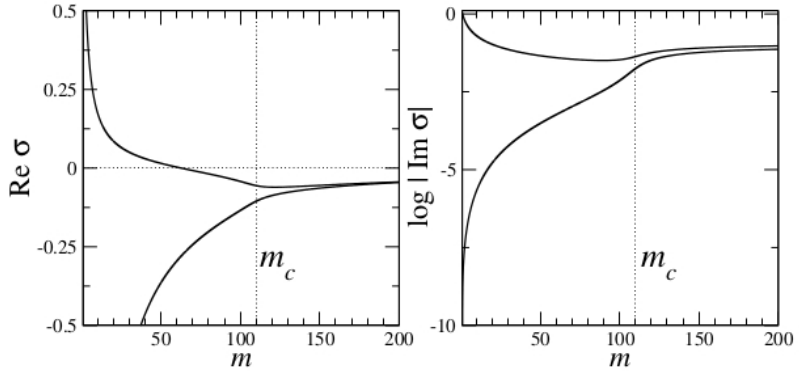

Figure 4.3: *As Figure 4.2 but with* $\mathcal{R} = 10$. *Note that the absence of merger of the real parts becomes clearer.*

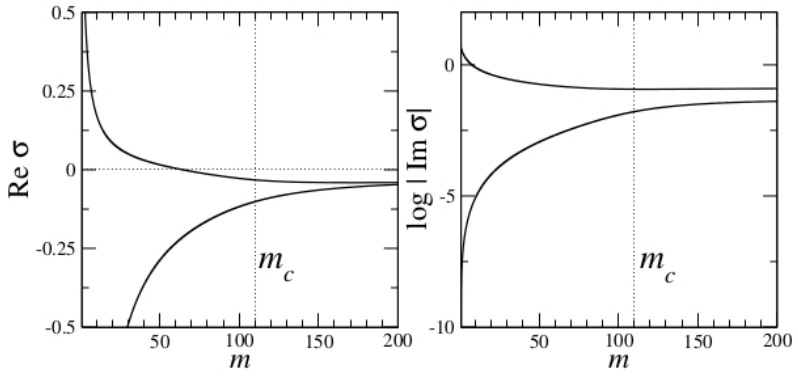

Figure 4.4: *As Figure 4.2 but with* $\mathcal{R} = 2$.

We can make some interesting observations from these figures which are not easily seen in the analysis. Firstly, it can be seen that for $\mathcal{R} > 10$ (approximately), there are modes with with a noticeably larger imaginary part to their frequency. These modes are seen to 'set in' near the critical value, m_c. These modes are associated with the dynamical instability as discussed in the previous section.

However, as $\mathcal{R}$ decreases further, we see (this is particularly clear in the $\mathcal{R} = 2$ graph, Figure 4.4) that there is no longer any clear change in the imaginary part near to m_c. Also, it can be seen that there is no longer the exact mode merger but that the dynamical instability 'sets in' at decreasingly near misses in the complex frequency plane. From this we infer that the dissipative aspect of the mutual friction becomes more significant away from the strong coupling limit. So far as the increase in the importance of the mutual friction is concerned, such results are to be expected.

Considering Figures 4.2, 4.3 and 4.4 in more detail, with particular reference to the right hand panels, we see that neither imaginary part changes sign in the displayed interval. As we are aware that one of the modes is unstable beyond m_c, the absence of a change in sign tells us that it is also unstable for all lower values of m. This is a significant departure from the linear models discussed in Chapters 2 & 3, where the instability is present only for a limited range of frequencies. (We rather blur the difference between spherical modes and plane waves in making this comparison, but it is clear that something unexpected is occurring in our differentially rotating model.) We should note that equations (4.69) and (4.76) are approximations based on the assumption that $m \gg m_c$ and do not apply to this regime, where $m < m_c$. We would, however, assume that for smaller m the growth time is much longer than for the dynamical unstable modes. We return to discuss this later in this chapter, where we show that this is a new secular

instability linked to the mutual friction parameters [66][179][180].

Of particular interest is the observation that this instability is active not only for small scale modes but also for large scale modes. Such large scale modes, in particular the $m = 2$ r-mode are also secularly unstable to gravitational wave emission [181]. Our results suggest that, for such large scale modes, the mutual friction, rather than damping, may provide an additional driving mechanism for the instability. Further, we explore whether, considering the scaling of the gravitational radiation reaction with the star's spin rate, the mutual friction instability is the dominant mechanism for slowly rotating stars.

Before considering such issues in detail, we consider whether we can find approximate solutions that mirror the behaviour shown by the numerical results. If sufficiently simple approximations can be produced, whilst retaining the key features of the numerical solutions, the key parameters that affect the behaviour of the instabilities can be distinguished.

By our use of the sum and difference velocities, U^m and u^m respectively, we obtained our two working equations, (4.57) and (4.58), which have these velocities as their two degrees of freedom. We can see that these variables are coupled solely by Δ. If this is small, then we will have modes that are either predominantly co-moving with the star, in which case U^m dominates over u^m, or counter moving, where u^m is dominant.

We first consider the co-moving case. Here we can assume that u^m approximates to zero in comparison with U^m. Since we are looking for solutions for $\tilde{\kappa}$, we chose whichever of the two equations has U^m depending on this. So equation (4.57) reduces to

$$(m+1)\tilde{\kappa} - 2 + \Delta(1 - x_{\rm p})(m-1)(m+2) = 0, \tag{4.79}$$

which leads to

$$\tilde{\kappa}_0 = \frac{1}{m+1}\left[2 - \Delta(1 - x_{\rm p})(m-1)(m+2)\right]. \tag{4.80}$$

This is clearly real for all real parameters and so, in this simplified model, all modes are stable.

Moving on to the counter-moving case, we assume that U^m approximates to zero in comparison with u^m. Here we use equation (4.58) which gives us

$$(1-\bar{\varepsilon})(m+1)\tilde{\kappa} - 2(1-\bar{\mathcal{B}}' + i\bar{\mathcal{B}}) + \Delta x_{\rm p}(m-1)(m+2) - \bar{\varepsilon}\Delta\left\{[m(m+1)-4]x_{\rm p}+2\right\}$$
$$- m(m+1)\Delta x_{\rm p}(1-\bar{\varepsilon})(\bar{\mathcal{B}}' + i\bar{\mathcal{B}}) + 2(1-\varepsilon_{\rm n})(\bar{\mathcal{B}}' - i\bar{\mathcal{B}})\Delta = 0. \tag{4.81}$$

So we have modes with frequency

$$\tilde{\kappa} = \frac{1}{(1-\bar{\varepsilon})(m+1)}\Big\{2(1-\bar{\mathcal{B}}' + i\bar{\mathcal{B}}) - \Delta x_{\rm p}(m-1)(m+2) + \bar{\varepsilon}\Delta\left\{[m(m+1)-4]x_{\rm p}+2\right\}$$
$$+ m(m+1)\Delta x_{\rm p}(1-\bar{\varepsilon})(\bar{\mathcal{B}}' + i\bar{\mathcal{B}}) - 2(1-\varepsilon_{\rm n})(\bar{\mathcal{B}}' - i\bar{\mathcal{B}})\Delta\Big\}. \tag{4.82}$$

We are, initially at least, only interested in the imaginary part of this solution as this is the indicator of instability. This is proportional to

$$2 + m(m+1)\Delta x_{\rm p}(1-\bar{\varepsilon}) + 2(1-\varepsilon_{\rm n})\Delta. \tag{4.83}$$

In the case of zero entrainment, this is always positive and so the modes are stable.

So far we have seen that in our simplest approximation the model remains stable for all modes. However, we have have only considered leading order terms in Δ to this point. If we consider both of our original equations, (4.57) and (4.58), in combining these we will clearly have terms in Δ^2. So we can estimate a solution to next order by

$$\tilde{\kappa} = \tilde{\kappa}_0 + \tilde{\kappa}_2\Delta^2. \tag{4.84}$$

After considerable manipulation (mostly performed by Maple) we arrive at

$$\tilde{\kappa}_2 = \frac{(m-1)(m+2)}{2(m+1)}\frac{x_{\rm p}(1-x_{\rm p})}{(\bar{\mathcal{B}}' - i\bar{\mathcal{B}})}\left[(m-1)(m+2) - m(m+1)(\bar{\mathcal{B}}' + i\bar{\mathcal{B}})\right]. \tag{4.85}$$

As previously, it is the imaginary part of this solution that interests us. Since, from both earlier in our work and [7], we know that instability exists in the strong coupling limit, this leads to a simplifying approximation of $\bar{\mathcal{B}}' \approx 1/x_{\rm p}$. This gives us, to first order in $\bar{\mathcal{B}}$,

$$\text{Im}\ \tilde{\kappa}_2 = -\frac{(m-1)(m+2)}{2(m+1)}x_{\rm p}(1-x_{\rm p})[m(m+1)(2-x_{\rm p}) + 2x_{\rm p}]\bar{\mathcal{B}}. \tag{4.86}$$

This is clearly always negative and tells us that these modes are unstable for all Δ. We can see that the growth of these unstable modes scales a $1/\bar{\mathcal{B}}$, which tells us that this is a secular instability ($\bar{\mathcal{B}}$ depends upon $\mathcal{R}$, the mutual friction coefficient). The relatively simple nature of equation (4.86) enables us to see more clearly the dependence of the instability on the parameters.

It is also relevant to establish the critical value for $\mathcal{R}$, $\mathcal{R}_c$, at which these instabilities 'appear'. This is clearly associated with a change of sign in the imaginary part of equation (4.85). This occurs when Im $\tilde{\kappa}_2 = 0$, giving

$$\mathcal{B}'_c \left(= \frac{\mathcal{R}_c^2}{1+\mathcal{R}_c^2} \right) = \frac{(m-1)\,(m+2)}{2m\,(m+1)} x_{\rm p}. \tag{4.87}$$

Having established the instability in the strong coupling case, we expand our analysis to the weak coupling case. It should be recalled that the assumption of zero entrainment still holds here. This is useful as it will confirm the expectation that, for $\mathcal{R} \ll \mathcal{R}_c$, the system should be stable. In the weak coupling case we have $\bar{\mathcal{B}}' \sim \bar{\mathcal{B}}^2$ and this gives a solution of

$$\text{Im } \tilde{\kappa}_2 = \frac{(m-1)^2(m+2)^2}{2(m+1)} x_{\rm p}(1-x_{\rm p}) \frac{1}{\bar{\mathcal{B}}}. \tag{4.88}$$

Here the modes are clearly always stable, as expected.

Whilst the approximation, equation (4.85), is more tractable than the full solution, its usefulness can only be determined when its prediction are compared with the numerical solutions. This comparison is best shown graphically and appears in Figure 4.5. Since all modes are unstable for $\mathcal{R} > 1$, we select a value for $\mathcal{R}$ such that $\mathcal{R}_c < \mathcal{R} < 1$. In this domain, the solution for all $\mathcal{R}$ is qualitatively the same. The instability is present for a range of multipoles up to some critical value, after which the modes become stable. To this end we select $\mathcal{R} = 0.5$ for Figure 4.5. It can be seen that equation (4.85) shows reasonable correspondence with the numerical results for low m, but becomes unreliable as m nears the critical value and fails to change sign at said value.

We can gain further insight into this new instability by producing plots with fixed m and varying $\mathcal{R}$. This is done in Figures 4.6 and 4.7, where we have chosen values of $m = 2$, Figure 4.6, and $m = 100$, Figure 4.7. From these figures we see that, as previously stated, the instability is present throughout the $\mathcal{R} \geq 1$ domain. We further see that it extends into the weak coupling regime as well. The approximation from

equation (4.85) is also included in these plots and we see that, for the low $m\,(=2)$ plot, Figure 4.6, this mirrors the numerical solutions. It does not, however, perform well for higher $m\,(=100)$ Figure 4.7. This is not surprising, since in equation (4.85) we have neglected the higher order terms in Δ. These terms become significant when multiplied by powers of a larger value for m. We conclude, nevertheless, that the approximation is useful, in so far as it indicates the behaviour in an important part of the parameter space.

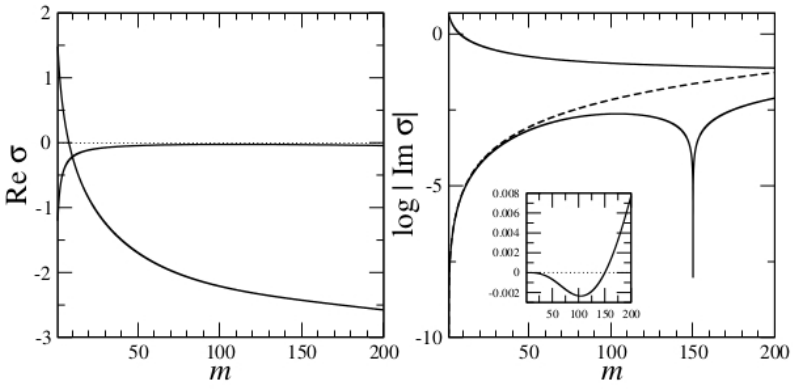

Figure 4.5: *As Figure 4.2 but with* $\mathcal{R} = 0.5$. *The inset panel shows the change of sign, from negative to positive, for the imaginary part of* $\tilde{\kappa}$. *This indicates that the secular instability is turning off. The dashed curve in the right hand panel corresponds to the approximate solution given by equation* (4.85). *This is accurate for low* m *but fails, in this case, near to the onset of the instability.*

Returning to the numerical results, it would be illuminating if we could show the details of our previous plots in a single plot. To this end Figure 4.8 is a 3-d plot which shows the key features of our solution for a range of value of both $\mathcal{R}$ and m. The 'trench' feature running through the graph represents the change of sign associated with the onset of the instability.

Whilst Figure 4.8 gives a 'feel' for what is happening as we vary the parameters, Figure 4.9 is possibly clearer, where we summarise the behaviour in the phase plane. This shows the unstable region in the $m - \mathcal{R}$ plane, with other key features indicated.

4.3.3 Astrophysical Context for the Dynamical Instability

As stated at the outset of this chapter, our aim was to show that the superfluid two-stream instability (as discussed in Chapter 2) might have applications in improving our understanding of some features of neutron star behaviour. In particular, we were hoping

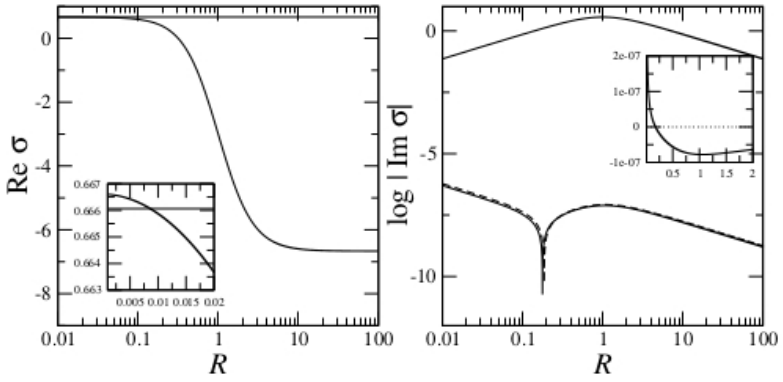

Figure 4.6: *Real and imaginary parts of r-modes with* $m = 2$, $x_{\rm p} = 0.1$ *and* $\Delta = 5 \times 10^{-4}$. *The inset panel on the right hand side shows a change of sign for an imaginary root, indicating that there is some critical value of* $\mathcal{R}$ *beyond which unstable modes are present. The approximation from equation* (4.85) *is again included as a dashed line. As was suggested by Figure 4.5, this is a good match at this low* m.

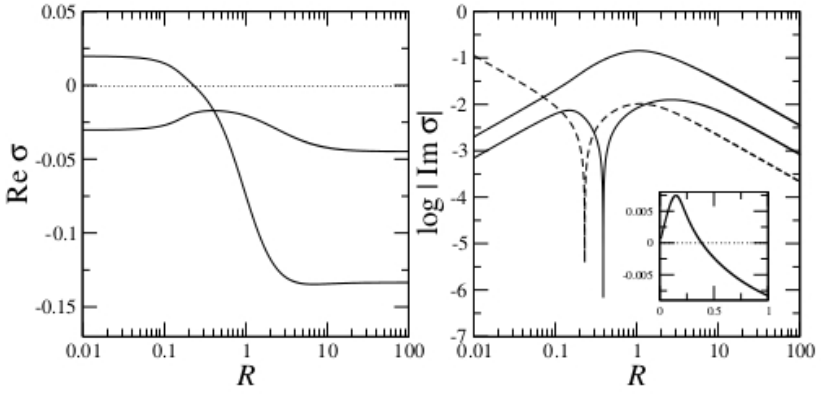

Figure 4.7: *As Figure 4.6, but with* $m = 100$. *Here we see that equation* (4.85) *is no longer a good approximation for the imaginary part.*

to show it as a possible trigger mechanism for vortex unpinning and the associated pulsar glitches. Whilst we have demonstrated the existence of both dynamical and secular instabilities in our model, we have yet to show that these are sufficient to cause the phenomenon in question. The first requirement in this case is that any instability grows quickly enough to overcome the dissipative action of viscosity within the neutron star.

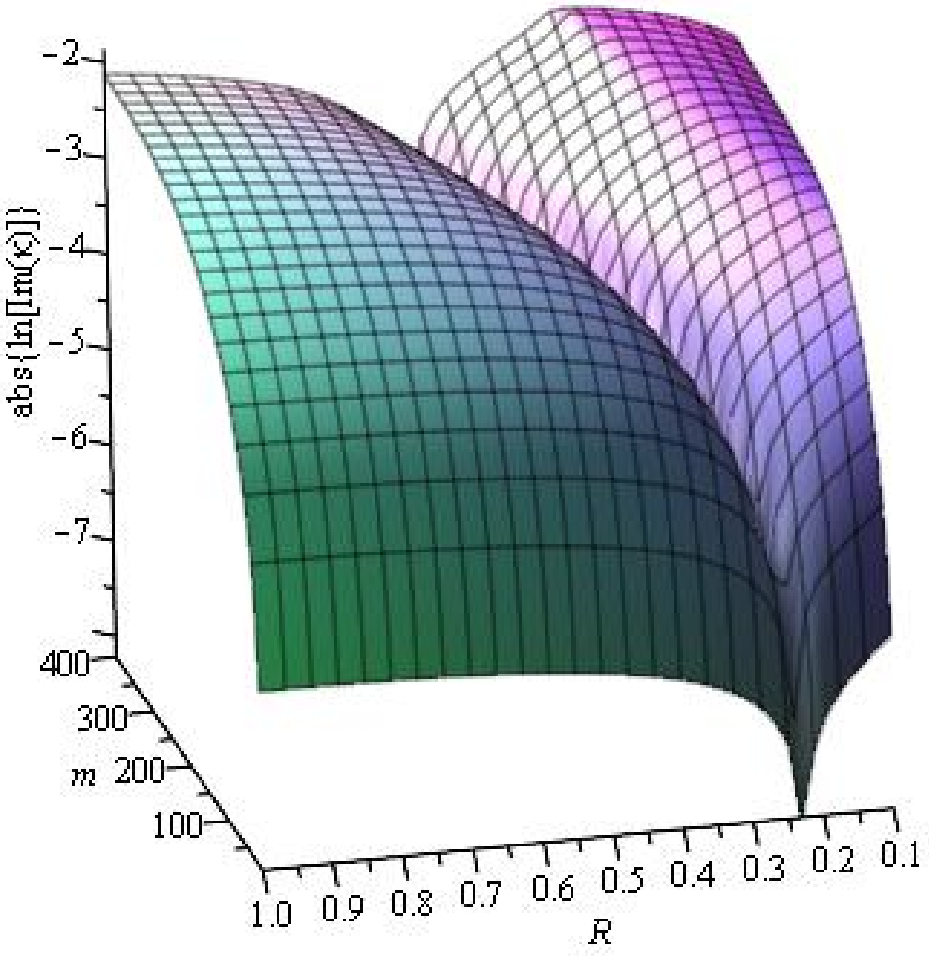

Figure 4.8: *Surface plot for the imaginary part of one of roots of equation* (4.60). *The 'trench' running through the plot indicates a change in sign. This shows the onset of the instability moving across the trench from left to right.*

We should ask whether the conditions prevailing in a neutron star (and especially within the core) are such that our model is relevant. Recent evidence suggests that both superfluid neutrons and protons will be present in the core temperature of a neutron star with Temperature below 10^9K [182][183]. (For our purpose, a mature neutron star is a star that has 'settled down' into a state where there is no longer rapid cooling, has a steady spin down and whose magnetic field is not rapidly altering.) Under such circumstances, and taking into account particle density and pressure, the core is sufficiently cold to contain both superfluid neutrons and protons.

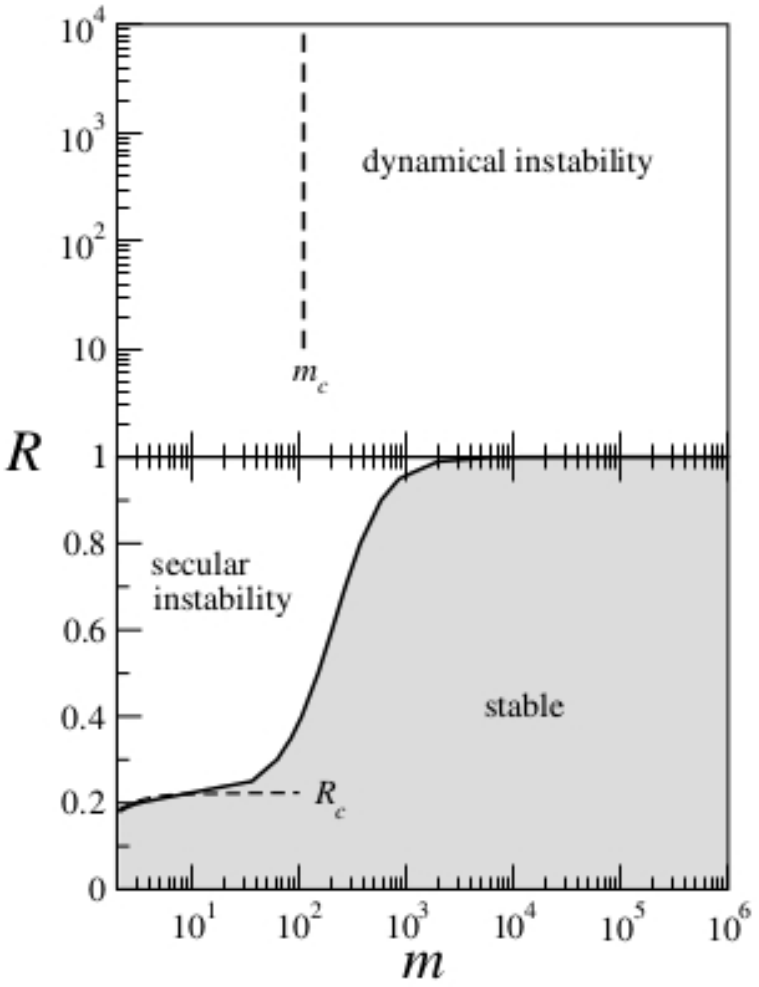

Figure 4.9: *Summary of the parameter space $\mathcal{R}$ vs m, indicating the different regions of instability for $x_{\rm p} = 0.1$ and $\Delta = 5 \times 10^{-4}$. The vertical dashed line indicates the critical multipole, m_c, where, in the strong coupling regime, the behaviour changes from secularly to dynamically unstable. The horizontal dashed line estimates the critical drag, $\mathcal{R}_c$, where the secular instability sets in for low m. We see that higher modes are always stable for $\mathcal{R} \lesssim 1$.*

Under these conditions there are two mechanisms which we would expect to damp the fluid motion [61][184][185]. The first is the vortex mutual friction. This, as we have seen, drives the instability under consideration, rather than suppressing it. The second of these mechanisms is the shear viscosity from electron-electron collisions [175]. The underlying physics of this mechanism has been discussed elsewhere [67] and does not greatly impinge upon our investigation. Of greater import is the shear viscosity damping timescale and how this compares with the growth timescale of the instability. We can estimate this damping timescale using an energy integral approach by

$$\tau_{\rm sv} = \frac{E_{\rm mode}}{2\dot{E}_{\rm sv}}, \tag{4.89}$$

where $E_{\rm mode}$ is the mode energy and $\dot{E}_{\rm sv}$ is the shear viscosity damping rate. Since we are only interested in an approximate value to give us a feel for how this compares with the instability time scale, we use the results for single fluid r-modes in a uniform density star as previously calculated in [186];

$$\tau_{\rm sv} = \frac{3}{4\pi}\frac{M}{\eta_{\rm ee}R}\frac{1}{(2m+3)(m-1)} \approx \frac{1.3\times10^6}{m^2}\left(\frac{0.05}{x_{\rm p}}\right)^{3/2}\frac{R_6^{7/2}}{M_{1.4}^{1/2}}T_8^2 s, \tag{4.90}$$

where $R_6 = R/10^6 cm$ and $M_{1.4}/M_\odot$ represent the radius and mass of the star, respectively. The shear viscosity coefficient, $\eta_{\rm ee}$ $(= \rho_{\rm p}\nu_{\rm ee})$, is given by [175]

$$\eta_{\rm ee} = 1.5\times10^{19}\left(\frac{x_{\rm p}}{0.05}\right)^{3/2}\rho_{14}^{3/2}T_8^{-2}\ {\rm g\ cm^{-1}\ s^{-1}}, \tag{4.91}$$

where $\rho_{14} = \rho/10^{14}$ g cm^{-3} and $T_8 = T/10^8$ K.

Using this approximation, we are able to make a comparison between the growth timescale for the instability, $\tau_{\rm grow}$, and that for the shear viscosity damping, $\tau_{\rm sv}$. We consider first the modes that exhibit dynamical instability (in the strong coupling regime). Such a comparison is indicated in Figure 4.10. We show the timescales as functions of the multipoles, m, and we include plots for the same two entrainment parameters used in Figure 4.1. The damping rate, $\tau_{\rm sv}$, is shown for two temperatures, 10^7 K and 5×10^7 K. (We discuss the relevance of these temperatures below)

Dynamically unstable r-modes exist for the range of m where the dashed line, representing $\tau_{\rm sv}$ lie above the solid line, representing $\tau_{\rm grow}$. We can see that $\tau_{\rm grow}$ levels off for $m \gtrsim m_c$, with increasing entrainment having a small effect on $\tau_{\rm grow}$ above this critical value. However, as suggested by equation (4.75), the inclusion of entrainment has a significant effect on the value of m_c.

As a final observation, returning to the selected temperatures, we note that the range of unstable modes decreases as the star cools. Generally, glitches are observed in younger pulsars and this is qualitatively consistent with the results displayed in Figure 4.10. It appears that the dynamical r-mode instabilities are 'squeezed out' of existence once the core temperature drops much below 10^7K. However, it has been shown [187] that the

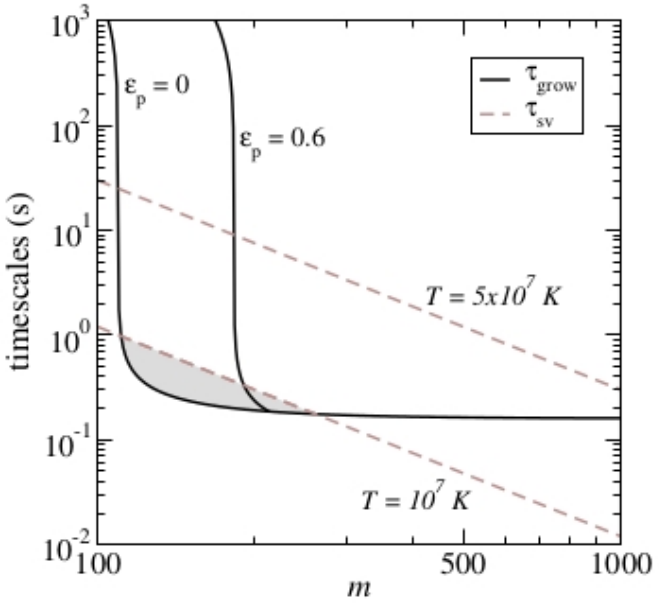

Figure 4.10: *A comparison of the r-mode instability and viscous damping timescales,* $\tau_{\rm grow}$ *and* $\tau_{\rm sv}$ *respectively, as obtained from equations* (4.69) *and* (4.90)*. These are shown as functions of* m *for pulsar parameters:* $P = 0.1$ *s,* $x_{\rm p} = 0.1$ *and* $\mathcal{R} = 10^4$*. Stellar mass and radius are set at the canonical values* $M_{1.4} = R_6 = 1$*. The shear viscosity damping rate,* $\tau_{\rm sv}$*, is shown for two temperatures,* 10^7 K*K and* 5×10^7 K*.* Δ *is fixed at* 5×10^{-4} *and* $\tau_{\rm grow}$ *is shown for two values of entrainment,* $\varepsilon_{\rm p} = 0$ *and* $\varepsilon_{\rm p} = 0.6$*. As an example, the unstable r-modes for* T= 10^7 K *are given by the shaded region.*

core temperature of a neutron star may remain above 10^8K for in excess of 10^5 years from the star's formation.

There remains one further piece of observational data that suggests a link between pulsar glitches and the r-mode instability for large m. By setting $\tau_{\rm grow} = \tau_{\rm sv}$, we can find a critical spin lag, Δ_c, above which the instability grows more quickly than it is damped [7]. By combining equations (4.69) and (4.90), and by setting m at the critical value, m_c, we obtain

$$\Delta_c \approx 3.3 \times 10^{-5} \left(\frac{x_{\rm p}}{0.05}\right)^{2/3} \left(\frac{P}{1\ {\rm s}}\right)^{2/3} \left(\frac{m_{\rm p}^*}{m_{\rm p}}\right)^{-1/3} T_8^{-4/3}. \tag{4.92}$$

It is necessary to compare this prediction for the onset of instability with the extrapolation of observed data. Fortunately [7], our model has only two components and, if we assume angular momentum is conserved (that is $I_c \Delta\Omega_c \approx -I_s \Delta\Omega_s$ where I_c and I_s are the two moments of inertia, while $\Delta\Omega_c$ and $\Delta\Omega_s$ represent the changes in the

corresponding spin frequencies) it is relatively straightforward to estimate the critical lag required.

The data regarding glitches suggests that approximately 2% of the total spin down is reversed in glitches [30] which implies $I_c/I_s \approx 0.02$. For a large glitch of the order of that observed in the Vela pulsar, we have $\Delta\Omega_c/\Omega_c \sim 10^{-6}$. This gives us a lag at the time of the glitch, Δ_g, of

$$\Delta_g \approx \frac{I_c}{I_s}\frac{\Delta\Omega_c}{\Omega_c} \approx 5 \times 10^{-4}. \tag{4.93}$$

This is sufficiently close to our estimate from equation (4.92) to suggest that the r-mode instability plays a role in large pulsar glitches. In common with the phenomenological discussion of glitches [30], our two fluid model operates in the strong drag limit where vortices are pinned to the charged lattice components. As discussed in Chapter 1, in this 'pinned' state a rotational lag will develop between the two components as the crust spins down. Once the critical lag is reached, a range of r-modes become unstable, with a growth time of only a few periods of rotation. It is reasonable to assume that it is the fluid motion associated with this instability that breaks the vortex pinning, which in turn triggers the glitch.

We note at this point that, as yet, we have made no detailed study of the non-linear behaviour of the fluid once the modes reach large amplitude. It has been demonstrated that the onset and initial growth of this instability in 1+1 dimensions are well described by linear perturbation theory [64]. The behaviour at late stages, when the instabilities dominate, has yet to be satisfactorily resolved.

To further relate the predictions of our model to available data regarding neutron star glitches, we reproduce a figure from [7], Figure 4.11. This figure details the maximum glitches allowed assuming a completely relaxed system, with $\Delta_g = \Delta_c$ and $I_c/I_s = 0.02$. Accurate temperature data is not available for most pulsars that exhibit glitches, so an estimation has been made using the 'heat blanket' model [188] and calibrating this model to the Vela pulsar ($T \approx 6.9 \times 10^7$ K) [189]. This leads to the following expression for pulsar temperature

$$T \approx 3.3 \times 10^8 \left(\frac{t_c}{1\text{yr}}\right)^{-1/6} \text{K}, \tag{4.94}$$

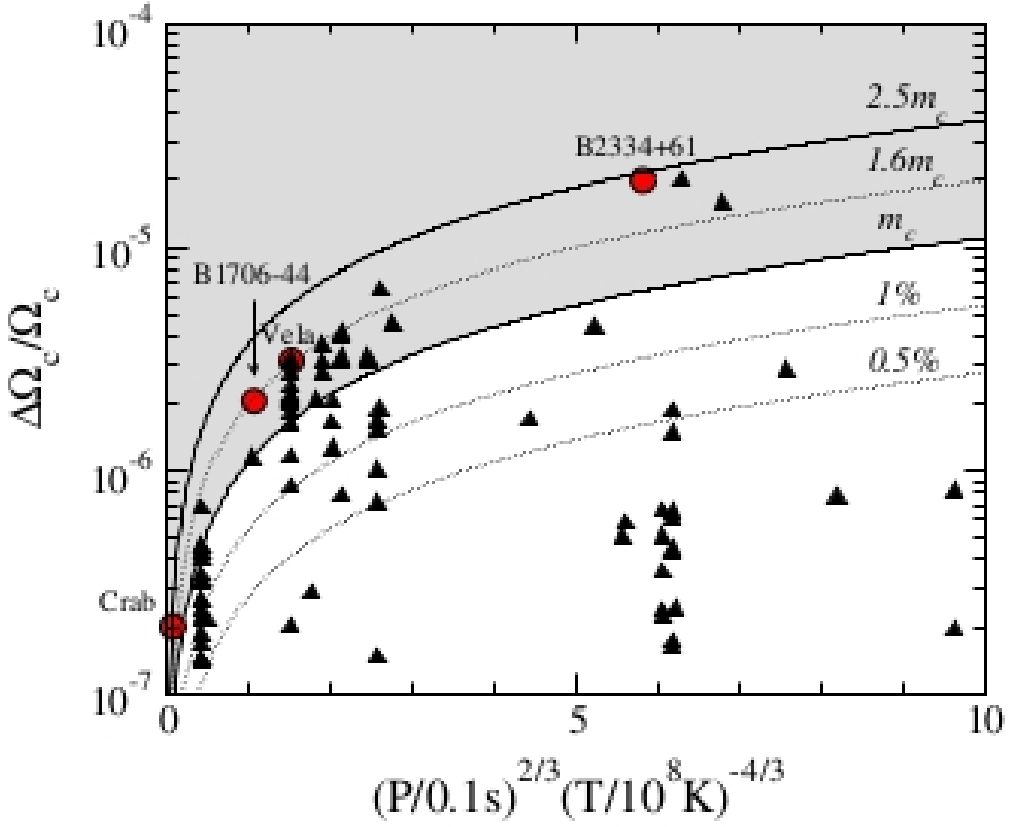

Figure 4.11: *Figure from [7]. The maximum glitches predicted by equation (4.92) compared with observations. The m_c curve represents the onset of the dynamical instability, with the shaded region unstable.*

where $t_c = P/2\dot{P}$ is the characteristic pulsar age.

The results from Figure 4.11 are encouraging in appraising our model. In particular, the model performs well when predicting the maximum glitch one would expect to see. It further lends credence to the idea that the system carries on evolving into the instability before the glitch happens. This is consistent with the more rapid growth of the higher modes. It is noted that both Vela and PSR B1706-44, for which temperature data is available, glitch when our model shows $m = 1.6m_c$, suggesting that the instability continues its evolution, after the first m-modes become unstable, until it is sufficiently widespread to trigger unpinning.

Whilst this model shows promising results, there is much to do to establish its validity completely. As well as the previously discussed non-linear evolution of the instability, further understanding of mutual friction parameters are required. To improve testing of the model, more accurate temperature data for glitching pulsars is needed. But none of these present insurmountable problems and this model offers real hope of modelling

neutron star glitches quantitatively as well qualitatively.

4.3.4 Discussion and Future Work

We have in this chapter provided an analysis of superfluid r-modes in a case of solid body rotation with lag between the two components. Whilst this has been considered in more detail than in previous work on the subject [7], (uncovering secular instability as well as somewhat extending the dynamical instability analysis from the strong coupling limit to a more general case) there remain many assumptions in the model that may need to be discarded if we are to obtain a more accurate picture of neutron star glitches.

As examples, we have assumed both uniform density and solid rotation. Clearly neither is physical and it would clearly improve the accuracy of the model if a more 'realistic' set of assumptions were used. However, such changes would remove several layers of simplification from the problem we addressed and may make an analytic approach intractable.

Overall the analysis shown in this chapter offer some results that have not been considered previously elsewhere. Whilst there has been much previous work on instabilities triggering superfluid turbulence and and results in the context of pulsar precession, we provide the first demonstration of this kind of instability for global mode oscillations. This work, along with [7], also considers perturbations in a new background configuration, that of differential rotation. The extra degree of freedom that this affords over previous studies leads to a problem that is in many ways richer and more enlightening.

One of the most interesting results was also the most unexpected, the secular instability. This was totally new to us as the previous work on this topic [7] had given no hint of its existence. We were surprised to find both secular and dynamical instabilities occupying almost distinct parts of the parameter space as shown in Figure 4.9. Again, as far as we are aware, the analysis in this chapter represents the first detailed study of a problem that has secularly unstable modes entering a regime in which they become dynamically unstable.

The analysis reveals that, instead of modes becoming unstable where real roots merge and form complex conjugate pairs, we have dynamical instabilities associated with near misses in the complex plane. This phenomenon certainly warrants further investigation.

Chapter 5

Superfluid Helium II as a Model for Neutron Star Cores

In Chapter 4 we considered r-mode instability for a differentially rotating, two component superfluid neutron star core. We showed that such a two component superfluid configuration exhibited unstable r-modes (both secularly and dynamically) and suggested that these may act as a trigger mechanism for vortex unpinning and the observed neutron star glitches. In this initial mathematical model, we have endeavoured to include as much detail as possible whilst keeping the mathematics tractable. As discussed in the closing remarks to Chapter 4, having produced such a model, we would like to investigate whether such a mechanism acts in other systems. In particular, we would be interested in some system that is realisable within a laboratory.

In Chapter 3, we discuss the possibility of using a mixture of Bose-Einstein Condensates as an analogue for a two component superfluid. We show that, although this approach shows promise, there remain several issues to overcome before such an analogue becomes fully realisable. Fortunately, there are other possible laboratory systems that offer the hope of demonstrating the key features of our model. One such candidate is the Helium II (He II). In the following sections we discuss why an appropriate laboratory set up using He II might exhibit these r-mode instabilities. We obtain the relevant parameters for He II over a range of temperatures, and apply these to the model used for a neutron star.

5.1 Why We Might Consider Helium II as a Good Analogue for Neutron Star Core

Our aim is to develop an analogue for the superfluid neutron - superconducting proton conglomerate of a neutron star core in a laboratory environment. It would seem logical that we should use materials that display similar properties to those making up said core. It would also make the realisation of such an analogue clearer if the physics of these laboratory materials were well understood. From what we know of its properties, He II leaps to mind as a candidate. The most obvious reasons for such a selection are listed here.

Firstly, this is well established science. The superfluidity effect was first observed in 1937 [52][51] and has since been described through phenomenological and microscopic theories. The properties of superfluid Helium are, by now, well understood and no 'new' physics seems to be required to fit it into the analogue of the neutron star model.

Secondly, we can describe superfluid Helium as a two component fluid, as is the case for the outer core of a neutron star. This description follows from the work of Landau [53] and Tisza [69], where it was noted that the entropy flow of He II does not always follow that of the centre of mass. From this it was "postulated that the velocity of flow of entropy was, for He II, a new variable independent of $\boldsymbol{v}$ (the velocity of the centre of mass)" [54]. This led to a description of He II as a fluid with two distinct, but coexisting, components. The first, an ideal superfluid component with all of the characteristics of such a state of matter. The second, a 'normal' fluid component, governed by the well known laws of fluid dynamics. It is this second component with which the entropy of the fluid is associated. As we demonstrate later in this chapter, the ratio of these two components present in the composite fluid varies with temperature; the proportion of the superfluid component increasing as we approach 0K. It is of particular interest for us to note the similarity with the neutron star core, which is composed of superfluid neutron vortices arranged in a lattice and a coexisting component of superconducting protons. In the case of He II under rotation, the superfluid component would form a vortex lattice coexisting with a 'sea' of normal fluid.

The formation of vortices in the superfluid component of He II was established in the 1950s, most notably by Hall and Vinen [171]. We also note that the normal fluid component can be modelled by solid rotation [180]. So, if He II is suitably confined and rotated, we have a structure that is qualitatively analogous to the standard model of a neutron star core.

Naturally, there are some issues with using He II as an analogue for the two component fluid of the neutron star core. In particular, our model of the core depends on the differential rotation between the two components. This builds up as a result of the pinning of the neutron vortices to the crystal lattice. Fortunately, an analogue for this system was constructed in the 1970s by Tsakadze and Tsakadze [79], where He II was placed in a spherical container, which was then rotated. Whilst we discuss their work in more detail in Chapter 2, we note that they were able to effectively pin the vortices by use of Plexiglass crystals glued to the inside of the container.

5.2 Instabilities in Rotating Helium II

We should note that the similarities discussed in the preceding section do not guarantee that rotating He II will display the same instabilities as those observed in our neutron star model. We are constrained by the physical nature of the Helium model with regard to mutual friction parameters as a function of temperature. In selecting a suitable temperature for the model, we are further restricted by the effect this has on the ratio of the two components. Such parameters have been established experimentally [54]. However, before considering applying such data, we first establish how these parameters relate to those used for the neutron - proton composite fluid.

In comparing the He II case with that of the neutron star, we consider the mutual friction force for each. To avoid confusion in comparing the dynamical equations governing the behaviour of He II with those from the neutron star model, we label variables as follows [54]:

In the Helium case we use the subscripts 'S' and 'N' for quantities relating to the superfluid and normal fluid components respectively. The non dimensional mutual friction coefficients we denote by 'B_{HV}' and 'B'_{HV}'. The solid angular velocity of the superfluid component is $\boldsymbol{\Omega}$ and from this, a unit vector $\hat{\boldsymbol{\Omega}}$ is defined by

$$\hat{\boldsymbol{\Omega}} = \frac{\boldsymbol{\Omega}}{|\Omega|}. \tag{5.1}$$

The relative linear velocity between the two components, $\boldsymbol{W}$ is given by

$$\boldsymbol{W} = \boldsymbol{v}_{\mathrm{S}} - \boldsymbol{v}_{\mathrm{N}}. \tag{5.2}$$

Finally, the overall density is given by ρ, whilst those of the superfluid and normal components are given by ρ_{S} and ρ_{N} respectively. We note that, since the two components have the same particle mass, the density fraction for each component is the same as the particle density ratio.

In the case of the differentially rotating neutron star model we follow the convention used in Chapter 4.

Hall and Vinen proposed that the mutual friction force, $\mathbf{F}_{\mathrm{ns}}$ between the normal and superfluid components could be expressed by

$$\mathbf{F}_{\mathrm{ns}} = -\left(B_{\mathrm{HV}}\rho_{\mathrm{N}}\rho_{\mathrm{S}}/\rho\right)\hat{\boldsymbol{\Omega}}\times\left(\boldsymbol{\Omega}\times\boldsymbol{W}\right) - \left(B'_{\mathrm{HV}}\rho_{\mathrm{N}}\rho_{\mathrm{S}}/\rho\right)\left(\boldsymbol{\Omega}\times\boldsymbol{W}\right). \tag{5.3}$$

For comparison we reproduce the mutual friction equation for the neutron star model, equation (4.29) from Chapter 4.

$$f_i^{\mathrm{x}} = \frac{\rho_{\mathrm{n}}}{\rho_{\mathrm{x}}}\mathcal{B}'n_v\epsilon_{ijk}\kappa^j w^k_{\mathrm{xy}} + \frac{\rho_{\mathrm{n}}}{\rho_{\mathrm{x}}}\mathcal{B}n_v\epsilon_{ijk}\hat{\kappa}^j\epsilon^{klm}\kappa_l w^{\mathrm{xy}}_m. \tag{5.4}$$

This we can rewrite in vector form as

$$\boldsymbol{f}^{\mathrm{x}} = -\left(\frac{\rho_{\mathrm{n}}}{\rho_{\mathrm{x}}}\mathcal{B}n_v\right)\hat{\boldsymbol{\kappa}}\times\left(\boldsymbol{\kappa}\times\boldsymbol{w}^{\mathbf{xy}}\right) - \left(\frac{\rho_{\mathrm{n}}}{\rho_{\mathrm{x}}}\mathcal{B}'n_v\right)\left(\boldsymbol{\kappa}\times\boldsymbol{w}_{\mathrm{xy}}\right). \tag{5.5}$$

We can see that equation (5.5) is simply equation (5.3) , with the minor exception that $\mathcal{B}'/B'_{\mathrm{HV}} = \mathcal{B}/B_{\mathrm{HV}} = 1/2x_{\mathrm{p}}$. Here x_{p} is the proton fraction in the neutron star case, which translates to the fraction of the normal fluid component in the Helium II case. This difference follows directly from our definition of $\tilde{\kappa}$ in the neutron star model.

So, by comparing the two mutual friction equations in component form, we have shown that the experimental parameter values for Helium II can also be applied, with the modification mentioned above, to equations (4.57) and (4.58) from Chapter 4. For convenience, said equations, without entrainment terms which we set to zero in this calculation, are reproduced here.

$$\begin{aligned}&[(m+1)\tilde{\kappa} - 2 + \Delta(1-x_{\mathrm{p}})(m-1)(m+2)]U^m\\ &-(1-x_{\mathrm{p}})\Delta x_{\mathrm{p}}(m-1)(m+2)u^m = 0\end{aligned} \tag{5.6}$$

$T(K)$	x_{p}	B_{HV}	B'_{HV}
1.30	0.045	1.526	0.616
1.35	0.058	1.466	0.535
1.45	0.091	1.351	0.385
1.50	0.111	1.296	0.317
1.55	0.135	1.243	0.255
1.60	0.162	1.193	0.198
1.65	0.193	1.144	0.149
1.70	0.771	1.100	0.107
1.75	0.268	1.059	0.075
1.80	0.313	1.024	0.052
1.85	0.364	0.996	0.041
1.90	0.420	0.980	0.040
1.95	0.482	0.981	0.045
2.00	0.553	1.008	0.043
2.10	0.741	1.298	-0.065
2.12	0.788	1.476	-0.143
2.14	0.842	1.790	-0.297
2.16	0.907	2.420	-0.683
2.17	0.950	3.154	-1.272
2.172	0.961	3.538	-1.549
2.174	0.973	4.227	-2.048
2.176	0.988	6.391	-3.613

Table 5.1: *Experimental values for the normal fluid component fraction and the dimensionless mutual friction coefficients from equation (5.3) for a range of temperatures* [54].

and

$$
\begin{aligned}
&- \left[(m-1)(m+2) - m(m+1)(\bar{\mathcal{B}}' + i\bar{\mathcal{B}})\right] \Delta U^m \\
&+ \Big\{(m+1)\tilde{\kappa} - 2(1 - \bar{\mathcal{B}}' + i\bar{\mathcal{B}}) + \Delta x_{\mathrm{p}}(m-1)(m+2) \\
&- m(m+1)\Delta x_{\mathrm{p}}(\bar{\mathcal{B}}' + i\bar{\mathcal{B}}) + 2(\bar{\mathcal{B}}' - i\bar{\mathcal{B}})\Delta\Big\} u^m = 0. \qquad (5.7)
\end{aligned}
$$

Here we use $\bar{\mathcal{B}}'$ $(= \mathcal{B}'/x_{\mathrm{p}})$ and $\bar{\mathcal{B}}$ $(= \mathcal{B}/x_{\mathrm{p}})$, so our substitution simplifies further to $\bar{\mathcal{B}}'/B'_{\mathrm{HV}} = \bar{\mathcal{B}}/B_{\mathrm{HV}} = 1/2$. It simply remains to obtain values for the parameters B'_{HV}, B_{HV} and ρ_{N}/ρ $(= x_{\mathrm{p}})$ for various values of temperature at which Helium II exhibits superfluidity. The required parameters were obtained from [54] and are reproduced in Table 5.1

A cursory inspection of this data suggests that we may observe different behaviour in the He II model from that manifested in the neutron star case. In the case of the neutron star, the terms $\bar{\mathcal{B}}'$ and $\bar{\mathcal{B}}$ are derived from a single dimensionless mutual friction coefficient, $\mathcal{R}$, which is assumed to be always positive. These two coefficients are related by

$$\mathcal{B}' = \mathcal{R}\mathcal{B} = \mathcal{R}^2/\left(1+\mathcal{R}^2\right). \tag{5.8}$$

In the case of the Helium data, this equation does not hold true. The ratio of B'_{HV} and B_{HV} cannot be used to generate the original values using equation (5.8). In some cases the ratio of the two parameters is negative, which is certainly not within the range of allowed parameters for the original model. This would seem to imply that we would expect quantitatively different behaviour from He II.

Further to this point, in Chapter 4 it can be seen that there exists some minimum critical value for $\mathcal{R}$, $\mathcal{R}_c \approx 0.2$, below which all modes are stable. Let us, for the moment, ignore the problems mentioned in the above paragraph and assume that it is predominantly the ratio of the two parameters that is critical as to when the instability occurs. Then we can see that, above a temperature of about 1.6K, the ratio of B'_{HV} and B_{HV} is smaller than the neutron star critical value for $\mathcal{R}$ of 0.2. This suggests that we are unlikely to find instabilities above this temperature. This assumption along with the neutron star results would lead us to, initially at least, to use data from the temperature for which this ratio is the highest, that is $T = 1.3K$.

A further difference between the experimentally determined data for He II and that used for our neutron star model is that of the ratio of the two components. In the case of He II, the particle ratio of the superfluid component to the normal fluid, x_{p}, increases as temperature falls. However, in the neutron star case, we assume, quite reasonably, that this ratio is a constant. As explained previously, in the neutron star case we used $x_{\mathrm{p}} = 0.1$

Having discussed how we might apply the Helium data mathematically, we still have the question as to whether such a system might be physically realisable in a laboratory. As mentioned in section 5.1, experiments using He II in a similar manner were actually undertaken in the Soviet Union in the 1970s [79]. Whilst we discuss these experiments in more detail in Chapter 2, a brief description of the key features of the required experimental set up is included here.

To most accurately mimic the behaviour of the neutron star core, it would be required that the He II sample fill a sealed spherical container. This container would be free to rotate about a single axis and the rate of this rotation would ideally be externally controllable. It is then necessary that the rotation of the container can be transferred to the two components so as to create a differential rotation between the normal and superfluid components. This can be achieved by pinning, through the introduction of

impurities to the container wall, the vortices generated in the superfluid component to the inside of the container so that they rotate exactly with the container. The rotation of the normal component can be coupled to the inner wall of the container by friction alone, so that it will 'lag' any change in rotation in the container. So, by spinning up the container, the two components can be made to exhibit, at least until the no$u_{\mathbf{q}}$rmal component catches up, a measurable differential rotation.

Having established that such an experiment is physically realisable and pointed out the inconsistencies with the neutron star case, we still have a table of 'real world' data that we can apply to our model. It seems sensible to consider first the data that most closely matches that which we used in the neutron star model. This is the data at $T = 1.3$K, which has a ratio of B_{HV} to B'_{HV} which is within the range that produced instabilities in the neutron star model and a value for x_{p} that is reasonably close. We note, though, that the values of $\bar{\mathcal{B}}'$ and $\bar{\mathcal{B}}$ that we obtain are much lower than those used in the neutron star model. The results of substituting the parameters given for this temperature into equations (4.57) and (4.58) are shown in Figures 5.1, 5.2 and 5.3. For this first group of figures we have set $\Delta = 1 \times 10^{-5}$. We show the real parts of both roots in Figure 5.1, whilst the two imaginary parts are shown separately in Figures 5.2 and 5.3.

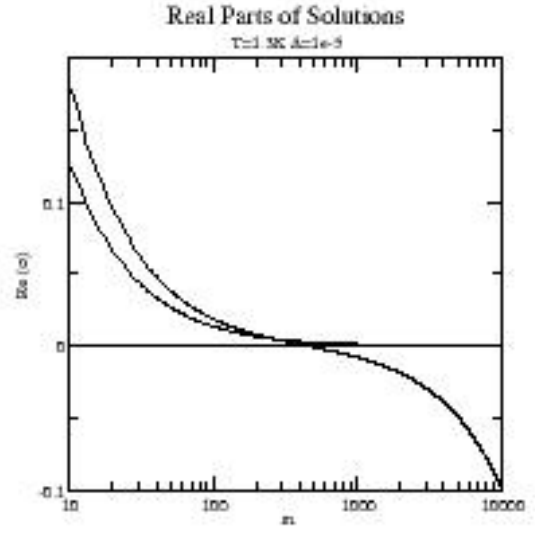

Figure 5.1: *Both real roots for* $\tilde{\kappa}$ *with* $T = 1.3K$ *and* $\Delta = 1 \times 10^{-5}$.

To show the presence of unstable modes, we require that the imaginary part of one of the roots be negative for these modes. It can be seen in Figure 5.3 that the imaginary part of one root is always positive and no instability is present. However, we see that in Figure 5.2, the solution dips below the x-axis, indicating a region of instability. Unfortunately, from the point of view of using Helium II as an analogue for our neutron star

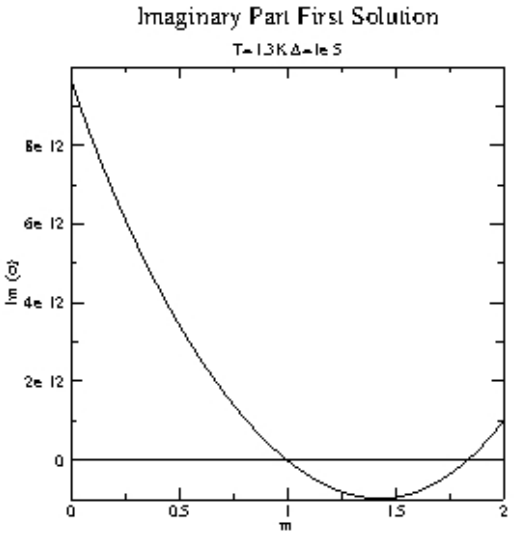

Figure 5.2: *Imaginary part of the first root for* $\tilde{\kappa}$ *with* $T = 1.3K$ *and* $\Delta = 1 \times 10^{-5}$.

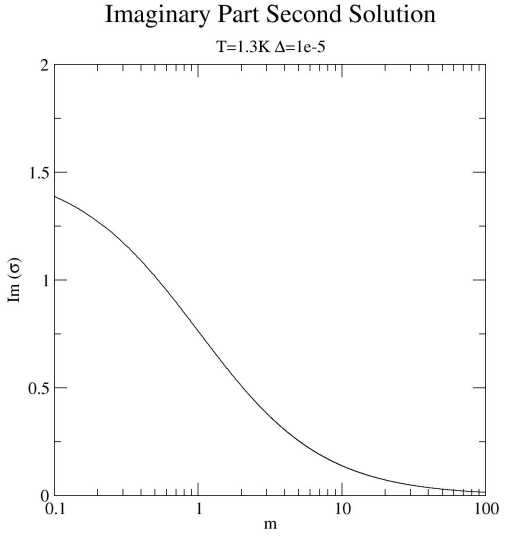

Figure 5.3: *Imaginary part of the second root for* $\tilde{\kappa}$ *with* $T = 1.3K$ *and* $\Delta = 1 \times 10^{-5}$.

model, this imaginary part of $\tilde{\kappa}$ becomes positive again before the $m = 2$ mode. This tells us that all modes are stable in this instance.

It should be pointed out that, in reality, m can take only positive integer values. In the graphs we treat it as a continuous variable only because this helps us to visualise the behaviour. So, where the function σ has a negative imaginary part for non-integer m

only, this has no physical meaning. Hence, in Figure 5.2, where both $m = 1$ and $m = 2$ are stable and the graph only dips below the x-axis only between these modes, this tells us all modes are stable.

We next consider the impact on our results of changing the differential rotation between the two component, Δ. We show the results for the imaginary part of the first root with $\Delta = 1 \times 10^{-3}$ in Figure 5.4 and with $\Delta = 1 \times 10^{-1}$ in Figure 5.5. The graphs for the real parts and the second imaginary part are not shown here as they show essentially the same structure as the graphs for $\Delta = 1 \times 10^{-5}$. It is, at this stage where we are endeavouring to show the existence of unstable modes, the imaginary part of only one root that is of real interest.

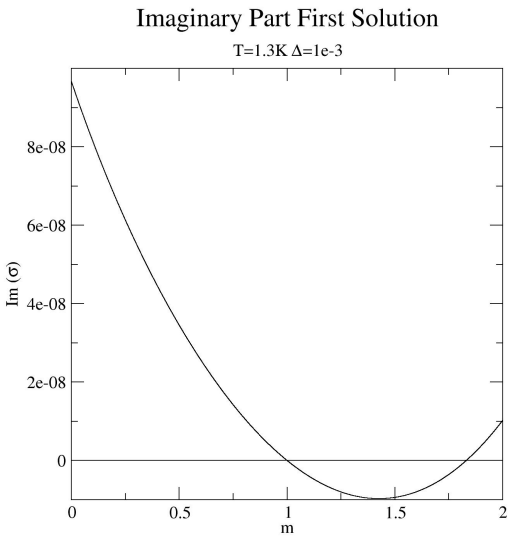

Figure 5.4: *As Figure 5.2 but with* $\Delta = 1 \times 10^{-3}$.

We see in Figures 5.4 and 5.5 the same behaviour as in Figure 5.2, with the imaginary part only becoming negative for a range of unphysical values between $m = 1$ and $m = 2$. This implies that a change in Δ does not significantly alter the qualitative behaviour of Helium II with regard to unstable modes.

When we compare the values of $\bar{\mathcal{B}}$ and $\bar{\mathcal{B}}'$ generated by Table 5.1, it was the parameters at $T = 1.3$K that suggested we would be most likely to find behaviour similar to the neutron star model. It is, however, worth exploring the behaviour at other temperatures as these give a range of parameters unconsidered in Chapter 4. Rather than repeat the procedure for all of the values given in the table, we select temperatures that offer extremes for our parameters, for instance close to a change of sign in $\bar{\mathcal{B}}'$. To this end we show plots for $T = 1.9$K ($\bar{\mathcal{B}}'$ small but positive), $T = 2.1$K ($\bar{\mathcal{B}}'$ small negative) and

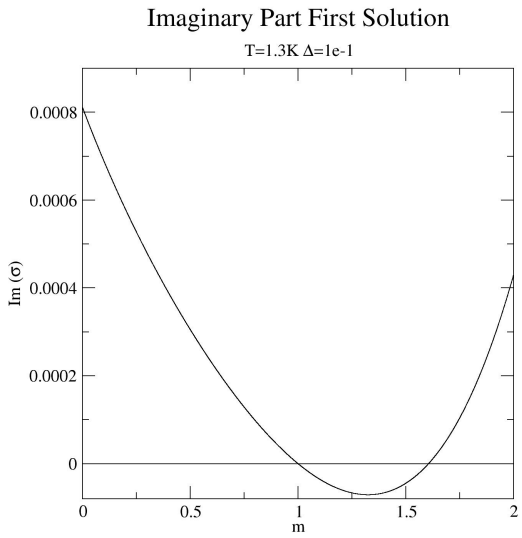

Figure 5.5: *As Figure 5.2 but with* $\Delta = 1 \times 10^{-1}$.

$T = 2.17$K ($\bar{\mathcal{B}}'$ more negative). These examples are shown in Figures 5.6, 5.7 and 5.8 respectively. In all cases, we use $\Delta = 1 \times 10^{-3}$.

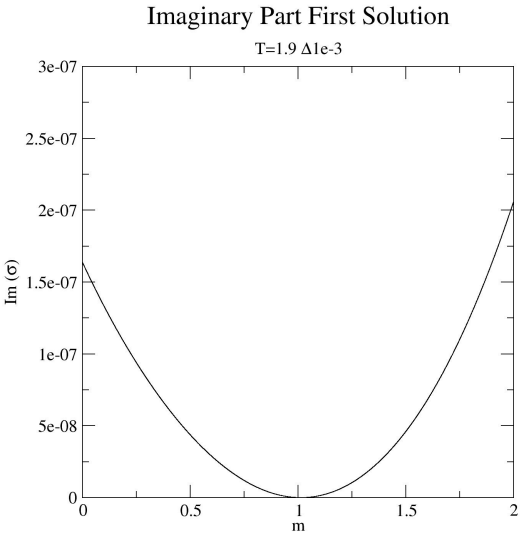

Figure 5.6: *As Figure 5.4 but with* $1.9K$.

We note that whilst the overall shape of the plots remains the same as we vary the temperature upwards, they become less like the results for the neutron star model. It is interesting to note, but only in passing, that the values of m, when we treat it as continuous variable, where the imaginary part of σ becomes negative shifts to the left of $m = 1$ when $\bar{\mathcal{B}}'$ becomes negative. More significantly, we note that there is still no

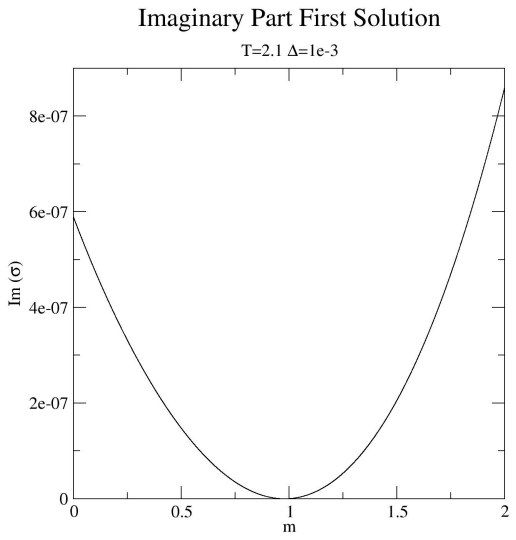

Figure 5.7: *As Figure 5.4 but with* $T = 2.10K$.

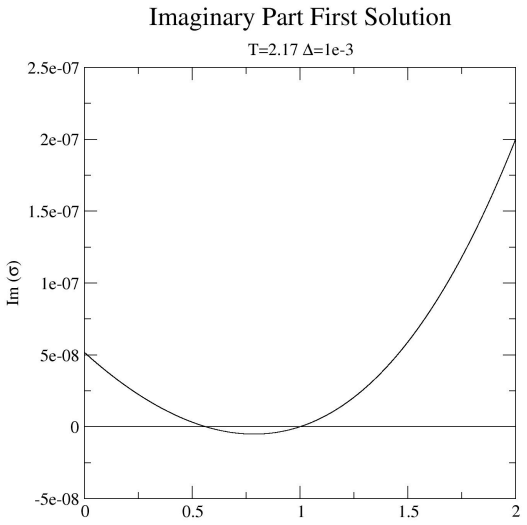

Figure 5.8: *As Figure 5.4 but with* $T = 2.17K$.

instability present for any real modes (that is, positive integer values of m).

The results from these plots lead us to the conclusion that we are unable to test for the neutron star r-mode instability using the two fluid model of He II as an analogue. It was earlier suggested that there might be issues in trying to reproduce this form of instability owing to discrepancies between the He II parameters and the single mutual friction coefficient in the neutron star model. However, it would be helpful if we could

express this failure in rather more concrete terms.

In Chapter 4 we showed, using equation (4.87), that there is a critical value for the parameter $\mathcal{B}'$ below which, for particular modes, m, the instability cannot manifest. In the case of the He II model, this translates to

$$\mathcal{B}'_{HV(c)} = \frac{(m-1)(m+2)}{4m(m+1)} \qquad m \in \mathbb{N} : m \geq 2 \tag{5.9}$$

It is clear that this is a minimum when $m = 2$, so this is the mode that will possess the lowest critical value for $\mathcal{B}'_{HV}$. For the $m = 2$ mode, we have $\mathcal{B}'_{HV(c)} = 0.667$. The highest value in Table 5.1 for $\mathcal{B}'_{HV}$ is 0.616, when $T = 1.3K$. So we can see that, with the range of data available, He II would not be expected to exhibit the r-mode instability being considered.

This might suggest that this experimental set up cannot be used to model the neutron star instability. There are, however, possibilities that might be considered to extend the range of parameters for $\mathcal{B}_{HV}$ and $\mathcal{B}'_{HV}$.

From Table 5.1, it can be seen that the value of both of these parameters increases as the temperature falls. If we infer from this feature that at a range of temperatures lower than those for which we have data, $\mathcal{B}'_{HV} > \mathcal{B}'_{HV(c)}$. So, initially, it might appear that finding data for lower temperatures or, failing this, extrapolating from existing data, might offer the chance to model the desired instability. This line of reasoning, unfortunately for our model, contains a major flaw. Again from Table 5.1, it can be seen that, as the temperature falls, the ratio of normal to superfluid components also decreases. It should be considered as to whether such a ratio of the two components can truly be regarded as a two component fluid, or whether it enters a single component regime. In particular, the low concentration of the normal fluid component implies that its behaviour can no longer be modelled as that of a liquid, but rather as a dilute gas.

We should note that this does not necessarily mean that such an experimental set up has no possible use in modelling the r-mode instability. It simply tells us that the physical parameters of the two components of He II are not appropriate. There might be other fluid combinations that exhibit the desired parameters. A possible example might involve a mixture of superfluid ^{4}He and normal ^{3}He, with the composite fluid at a temperature where the superfluid component of ^{4}He dominates. Unfortunately, mutual friction parameters are not readily available for this combination of fluids.

Another possibility for an analogue is the use of superfluid ^{3}He. Although this is not usually described by the two fluid model, it does form several superfluid phases [141]. Whether some composite of these phases might produce the desired parameters is open to question. Measurements have been undertaken for the $\mathcal{B}$ and $\mathcal{B}'$ in ^{3}He [190]. However, they appear to display strange characteristics near the critical temperature and further work is needed.

As a final remark, we should note that the mutual friction parameters used for the Helium calculations assumed that the vortices were free to move. It has been calculated [191] that in the case of pinned vortices the effective parameters are increased. At low temperatures, below about 1.3 K, this difference is marginal. It has been shown that, as the temperature increases towards the *lambda* point, the differences become more significant. It is, therefore, possible that an experiment with pinned vortices may raise the effective mutual friction sufficiently so that it exceeds the critical value given by equation (4.87). This offers an interesting extension to the work in this chapter.

Chapter 6

Heat Flow Instability with Entropy as a Dynamical Entity

6.1 Introduction

In this chapter we consider a somewhat unusual application of the two-stream instability, that of thermodynamical instabilities associated with heat flow in a fluid. This is motivated by previous work in causal heat conductivity [192] which describes a mechanism for the transfer of heat at finite speed. We first consider why such instabilities might occur in the case of heat flow.

We initially recall the two fluid model for superfluid Helium-4 developed by Landau [53][193]. Here the Helium was described as a composite of two inter-penetrating fluids: a perfect, zero entropy superfluid; and a normal fluid component with which the entropy of the Helium-4 is associated. This model has been the accepted standard for the macroscopic description of superfluid Helium-4 almost since its inception [47]. Whilst it has been refined over the years [194][49], the Landau model has proved invaluable in furthering our understanding of superfluid behaviour and remains a cornerstone of low temperature fluid dynamics.

However, it is possible to refine this model by considering entropy itself to be a dynamical entity. In fact, such a concept can be extended to a fluid that is not necessarily a superfluid. The foundation of this is the concept of variational multifluid dynamics [170]. Building upon this approach, the inclusion of entropy as a dynamical entity, with many of the properties of a classical fluid, leads to a description of heat transfer that was compatible with relativity [192]. The use of Fourier's law contravenes one of the principal tenets of special relativity, in that heat is propagated instantaneously, whereas

the treatment of entropy as a dynamical entropy leads to heat propagation at finite speed.

The idea of treating entropy as a massless component in a composite fluid (along with a massive component constituted by the atomic material) suggests that a variation of the two-stream instability might become manifest. A brief consideration of this shows that we have the conditions, with some modifications, present in the analysis in Chapter 1. We have a two component fluid and, via entrainment, these two components are coupled. We have the possibility of a relative flow between the components. The major difference, from a mathematical standpoint, between this case and the case of two massive components lies in the particle conservation laws when applied to entropy.

The treatment of entropy in this manner has already been of some interest in describing heat flow in relativity and other cosmological applications [195][196][197]. Because of the similarities with the two fluid case, it seems reasonable that we investigate possible thermodynamical instabilities that might arise in Newtonian physics. We begin this analysis with a description of the mathematics of causal heat flow as given in [192].

6.1.1 Causal Heat Flow

We start by considering a simple system, that of two interpenetrating fluid components. The first, which we identify by the constituent index n, consists of "massive" particles with mass m and number density n. We assume this component to possess a velocity v_i^{n}. The second, identified by the constituent index s, is the massless entropy. This has number density s and velocity v_i^{s}. It is assumed that there exists some entrainment between the two fluids, denoted by the parameter α. Following the variational analysis [170], the canonical momentum of each component is

$$\pi_i^{\mathrm{n}} = mnv_i^{\mathrm{n}} - 2\alpha w_i^{\mathrm{ns}}, \tag{6.1}$$

for the massive component and

$$\pi_i^{\mathrm{s}} = 2\alpha w_i^{\mathrm{ns}}, \tag{6.2}$$

for the entropy.

Here we have used the relative velocity between the two component, w_i^{ns}, which is given by

$$w_i^{\mathrm{ns}} = v_i^{\mathrm{n}} - v_i^{\mathrm{s}}. \tag{6.3}$$

From the variational analysis, which starts with the energy functional E, it can be shown that

$$\alpha = \left(\frac{\partial E}{\partial w_{\mathrm{ns}}^2}\right)_{n,s}. \tag{6.4}$$

It has been shown [198][61] that, the momentum equations for a dissipative two-component system can be written as

$$f_i^{\mathrm{n}} = \partial_t \pi_i^{\mathrm{n}} + \nabla_j \left(v_{\mathrm{n}}^j \pi_i^{\mathrm{n}} + D_i^{\mathrm{n}j}\right) + n\nabla_i \left(\mu_n - \frac{1}{2} m v_{\mathrm{n}}^2\right) + \pi_j^{\mathrm{n}} \nabla_i v_{\mathrm{n}}^j \tag{6.5}$$

and

$$f_i^{\mathrm{s}} = \partial_t \pi_i^{\mathrm{s}} + \nabla_j \left(v_{\mathrm{s}}^j \pi_i^{\mathrm{s}} + D_i^{\mathrm{s}j}\right) + s\nabla_i T + \pi_j^{\mathrm{s}} \nabla_i v_{\mathrm{s}}^j. \tag{6.6}$$

Here $D_i^{\mathrm{n}j}$ and $D_i^{\mathrm{s}j}$ represent the dissipation from n and s respectively, whilst f_{n}^i and f_{s}^i indicate the forces acting on each of the two components. The chemical potentials of the two components are given by the normal definition, that is

$$\mu_{\mathrm{n}} = \left(\frac{\partial E}{\partial n}\right)_{s,w_{\mathrm{ns}}} \tag{6.7}$$

and

$$\mu_{\mathrm{s}} = \left(\frac{\partial E}{\partial s}\right)_{n,w_{\mathrm{ns}}} \equiv T. \tag{6.8}$$

Although we should note that equation (6.8) gives the definition of temperature for thermal equilibrium, its use here seems to fit with the model naturally.

Assuming no particle creation or destruction gives rise to mass conservation, leading to

$$\partial_t n + \nabla_j \left(n v_{\mathrm{n}}^j\right) = 0. \tag{6.9}$$

However, we must allow for the possible increase in entropy. So the equivalent of equation (6.9) for the entropy component is

$$\partial_t s + \nabla_j \left(s v_{\mathrm{s}}^j \right) = \Gamma_{\mathrm{s}}, \tag{6.10}$$

where $\Gamma_{\mathrm{s}} \geq 0$.

It is assumed that we are working with a closed system with no external forces and no energy is added, so

$$f_i^{\mathrm{s}} = -f_i^{\mathrm{n}} \tag{6.11}$$

and

$$D_{ij} = D_{ij}^{\mathrm{n}} + D_{ij}^{\mathrm{s}}, \tag{6.12}$$

where D_{ij} is the total dissipation.

By considering (for the sake of keeping our algebra manageable) only the linear friction component of the total dissipative forces [61], we arrive at

$$T\Gamma_{\mathrm{s}} = -f_i^{\mathrm{n}} w_{\mathrm{ns}}^i \tag{6.13}$$

and

$$-f_i^{\mathrm{n}} = 2\mathcal{R} w_i^{\mathrm{ns}}, \tag{6.14}$$

where $\mathcal{R}$ is the resistivity coefficient. This is essentially the classic approach to heat conductivity.

Next a heat flux vector is introduced, which is defined by

$$q^i = sT w_{\mathrm{sn}}^i, \tag{6.15}$$

and equation (6.10) is rewritten as

$$\partial_t s + \nabla_i \left(s v_{\mathrm{n}}^i + s w_{\mathrm{sn}}^i \right) = \Gamma_{\mathrm{s}}. \tag{6.16}$$

This leads to a expression for $\Gamma_{\rm s}$ given by

$$\Gamma_{\rm s} = 2\mathcal{R}\left(\frac{q}{sT}\right)^2, \tag{6.17}$$

with $\mathcal{R} \geq 0$.

If we consider the case of vanishing entrainment, it follows from equation (6.6) that

$$q_i = -\frac{1}{2}\frac{s^2T}{\mathcal{R}}\nabla_i T. \tag{6.18}$$

Thus far, the traditional approach to heat flow has been followed, even though entropy has been used as a dynamical variable. It is, therefore, hardly surprising that Fourier's law, $q_i = -\kappa\nabla_i T$, has been recovered. But this does give an expression for the thermal conductivity, κ, in terms of the preferred variables;

$$\kappa = \frac{1}{2}\frac{s^2T}{\mathcal{R}}. \tag{6.19}$$

Having recovered Fourier's law through following the traditional approach, the analysis moves on to apply the model in the context of extended irreversible thermodynamics [199]. For the sake of simplicity, it first considers heat conduction in a solid, as the absence of a mobile massive fluid component makes this a simpler case. As such this is not, in detail, of great interest at this juncture. However, there are some concepts introduced that are of major import to our work and these are included here.

By considering the solid case, we can assume that $v_{\rm n} = 0$. Also by only including the resistive contribution to the dissipation, we have

$$D^{\rm s}_{ij} = 0 \tag{6.20}$$

and

$$f^{\rm s}_i = 2\mathcal{R}w^{\rm ns}_i. \tag{6.21}$$

Under these conditions equation (6.6) reduces to the more tractable

$$\partial_t\pi^{\rm s}_i - \nabla_j\left(\frac{1}{2\alpha}\pi^j_{\rm s}\pi^{\rm s}_i\right) - \pi^{\rm s}_j\nabla_i\left(\frac{1}{2\alpha}\pi^j_{\rm s}\right) + s\nabla_i T = \frac{\mathcal{R}}{\alpha}\pi^{\rm s}_i. \tag{6.22}$$

By recalling that $\pi_i^s = 2\alpha_i^{\rm ns}$ and $w_i^{\rm ns} = -w_i^{\rm sn}$, this can be rewritten as

$$-\partial_t\left(2\alpha w_i^{\rm sn}\right) - \nabla_j\left(2\alpha w_{\rm sn}^j w_i^{\rm sn}\right) - \alpha\nabla w_{\rm ns}^2 + s\nabla_i T + 2\mathcal{R}w_i^{\rm sn} = 0. \tag{6.23}$$

By making use of equation (6.15) and then linearising equation (6.23) with respect to thermal equilibrium ($q^i = 0$), we arrive at

$$-\partial_t\left(\frac{2\alpha}{sT}q_i\right) + s\nabla_i T + \frac{2\mathcal{R}}{sT}q_i = 0. \tag{6.24}$$

This is in the form of a Cattaneo equation and can rewritten, by the introduction of a thermal relaxation time, τ ($= -\alpha/\mathcal{R}$), as

$$\tau\partial_t q_i + q_i = -\kappa\nabla_i T. \tag{6.25}$$

From the definition of the thermal relaxation time, we can infer that $\alpha \leq 0$. It can be seen that, by this approach, a model for the propagation of heat at finite speed has been produced.

The inclusion of non-local terms is considered and finally a more general model with $v_{\rm n} \neq 0$ is developed. This contains some very long winded algebra which is not included here. We do include the resulting momentum equations for the two components as this is central to the instability analysis that follows. To keep the problem tractable, the non-local terms are not included here. Firstly we have the massive component,

$$\rho\left(\partial_t + v_{\rm n}^l\nabla_l\right)v_i^{\rm n} + \nabla_i p = 0, \tag{6.26}$$

and then for the entropy component

$$\left(\partial_t + v_{\rm n}^j\nabla_j\right)q_i + \frac{1}{\tau}q_i + q_i\nabla_j v_{\rm n}^j + q_j\nabla_i v_{\rm n}^j = -\frac{\kappa}{\tau}\nabla_i T. \tag{6.27}$$

We now have two conservation equations, (6.9) (6.16), and two momentum equations, (6.26) (6.27), which "fully" describe the fluid's macroscopic behaviour. In the following sections of this chapter we explore the dynamical stability of this two fluid model.

6.2 Dynamical Stability in a Static Background

Before moving on to consider a more general case, we first look at the dynamical stability of the fluid model in the simplest case, that of a static background. Here, we assume that our two component fluid is of uniform temperature, pressure and density. We further assume that the fluid is at rest with respect to the reference frame used. As such, the fluid can be said to be in thermodynamic equilibrium, with no net heat flow, and, so, the entropy density is both constant and uniform. To this background we apply small plane wave perturbations and search for frequencies at which these perturbations grow, indicating dynamical instability.

It may seem that this configuration is relatively trivial but it provides some understanding of the behaviour of our fluid mode under perturbation. Also, since we use a different method of calculation in the more general case, it serves as a "sanity check" for our later calculations.

One further observation is that, in the static case, we work in one spatial dimension only. This is such that the results are consistent with those from the more general case discussed later. Although it is the case that a full three dimensional solution to the more general case might be found, the algebra for this quickly becomes intractable. As is seen in the next section, the "more general case" mentioned here is not a fully general solution for the same reason.

As our starting point, we take, in one dimensional form, the conservation equations and the momentum equations derived for each of our two components above. That is equations (6.9), (6.16), (6.24) and (6.26). We note that equation (6.24) is equivalent to equation (6.27). It is preferred as it is a simplification of the momentum equation, better suited to our problem.

$$\partial_t \rho + \partial_x (\rho v) = 0, \tag{6.28}$$

$$\partial_t s + \partial_x (sv + sw) = \frac{2\mathcal{R}}{T} \left(\frac{q}{sT}\right)^2 = \Gamma_s, \tag{6.29}$$

$$\rho (\partial_t + v\partial_x) v + \partial_x p = 0, \tag{6.30}$$

$$-\partial_t \left(\frac{2\alpha}{sT} q_i\right) + s\nabla_i T + \frac{2\mathcal{R}}{sT} q_i = 0 \tag{6.31}$$

Here, for convenience only, we have neglected the indices n and s. It should be made clear that, from here onwards, w relates to $w_{\rm sn}$, and v is $v_{\rm n}$. We note also that, because of the static nature of the background, for any variable X with background value X_0, $\partial_x X_0 = 0$ and $\partial_t X_0 = 0$. This background is perturbed such that for a variable, X we have

$$X = X_0 + \delta X, \tag{6.32}$$

where X_0 is the background value of the variable. So the four equations above give us four perturbation equations (where the background has been removed.):

$$\partial_t \delta\rho + \partial_x (\rho v) = 0, \tag{6.33}$$

$$\partial_t \delta s + \partial_x \left(sv + \frac{q}{T} \right) = 0, \tag{6.34}$$

$$\rho \partial_t v + \partial_x \delta p = 0, \tag{6.35}$$

$$\partial_t \left(\frac{2\alpha}{sT} q \right) + s\partial_x \delta T + 2\mathcal{R}\frac{q}{sT} = 0. \tag{6.36}$$

We should note that equation (6.33) has density, ρ, rather than particle density as a parameter.

At this point we have four equations in six unknowns. To resolve this we make the not unreasonable assumption that both entropy density and total pressure are functions of temperature and the density of the massive components. So the perturbed terms in entropy number density and total pressure can be rewritten as

$$\delta s = \left(\frac{\partial s}{\partial \rho} \right)_T \delta\rho + \left(\frac{\partial s}{\partial T} \right)_\rho \delta T \tag{6.37}$$

and

$$\delta p = \left(\frac{\partial p}{\partial \rho} \right)_T \delta\rho + \left(\frac{\partial p}{\partial T} \right)_\rho \delta T. \tag{6.38}$$

We can simplify the perturbed equations by substituting in the previously defined relaxation time, τ, and thermal conductivity, κ. These definitions are reproduced here for ease of reading:

$$\tau = -\frac{\alpha}{\mathcal{R}}, \tag{6.39}$$

$$\kappa = \frac{s^2 T}{\mathcal{R}}. \tag{6.40}$$

We further assume that the perturbations of our four remaining variables are plane waves. This leads us to

$$v = \bar{v} e^{i(\omega t + kx)}, \tag{6.41}$$

$$q = \bar{q} e^{i(\omega t + kx)}, \tag{6.42}$$

$$\delta\rho = \bar{\rho} e^{i(\omega t + kx)}, \tag{6.43}$$

$$\delta T = \bar{T} e^{i(\omega t + kx)}. \tag{6.44}$$

Here $\bar{X}$ represents the magnitude of the plane wave perturbation applied to the variable X. Applying these various substitutions to our four perturbed equations leads us to:

$$i\omega\bar{\rho} + ik\rho\bar{v} = 0, \tag{6.45}$$

$$i\omega\left[\left(\frac{\partial s}{\partial \rho}\right)_T \bar{\rho} + \left(\frac{\partial s}{\partial T}\right)_\rho \bar{T}\right] + ik\left[s\bar{v} + \frac{\bar{q}}{T}\right] = 0, \tag{6.46}$$

$$i\omega\rho\bar{v} + ik\left[\left(\frac{\partial p}{\partial \rho}\right)_T \bar{\rho} + \left(\frac{\partial p}{\partial T}\right)_\rho \bar{T}\right] = 0, \tag{6.47}$$

$$i\omega\tau\bar{q} + \bar{q} + ik\kappa\bar{T} = 0. \tag{6.48}$$

It can clearly be seen that the first of these equations, equation (6.45), gives $\bar{\rho}$ as a function of $\bar{v}$. Similarly, the fourth of these, equation (6.48), gives $\bar{T}$ as a function of $\bar{q}$.

Substituting the relationships from these equations into the two remaining equations, (6.47) and (6.46), whilst multiplying the first, (6.47), by k leads to the following two intermediate equations:

$$\left[\omega - \frac{k^2}{\omega}\left(\frac{\partial p}{\partial \rho}\right)_T\right](\rho \bar{v} k) - \left(\frac{i\omega\tau + 1}{i\kappa}\right)(k\bar{q})\left(\frac{\partial p}{\partial T}\right)_\rho = 0, \tag{6.49}$$

$$(\rho k \bar{v})\left[\rho\left(\frac{\partial s}{\partial \rho}\right)_T - s\right] - (k\bar{q})\left[\frac{1}{T} - \frac{\omega\,(i\omega\tau + 1)}{i\kappa k^2}\left(\frac{\partial s}{\partial T}\right)_\rho\right] = 0. \tag{6.50}$$

At this point we consider the partial differentials and whether substitutions for known quantities can be found for any of them. To this end we consider the speed of the first sound in the medium, c_0. If we consider that only a pure sound wave is present, then we can assume that $q = 0$, as any heat flow in a super-fluid is related to the second sound[49]. The absence of heat flow implies uniform temperature[200], so we can assume that $\delta T = 0$. If we apply this to the second of our intermediate equations, (6.50), we arrive at

$$\frac{\omega^2}{k^2} = \left(\frac{\partial p}{\partial \rho}\right)_T \equiv c_0^2, \tag{6.51}$$

by the usual definition for the speed of the first first sound.

We next consider the case where, as a first approximation, heat is transferred solely by thermal diffusion. This implies that there is no thermal relaxation time, so $\tau = 0$. Further, no heat is transferred by convection, hence $\bar{v} = 0$. If we substitute these assumptions into the first of our intermediate equations, (6.49), we obtain

$$\frac{1}{T} - \frac{\omega}{i\kappa k^2}\left(\frac{\partial s}{\partial T}\right)_\rho = 0. \tag{6.52}$$

But the standard definition of specific heat capacity, c_v, is given by [160]

$$c_v = T\left(\frac{\partial s}{\partial T}\right), \tag{6.53}$$

with all other variables held constant. So the specific heat capacity can be written as

$$c_v = \frac{i\kappa k^2}{\omega}. \tag{6.54}$$

At this juncture it is also convenient to introduce two new constants. The first is a 'thermal diffusivity' term[1] χ, which we define by

$$\chi = \frac{\kappa}{c_v}. \tag{6.55}$$

The second term is a diffusion time,

$$t_d = \left|\frac{1}{\omega}\right|. \tag{6.56}$$

It should be noted that in both the case of the thermal diffusivity and diffusion time, the ω referred to relates to the diffusive case discussed above and not to the general case. So, in general, $\omega t_d \neq 1$.

This also gives us a relation between the thermal diffusivity and the diffusion time,

$$t_d = \frac{1}{k^2\chi} = \frac{c_v}{\kappa k^2}. \tag{6.57}$$

Including these new constants in the two intermediate equations, (6.49) and (6.50), leads us to

$$\frac{k^2}{\omega}\left[\frac{\omega^2}{k^2} - c_0^2\right](\rho k\bar{v}) + \frac{i}{\kappa}\left(\frac{\partial p}{\partial T}\right)_s (1 + i\omega\tau)(k\bar{q}) = 0, \tag{6.58}$$

$$\left[\left(\frac{\partial s}{\partial \rho}\right)_T - \frac{s}{\rho}\right](\rho k\bar{v}) - \frac{1}{T}\left[1 + i\omega t_d\,(1 + i\omega\tau)\right](k\bar{q}) = 0. \tag{6.59}$$

We can now combine these two equations, which, after some manipulation, gives the dispersion relation

$$\begin{aligned}&\left[\frac{\omega^2}{k^2} - c_0^2\right]\left[1 + i\omega t_d\,(1 + i\omega\tau)\right] \\ &+ \frac{i\omega}{\kappa k^2}\left(\frac{\partial p}{\partial T}\right)_s (1 + i\omega\tau)\left[\left(\frac{\partial s}{\partial \rho}\right)_T - \frac{s}{\rho}\right] = 0.\end{aligned} \tag{6.60}$$

Before progressing to a more general solution to the stability of a static background, we solve the simpler, purely diffusive case for pure sound waves. Here the relaxation time,

[1] We define this term, for convenience, using the specific heat capacity, rather than the standard definition which uses the volumetric heat capacity[201].

τ is zero. We shall assume that the diffusion time is sufficiently large such that $\omega t_d \gg 1$. So, we are able to divide through by $i\omega t_d$. This reduces equation (6.60) to

$$\left[\left(\frac{\omega}{k}\right)^2 - c_0^2\right]\left(1 - \frac{i}{\omega t_d}\right) + \frac{T}{t_d \kappa k^2}\left(\frac{\partial p}{\partial T}\right)_\rho \left[\left(\frac{\partial s}{\partial \rho}\right)_T - \frac{s}{\rho}\right] = 0. \tag{6.61}$$

As we are now discussing the purely diffusive case, we can no longer assume zero heat flow. Under these circumstances, the previously stated identity for the speed of sound no longer applies. Instead, it would be more accurate to write

$$\frac{\omega}{k} \sim c_0. \tag{6.62}$$

It is more useful to interpret this as

$$\frac{\omega}{k} = c_0\left(1 + a + ib\right), \qquad (a, b \ll 1), \qquad (a, b \in \Re). \tag{6.63}$$

This leads us to the (first order in a and b) approximation

$$\left[\left(\frac{\omega}{k}\right)^2 - c_0^2\right] = 2c_0^2\left(a + ib\right), \tag{6.64}$$

which enables us to express ω, to first order again, by

$$\frac{1}{\omega t_d} \sim \frac{(1 - a - ib)}{k c_0 t_d}. \tag{6.65}$$

Here we note that, in the case of the plane wave perturbations applied in this exercise, growing solutions (instabilities) occur when the real part of $i\left(\omega t + kx\right)$ is positive, leading to exponential growth. If we assume that the wave number, k, is always real and positive, then we have instabilities when the imaginary part of ω is negative. Considering this, it can be seen that instabilities will only be observed if $b < 0$.

For convenience, we reproduce equation (6.61).

$$\left[\left(\frac{\omega}{k}\right)^2 - c_0^2\right]\left(1 - \frac{i}{\omega t_d}\right) + \frac{T}{t_d \kappa k^2}\left(\frac{\partial p}{\partial T}\right)_\rho \left[\left(\frac{\partial s}{\partial \rho}\right)_T - \frac{s}{\rho}\right] = 0. \tag{6.66}$$

We note that the second term in this equation is wholly real. Hence, the first term must also be wholly real. Using this and making the substitutions suggested above, we have

$$\left[\left(\frac{\omega}{k}\right)^2 - c_0^2\right](1 + i\omega t_d) = 2c_0^2\left[\left(a + \frac{b}{kc_0 t_d}\right) + i\left(b - \frac{a}{kc_0 t_d}\right)\right]. \tag{6.67}$$

Having already established that the right hand side of this equality must be real, it follows that the imaginary part of the left hand side must be zero. This can only be the case if

$$b = \frac{a}{kc_0 t_d}. \tag{6.68}$$

As all of the constants used here are positive, this also reveals that a and b must share the same sign. This tells us that it is sufficient to solve for a to find if there are instabilities present. So we can substitute for b into equation (6.67), obtaining

$$2c_0^2\left(a + \frac{a}{kc_0 t_d}\frac{1}{kc_0 t_d}\right) + \frac{T}{k^2\kappa t_d}\left(\frac{\partial p}{\partial T}\right)_\rho\left[\left(\frac{\partial s}{\partial \rho}\right)_T - \frac{s}{\rho}\right] = 0. \tag{6.69}$$

As we previously stated that $\omega t_d \gg 1$, then we can make the approximation that

$$\left(\frac{1}{kc_0 t_d}\right)^2 \ll 1. \tag{6.70}$$

Substituting this into preceding equation, (6.69), and making the earlier substitution for heat capacity, (6.54), gives us

$$a \sim -\frac{T}{2c_v i c_0^2}\left(\frac{\partial p}{\partial T}\right)_\rho\left[\left(\frac{\partial s}{\partial \rho}\right)_T - \frac{s}{\rho}\right]. \tag{6.71}$$

Upon initial inspection this gives us no real clue as to the sign of a. This is because, in our rather naive model, we have made no mention of the relationship between pressure and temperature or of that between the density of the massive component and entropy density. Intuitively, as well as from the gas laws (Amonton's Law), it is reasonable to assume that pressure increases in some manner with increasing temperature. We further assume that entropy does not substantially depend upon the density of the massive component. This leads us to the conclusion that a is always positive and so, in the diffusion only case, the pure sound wave perturbations are always stable.

We return to a more general dispersion relation for our static background. To make this easier to follow, we here reproduce equation (6.60).

$$\left[\frac{\omega^2}{k^2} - c_0^2\right][1 + i\omega t_d\,(1 + i\omega\tau)] + \frac{i\omega}{\kappa k^2}\left(\frac{\partial p}{\partial T}\right)_s (1 + i\omega\tau)\left[\left(\frac{\partial s}{\partial \rho}\right)_T - \frac{s}{\rho}\right] = 0. \tag{6.72}$$

Since we are no longer dealing with a purely dispersive case, we must assume that we have a non-zero thermal relaxation time. It is also convenient, and serves to condense the algebra, if we introduce a phase velocity, σ, for our perturbations. This is defined by

$$\sigma = \frac{\omega}{k}. \tag{6.73}$$

Clearly, as k is assumed to be always real and positive, the real and imaginary parts of σ will always have the same sign as ω.

For further convenience, we can condense equation (6.72) by defining

$$A = \frac{T}{\kappa k}\left(\frac{\partial p}{\partial T}\right)_\rho \left[\frac{s}{\rho} - \left(\frac{\partial s}{\partial \rho}\right)_T\right].$$

So, with a little manipulation, equation (6.72) becomes

$$\left(\sigma^2 - c_0^2\right)\left[\left(k^2\sigma^2 t_d\tau\right) - ik\sigma t_d - 1\right] + i\sigma\,(1 + ik\sigma\tau)\,A = 0. \tag{6.74}$$

Since we have already established the first sound as stable solutions, we shall assume that any further solutions represent second sound waves. We, therefore, assume that the speed of these solutions is much lower than that of pure sound waves. From this, we can make use of the approximation that $\sigma^2 \ll c_0^2$, and so we can rewrite the above equation, (6.74), as

$$\sigma^2\left(k^2 t_d\tau + \frac{k\tau A}{c_0^2}\right) - i\sigma\left(kt_d + \frac{A}{c_0^2}\right) - 1 = 0. \tag{6.75}$$

We can, with some justification, assume that $kt_d \gg A/c_0^2$. And, recalling our definition for thermal diffusivity, χ, the quadratic in σ, equation (6.75), becomes

$$\sigma^2 - \frac{i}{k\tau}\sigma - \frac{\chi}{\tau} = 0. \tag{6.76}$$

This solves to

$$\sigma = \frac{1}{k\tau}\left(\frac{i}{2} \pm \sqrt{\frac{-1}{4} + k^2\tau\chi}\right). \tag{6.77}$$

We note that $k^2\tau\chi$ is always positive. Here there are three 'families' of solutions dependent on the value of $k^2\tau\chi$:

i) $k^2\tau\chi < 1/4$. This gives two oscillation free solutions, both of which decay exponentially with time.

ii) $k^2\tau\chi = 1/4$. This gives a single oscillation free solution which decays exponentially with time.

iii) $k^2\tau\chi > 1/4$. This gives two, out of phase, wave solutions of the same frequency, which decay exponentially at the same rate.

There are no growing solutions in this model and, hence, there are no instabilities inherent to the two component model in the static background. Our model also suggests that wave solutions only exist for wave numbers above the $k^2\tau\chi = 1/4$ threshold, dependent upon the relaxation time and the thermal diffusivity.

It is interesting to note that these Newtonian results are consistent with the relativistic two-stream results from Samuelsson et al[202], which also shows that the static case is dynamically stable. In the next section we consider the dynamical stability of a non-static (stationary) background.

6.3 Stationary Background with Zero Flow in the Massive Component

Here we consider the flow between two reservoirs as shown in Figure 6.1. As described, the background represents a stationary flow for the entropy with the massive component static. This represents a "half way house" between the static case above and a more general solution. As the background is no longer truly static, some of the previous assumptions will no longer apply. Therefore the mathematical treatment requires a rather different approach.

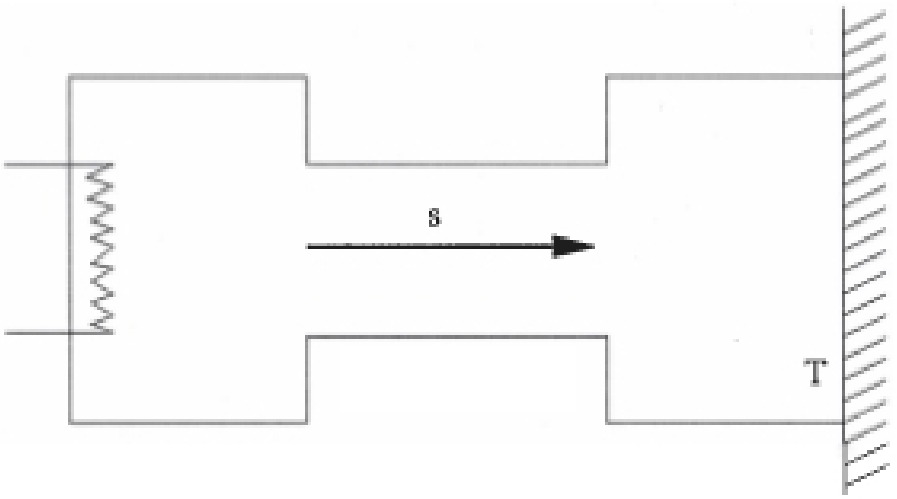

Figure 6.1: *Relative flow induced by "pumping" heat through a recipient containing He II. The heater on the left is the source, while the thermal bath on the right is the sink. The ^{4}He fluid is static (v_n =0) but there is stationary entropy flow ($v_s \neq 0$).* [8]

As in the static example, we take four "governing" equations from [192]. In common with the this static case, non-local terms are not included. In this case we use equation (6.27) rather than (6.24), as we believe the information is easier to manage in this form for the approach used in this section. In order to keep the algebra simple at this stage, we reproduce these equations here in a one dimensional form:

$$\partial_t \rho + \partial_x (\rho v) = 0, \tag{6.78}$$

$$\partial_t s + \partial_x (sv) + \partial_x (sw) = \frac{2\mathcal{R}}{T} \left(\frac{q}{sT}\right)^2 = \frac{2\mathcal{R}}{T} w^2, \tag{6.79}$$

$$\rho (\partial_t + v\partial_x) v + \partial_x p = 0, \tag{6.80}$$

$$\partial_t q + v\partial_x q + \frac{1}{\tau} q + 2q\partial_x v = -\frac{\kappa}{\tau} \partial_x T. \tag{6.81}$$

We first consider the background. We denote all variables in the background with the subscript 0. Since this is stationary, for any variable X_0 we have $\partial_t X_0 = 0$. Further, as the massive component is static, we have $v_0 = 0$. Substituting this into equations (6.78), (6.79), (6.80) and (6.81) gives us these relations in the background.

From (6.80) we have

$$\partial_x p_0 = 0. \tag{6.82}$$

And from (6.81) we recover Fourier's law

$$q_0 = -\kappa \partial_x T_0. \tag{6.83}$$

Since the fluid is stationary we can assume that the heat flow is constant. This leads to a linear temperature distribution in the background, so

$$T_0 = Ax + B, \tag{6.84}$$

and, hence

$$q_0 = -A, \tag{6.85}$$

Where A and B are real constants.

It is also reasonable to assume that the entropy at any point within the region under consideration remains constant. So we can make the assumption that the velocity of the entropy flow is the same across this region [2] and state that

$$\partial_x w_0 = 0. \tag{6.86}$$

Returning to our original equations, (6.78), (6.79), (6.80) and (6.81), we have four equations in eight unknowns. This assumes that we treat the conductivity, κ and the relaxation time, τ, as constants. It is necessary that we eliminate three of these unknowns.We start with the entropy density, s. We consider the entropy density of a phonon gas given by [43]

$$s = \frac{16\pi^5}{45} k_{\mathrm{B}} \left(\frac{k_{\mathrm{B}} T}{2\pi\hbar c_0} \right)^3 \left(1 - \frac{w^2}{c_0^2} \right), \tag{6.87}$$

where $\hbar$ is the reduced Planck constant and k_{B} is the Boltzmann constant. If we assume the relative velocity to be much lower than the speed of sound, $c_0 \gg w$, then we can simplify this expression to

[2] This is slight oversimplification and is made only to keep the algebra manageable. We discuss this later.

$$s = DT^3, \tag{6.88}$$

where

$$D = \frac{16\pi^5}{45}\frac{k_B^4}{(2\pi\hbar c_0)^3}. \tag{6.89}$$

Secondly, we can eliminate the resistive friction coefficient, $\mathcal{R}$, by using equation (6.19). Rearranging this and using the above substitution for s gives

$$\mathcal{R} = \frac{D^2T^7}{2\kappa}. \tag{6.90}$$

Thirdly, we address the pressure. We assume that there are two distinct parts to this pressure. One is associated with the massive component, which is assumed to be barotropic. This will be denoted by p_{Baro}. We can define small changes in this part of the pressure by

$$\delta p_{Baro} = \frac{\partial p}{\partial \rho}\delta\rho. \tag{6.91}$$

The other part, ψ, comes from the phonon gas pressure and is given by [43]

$$\psi = \frac{1}{4}DT^4. \tag{6.92}$$

Finally, the heat flow, q, needs to be considered. Whilst we have defined the background flow as $q = -\kappa A$, this will not apply to small perturbations of the fluid. To this end we use equation (6.15). Substituting for the entropy density gives

$$q = DT^4 w. \tag{6.93}$$

This leads to perturbations in q being given by

$$\delta q = DT_0^4\delta w + 4DT_0^3 w_0\delta T. \tag{6.94}$$

Before going further, it can be seen that applying these substitutions to equation (6.79) considerably simplifies the problem. Substituting for s and T gives

$$D\partial_t T^3 + D\partial_x\left(T^3 v\right) + D\partial_x\left(T^3 w\right) = \frac{D^2T^6w^2}{\kappa}. \tag{6.95}$$

This leads to

$$\begin{aligned} &3DT^2\partial_t T + DT^3\partial_x v + 3DT^2 v\partial_x T \\ &+ DT^3\partial_x w + 3DT^2 w\partial_x T = \frac{D^2T^6w^2}{\kappa}, \end{aligned} \tag{6.96}$$

which simplifies to

$$\begin{aligned} &3\partial_t T + T\partial_x v + 3v\partial_x T \\ &+ T\partial_x w + 3w\partial_x T - \frac{DT^4w^2}{\kappa} = 0. \end{aligned} \tag{6.97}$$

We are now in a position to apply small perturbations, such that $X = X_0 + \delta X$ to our starting equations, (6.78), (6.79), (6.80) and (6.81). This gives us

$$\partial_t\left(\rho_0 + \delta\rho\right) + \partial_x\left[\left(\rho_0 + \delta\rho\right)v_0 + \delta v\right] = 0, \tag{6.98}$$

$$\begin{aligned} &3\partial_t\left(T_0 + \delta T\right) + \left(T_0 + \delta T\right)\partial_x\left(v_0 + \delta v\right) + 3\left(v_0 + \delta v\right)\partial_x\left(T_0 + \delta T\right) \\ &+ \left(T_0 + \delta T\right)\partial_x\left(w_0 + \delta w\right) + 3\left(w_0 + \delta w\right)\partial_x\left(T_0 + \delta T\right) \\ &- \frac{D\left(T_0 + \delta T\right)^4\left(w_0 + \delta w\right)^2}{\kappa} = 0, \end{aligned} \tag{6.99}$$

$$\begin{aligned} &\left(\rho_0 + \delta\rho\right)\partial_t\left(v_0 + \delta v\right) + \left(\rho_0 + \delta\rho\right)\left(v_0 + \delta v\right)\partial_x\left(v_0 + \delta v\right) \\ &+ \partial_x\left(p_0 + \delta p\right) = 0, \end{aligned} \tag{6.100}$$

$$\begin{aligned} &\partial_t\left(q_0 + \delta q\right) + \left(v_0 + \delta v\right)\partial_x\left(q_0 + \delta q\right) + \frac{1}{\tau}\left(q_0 + \delta q\right) \\ &+ 2\left(q_0 + \delta q\right)\partial_x\left(v_0 + \delta v\right) + \frac{\kappa}{\tau}\partial_x\left(T_0 + \delta T\right) = 0. \end{aligned} \tag{6.101}$$

Making the suggested substitutions, eliminating background and zero terms, and linearising in perturbations yields

$$\partial_t \delta\rho + \rho_0 \partial_x \delta v = 0, \tag{6.102}$$

$$\begin{aligned} &3\partial_t \delta T + T_0 \partial_x \delta v + 3\delta v \partial_x T_0 + T_0 \partial_x \delta w \\ &+ 3w_0 \partial_x \delta T + 3\delta v \partial_x T_0 - \frac{2D}{\kappa} T_0^4 w_0 \delta w - \frac{4D}{\kappa} T_0^3 w_0^2 \delta T = 0, \end{aligned} \tag{6.103}$$

$$\rho_0 \partial_t \delta v + \rho_0 v_0 \partial_x \delta v + c_0^2 \partial_x \delta\rho + DT_0^3 \partial_x \delta T + 3DT_0^2 \delta T \partial_x T_0 = 0, \tag{6.104}$$

$$\begin{aligned} &DT_0^4 \partial_t \delta w + 4DT_0^3 w_0 \partial_t \delta T + \frac{1}{\tau} DT_0^4 \delta w \\ &\frac{4}{\tau} DT_0^3 w_0 \delta T - 2\kappa A \delta v + \frac{\kappa}{\tau} \delta T = 0. \end{aligned} \tag{6.105}$$

For the sake of tractability we assume that the perturbations applied are plane waves of the form $\delta X = \bar{X} \exp\left[i\left(\omega t + kx\right)\right]$, where $\bar{X}$ is the amplitude. We then introduce a phase velocity for these perturbations, $\sigma\,(= \omega/k)$. Our four perturbation equations become

$$0 = \sigma\bar{\rho} + \rho_0 \bar{v}, \tag{6.106}$$

$$\begin{aligned} 0 =& 3i\sigma\bar{T} + iT_0\bar{v} + \frac{3A}{k}\bar{v} + iT_0\bar{w} + 3iw_0\bar{T} \\ &+ \frac{3A}{k}\bar{w} - \frac{2DT_0^4 w_0}{\kappa k}\bar{w} - \frac{4DT_0^3 w_0^2}{\kappa k}\bar{T}, \end{aligned} \tag{6.107}$$

$$0 = i\sigma\rho_0\bar{v} + ic_0^2\bar{\rho} + iDT_0^3\bar{T} + \frac{3ADT_0^2}{k}\bar{T}, \tag{6.108}$$

$$\begin{aligned} 0 =& i\sigma DT_0^4\bar{w} + i4\sigma DT_0^3 w_0\bar{T} + \frac{DT_0^4}{\tau k}\bar{w} \\ &+ \frac{4DT_0^3 w_0}{\tau k} - i2\kappa A\bar{v} + \frac{i\kappa}{\tau}\bar{T}. \end{aligned} \tag{6.109}$$

We can now solve to obtain a dispersion relation for σ by simple Gaussian elimination. As previously, the solution will represent unstable perturbations if the imaginary part

of σ is negative. Before proceeding with a stationary solution, it is worthwhile to make a sanity check with regard to the previous static case. This can be achieved by setting A and w_0 to zero. Further, to be consistent with the previous calculation, we assume that the pressure contribution from the phonon gas, ψ, is insignificant when compared with that from the massive component, p_{Baro}. It is also useful, in this context, to find a substitution for D. Given our previous definition for the entropy we can express the heat capacity, c_v, as

$$c_v = T\left(\frac{\partial s}{\partial T}\right) = 3DT^3. \tag{6.110}$$

But in equation (6.55) we defined

$$c_v = \frac{\kappa}{\chi}. \tag{6.111}$$

So we can approximate D by

$$D \approx \frac{\kappa}{3\chi T_0^3}.$$

In this static case we obtain

$$\left(c_0^2 - \sigma^2\right)\left(\sigma^2 k\tau - \sigma - \chi k\right) = 0. \tag{6.112}$$

This is identical to our previous solution, equation (6.76) and tells us that all values of σ are stable. Having obtained the same solution through two differing methods reinforces the validity of our results.

We now return to the stationary case. We would first like to obtain w_0 in terms of the other parameters. This we can do from the early definition of heat flow, equation (6.15). From this we obtain

$$w_0 = \frac{-\kappa A}{DT_0^4} = \frac{-\kappa A}{D\left(Ax + B\right)^4}, \tag{6.113}$$

which approximates to a constant (which was our earlier assumption) for small A and x. So the previous statement that $\partial_x w_0 = 0$ is valid for small temperature gradients over short length scales.

If we apply this substitution, along with that for D, we arrive at a full dispersion relation for σ,

$$0 = \left(c_0^2 - \sigma^2\right)\left[-\sigma^2 T_0^2\tau + \sigma\left(\frac{iT_0^2}{k} + \frac{i24\chi\tau}{k} - A\chi T_0\tau\right) - \frac{i4A\chi T_0}{k} + \frac{24\chi A^2}{k^2} + \chi T_0^2\right]. \tag{6.114}$$

So we again have the speed of the first sound as two of the solutions. The remaining two solutions are given by

$$\begin{aligned}\sigma =& \frac{1}{2T_0^2 k\tau}\left[i\left(T_0^2 + 24\chi A^2\tau\right) - A\chi T_0 k\tau\right.\\ &\pm\left(-T_0^4 + 48T_0^2\chi A^2\tau - 576\chi^2A^4\tau^2 + A^2\chi^2T_0^2k^2\tau^2\right.\\ &\left.\left.+4T_0^4\tau\chi k^2 - i18T_0^3A\chi k\tau - i48\chi^2A^3\tau^2T_0k\right)^{1/2}\right].\end{aligned} \tag{6.115}$$

Whilst the behaviour of the fluid is not clear from this, there are some limiting cases that offer a measure of illumination. Firstly, we consider the short wavelength (high frequency) limit. Here, as $k \to \infty$, we have

$$\sigma \to \frac{-1}{2T_0\tau}\left(A\chi\tau \pm \sqrt{A^2\chi^2\tau^2 + 4T_0^2\chi\tau}\right). \tag{6.116}$$

It is clear that the discriminant of this solution is always positive. So, for very high k and its associated short wavelength, the perturbations are stable.

The second limiting case is that of small temperature gradient. Here we assume that $A \ll 1$ (Consistent with the assumption $\partial_x w_0 = 0$). This allows us to linearise in A and so equation (6.115) becomes

$$\begin{aligned}\sigma \approx& \frac{1}{2T_0^2 k\tau}\left[iT_0^2 - A\chi T_0 k\tau\right.\\ &\left.\pm\left(-T_0^4 + 4T_0^4\tau\chi k^2 - i18T_0^3A\chi k\tau\right)^{1/2}\right].\end{aligned} \tag{6.117}$$

Assuming that we have some relaxation time much greater than one second , we can further approximate using [3]

$$\tau\chi k^2 \gg 1, \tag{6.118}$$

Applying this to equation (6.117) gives us

$$\sigma \approx \frac{1}{2T_0^2 k\tau}\left[iT_0^2 - A\chi T_0 k\tau \pm 2T_0^2 k\sqrt{\tau\chi}\left(1 - i\frac{9A}{T_0 k}\right)^{1/2}\right]. \tag{6.119}$$

But we know that for some real positive number y

$$\Im\left(\sqrt{1-iy}\right) = -\frac{1}{2}\sqrt{2\sqrt{1+y^2}-2}. \tag{6.120}$$

For positive y, this is always negative. So the perturbations are unstable if

$$T_0^2 < \Im\left[2T_0^2 k\sqrt{\tau\chi}\left(1 - i\frac{9A}{T_0 k}\right)^{1/2}\right], \tag{6.121}$$

or (squaring both terms to remove the first layer of square roots)

$$T_0^4 < \left(4T_0^4 k^2\tau\chi\right)\left[\frac{1}{4}\left(2\sqrt{1+\frac{81A^2}{T_0^2 k^2}}\right) - 2\right]. \tag{6.122}$$

Rearranging gives

$$T_0^4\left(1+2k^2\tau\chi\right) < 2k^2 T_0^4\tau\chi\sqrt{1+\frac{81A^2}{T_0^2 k^2}}. \tag{6.123}$$

Linearising a binomial expansion in A^2 (justified for small A) and squaring, we have

$$\left(1+2k^2\tau\chi\right)^2 < \left(2k^2\tau\chi\right)^2\left(1+\frac{81A^2}{T_0^2 k^2} + \mathcal{O}\left(A^4\right)\right). \tag{6.124}$$

Which leads to

[3] This assumption is a little more involved than this. From equation (6.89), we have a value for D of approx 980 J K^{-4}. Equation (6.55), shows that the value of χ depends on T^{-3} and the thermal conductivity, κ. Regardless of the relaxation time, this restricts the range of k to which this approximation can be applied, making it valid only for k greater than some critical value. This assumption is valid for the greatest range of k in a low temperature fluid possessing high thermal conductivity.

$$1 + 4k^2\tau\chi < \frac{162\tau\chi A^2}{T_0^2}. \tag{6.125}$$

This tells us that the perturbations are unstable for temperature gradients, A, such that

$$A > \sqrt{\frac{1 + 4k^2\tau\chi T_0^2}{162\tau\chi}}. \tag{6.126}$$

This can be further simplified if we again use the assumption (6.118) that $\tau\chi k^2 \gg 1$. This yields

$$A > \frac{\sqrt{2}kT_0}{9}, \tag{6.127}$$

or, more usefully

$$k < \frac{9\sqrt{2}A}{2T_0}. \tag{6.128}$$

Since we have assumed that A is small, we have shown that the instabilities of the described background occur only at very long wavelengths. It is possible that, at such frequencies, some of the assumptions made (particularly that w_0 is a constant) are not valid. It is also unclear as to whether, with the assumption of small x, these low frequency instabilities lie within the regime our model covers.

This does, however, serve as a first proof of principle that the two-stream instability might manifest as a thermodynamical instability when heat flows in a fluid. It remains to find a way such that the simplifications do not exclude the range of wavelengths where the instabilities seem most likely to be observed.

6.4 The Problems Associated with a more General Case

After calculating the stability of the special cases, we would like to consider a more general case. Here, we look at some 1-d region of the fluid, where the temperatures at the ends of this region are kept constant. The mechanism by which this is achieved does not concern us. The important difference with the previous example is that both components of the fluid are free to flow. Again, if the system is left to 'settle' for a long period, we can assume that the background will be stationary.

This initially appears to be a relatively simple extension of the earlier examples. The only immediately obvious difference being that $v_0 \neq 0$. Unfortunately, the analysis is far more complicated than this and many of the previous assumptions are no longer valid.

The major problem arises from the temperature gradient. Since we have two flows in the background, we can no longer really justify the heat flow being constant at all points. As such, we can no longer assume that the temperature gradient is linear over the region under consideration. Two possible solutions to this issue were tried each of which presented their own issues.

The first was that, as a simplifying approximation, a linear gradient was simply imposed on the fluid in the background. This was initially alluring but it quickly became apparent that this condition made the combination of a consistent background and a soluble problem impossible. Here we briefly discuss the approach followed and the inconsistencies that resulted.

To maintain some degree of tractability, it is clear that we would like the gradient of as many variables as possible to be zero. By imposing a linear temperature gradient and assuming Fourier's Law, we have $\partial_x q_0 = 0$. We further adopted the approximations that both p_0 and ρ_0 were spatially constant. From equation (6.78), this led to

$$\partial_x v_0 = 0. \tag{6.129}$$

However, when the substitution $s = DT^3$ was applied to equation (6.79), we arrived at values for both v_0 and w_0 that were dependent upon non linear powers of T_0. This inconsistency made it necessary to linearise in T_0 and we were forced to assume that the temperature gradient could on be regarded as linear on small length scales. When we continued, instabilities were shown to manifest only at low frequencies. It was unclear whether that these instabilities were a genuine phenomenon or simply a result of the linearising approximations we made. Even if they could be shown to be genuine, it is again unclear if the length scales used to linearise T_0 encompasses these longer wavelength instabilities.

The second approach was considerably more involved. It was suggested that by injecting energy continuously along the region under consideration, a linear temperature distribution might be imposed. This approach did not lead to any results as it was necessary to first have the initial temperature distribution, which was not known.

In summary, although we failed to establish a general case for this class of thermodynamical instability, we did demonstrate a first proof of principle of its existence in a limited stationary background.

Given the ubiquitous nature of the two-stream instability it was certainly a worthwhile exercise to investigate it in the context of causal heat flow. The similarities between the governing equations for such heat flow and those for a simple two fluid case, it still seems likely that this instability can still be demonstrated.

The difficulties in the problem, distinct from the two fluid case, arose because of allowing for increasing entropy. Even in the case where the flow of the massive component in the background was restricted to zero, this presented difficulty. This led to a number of assumptions and linear approximations that restricted the validity of the analysis to shorter wavelengths, where we had shown the perturbations to be stable.

The major issue that was encountered involved developing a background state that was self consistent but tractable to analysis. Clearly the simplest background state would to have all variables constant, both spatially and temporally. This, of course, gave us a static background where the system was shown to be stable.

The introduction of entropy flow into the background immediately led to difficulties, as this affected all of the other parameters, with the exception of the flow of the massive component. The main issue arose from the need to find a substitution for the entropy density in terms of the other variables. The use of the phonon gas model, whilst initially appealing, gave to numerous terms that were non-linear in temperature. The use of linear approximations maintained relative simplicity at the expense of restricting the regime where the solutions apply.

Considering the time that went into this problem, the paucity of results at first appears disappointing. However, we have identified why the problem presents so many difficulties. It is hoped that the problem may be addressed at some future time with many of the pitfalls already known.

Chapter 7

Summary and Discussion

The aim of this thesis has been throughout to consider whether some characteristics of neutron star physics might be modelled in terrestrial laboratories. This appears to be a sadly neglected area where researchers from different disciplines have been unaware of applications of their work outside of their own area of speciality. As can be seen from the literature cited in Chapter 2, the range of analogous behaviour between low temperature physics and astrophysics is enormous. As stated, the review of possible analogues is by no means comprehensive. To discuss in any detail all of these methods for modelling neutron star behaviour is well beyond the scope of a single thesis.

It was decided that it was better to focus on a single feature and to consider in more detail its role in neutron star behaviour and that of any possible analogue systems. The feature chosen was the two-stream instability, which previous research had shown was likely to be important in the understanding of neutron star physics [2]. The study of this instability in neutron stars was worthwhile in itself as it was believed that it may play a role in triggering neutron star glitches [7]. This instability is a widespread phenomenon, manifesting in many areas of physics including: plasma physics [57]; cosmology [203]; superfluid Helium [8]; and pulsar magnetospheres [204]. The ubiquitous nature of this instability suggests that it is likely to be found in almost any two component system that we might chose to model neutron star cores.

With this in mind, in Chapter 3 we showed that previously observed dynamical instabilities in binary Bose-Einstein Condensates [6] were a variant of the two-stream instability. By using the hydrodynamic equations for a two component condensate, we showed that there existed a critical relative velocity for the onset of this instability. Whilst showing that a binary condensate was mathematically analogous to a chemically coupled two component fluid, attempts to model entrainment in Bose-Einstein Condensates proved more difficult. The problems arose not in the mathematics, where it was a relatively

simple task to produce the governing equations for the binary condensate. It is the physical realisation of these governing equations into a working model that still presents us with a problem. It is to be hoped the foundations laid here be built upon to fully realise a solution.

In Chapter 4, we considered some of the implications of the two-stream instability for actual neutron star physics. By considering a differentially rotating two component fluid, we showed that the instability could locally stimulate growth in the r-modes. It was seen that, if these local instabilities were sufficiently widespread and growth was rapid enough to overcome any damping effects, this might act as a trigger mechanism for pulsar glitches through vortex unpinning. In an example of serendipity, our research in this area also found a previously unknown secular instability which drifts into the regime of dynamical instability with increasing differential rotation.

Having established an important consequence of the two-stream instability in neutron stars, we considered in Chapter 5 whether it might be possible to find an analogue for this in superfluid Helium. Here we observed some of the limitations of an apparently appealing analogue. It was seen that the mutual friction parameters for the two fluid model of Helium did not fall within the range required for the instability to manifest. So we showed that, even though two physical systems might appear qualitatively similar, they will not necessarily be quantitatively close enough to serve as analogues for each other. It remains the case that some other fluid/superfluid combination may produce better results.

Finally, in Chapter 6, we attempted to extend the scope of the two-stream instability into the realm of heat flow. This represents a natural extension of variational multi-fluid dynamics. It also proved the most frustrating topic included in this thesis, in that the large amount of time invested failed to produce results for a general case. We were, however, able to produce results for special cases and establish, in principle, that a thermodynamical instability becomes manifest at some critical temperature gradient in a fluid.

Overall, in this thesis we have extended the realm of the two-stream instability into the areas of Bose-Einstein Condensates and heat flow; we have shown that, by applying it to differential rotation, it produces r-mode instabilities which might act as triggers for pulsar glitches; and we have demonstrated a wide range of analogues for neutron star physics, highlighting their possible applications along with some of their limitations.

References

[1] J. Kistemaker. The vapour pressure of liquid helium from the λ-point to 1.3 K. *Physica*, 12:272–280, August 1946.

[2] N. Andersson, G. L. Comer, and R. Prix. The superfluid two-stream instability. *Monthly Notices of the Royal Astronomical Society*, 354:101–110, October 2004.

[3] J. S. Tsakadze and S. J. Tsakadze. PHYSICS OF OUR DAYS: Superfluidity in pulsars. *Soviet Physics Uspekhi*, 18:242–250, March 1975.

[4] C. F. Barenghi, R. J. Donnelly, and W. F. Vinen. Thermal excitation of waves on quantized vortices. *Physics of Fluids*, 28:498–504, February 1985.

[5] W. F. Vinen. Mutual Friction in a Heat Current in Liquid Helium II. I. Experiments on Steady Heat Currents. *Royal Society of London Proceedings Series A*, 240:114–127, April 1957.

[6] P.T. Leung C.K. Law, C.M. Chan and M.C.Chu. Critical velocity in a binary mixture of moving bose condensates. *Physical Review A*, 63(063612), 2001.

[7] K. Glampedakis and N. Andersson. Hydrodynamical Trigger Mechanism for Pulsar Glitches. *Physical Review Letters*, 102(14):141101–+, April 2009.

[8] G.L. Prix, R. Comer and N. Andersson. Two-stream instability in superfluid helium. *In Preparation.*

[9] N. Andersson, K. Glampedakis, and M. Hogg. Superfluid instability of r-modes in "differentially rotating" neutron stars. *Physics Review D*, 87(6):063007, March 2013.

[10] S. Shapiro and S. Teukolsky. *Black Holes, White Dwarfs and Neutron Stars.* John Wiley and Sons, 1983.

[11] W. Baade and F Zwicky. Remarks on super-novae and cosmic rays. *Physical Review Letters*, 46(1):76–77, 1934.

[12] J. R. Oppenheimer and G. M. Volkoff. On Massive Neutron Cores. *Physical Review*, 55:374–381, February 1939.

[13] V. A. Ambartsumyan and G. S. Saakyan. The Degenerate Superdense Gas of Elementary Particles. *Astronomicheskii Zhurnal*, 37:193, 1960.

[14] T. Hamada and E. E. Salpeter. Models for Zero-Temperature Stars. *Astro-Physical Journal*, 134:683, November 1961.

[15] A. G. Cameron. Neutron Star Models. *Astro-Physical Journal*, 130:884, November 1959.

[16] R. Giacconi, H. Gursky, F. R. Paolini, and B. B. Rossi. Evidence for x rays from sources outside the solar system. *Physical Review Letters*, 9:439–443, Dec 1962.

[17] H. Gursky, R. Giacconi, F. R. Paolini, and B. B. Rossi. Further Evidence for the Existence of Galactic x Rays. *Physical Review Letters*, 11:530–535, December 1963.

[18] M. Schmidt. 3C 273 : A Star-Like Object with Large Red-Shift. *Nature*, 197:1040, March 1963.

[19] E. E. Salpeter. Superdense Equilibrium Stars. page 393, 1965.

[20] A. Hewish, S. J. Bell, J. D. H. Pilkington, P. F. Scott, and R. A. Collins. Observation of a Rapidly Pulsating Radio Source. *Nature*, 217:709–713, February 1968.

[21] T. Gold. Rotating Neutron Stars as the Origin of the Pulsating Radio Sources. *Nature*, 218:731–732, May 1968.

[22] F. Hoyle, J. V. Narlikar, and J. A. Wheeler. Electromagnetic Waves from Very Dense Stars. *Nature*, 203:914–916, August 1964.

[23] S. Tsuruta and A. G. W. Cameron. Cooling and detectability of neutron stars. *Canadian Journal of Physics*, 44:1863, 1966.

[24] S. Tsuruta and A. G. W. Cameron. Some effects of nuclear forces on neutron-star models. *Canadian Journal of Physics*, 44:1895, 1966.

[25] L. Woltjer. X-Rays and Type i Supernova Remnants. *Astro-Physical Journal*, 140:1309–1313, October 1964.

[26] J. A. Wheeler. Superdense Stars. *Annual Review of Astronomy and Astro-Physics*, 4:393, 1966.

[27] F. Pacini. Energy Emission from a Neutron Star. *Nature*, 216:567–568, November 1967.

[28] V. L. Ginzburg and V. V. Zaitsev. Magnetic Models of Pulsars and Rotating Neutron Stars. *Nature*, 222:230–231, April 1969.

[29] P. E. Reichley and G. S. Downs. Observed Decrease in the Periods of Pulsar PSR 0833-45. *Nature*, 222:229–230, April 1969.

[30] A. G. Lyne, S. L. Shemar, and F. G. Smith. Statistical studies of pulsar glitches. *Mon. Not. R. Astron Soc.*, 315:534–542, July 2000.

[31] S. L. Shemar and A. G. Lyne. Observations of pulsar glitches. *Mon. Not. R. Astron Soc.*, 282:677–690, September 1996.

[32] M. Ruderman. Crust-breaking by neutron superfluids and the VELA pulsar glitches. *Astrophysical Journal*, 203:213–222, January 1976.

[33] M. Ruderman. Neutron Starquakes and Pulsar Periods. *Nature*, 223:597–598, August 1969.

[34] F. Crawford and M. Demiański. A Comparison of Measured Crab and Vela Glitch Healing Parameters with Predictions of Neutron Star Models. *Astrophysical Journal*, 595:1052–1057, October 2003.

[35] M. A. Alpar and C. Ho. Expectancy of large pulsar glitches. *Mon. Not. R. Astron. Soc*, 204:655–667, August 1983.

[36] P. W. Anderson and N. Itoh. Pulsar glitches and restlessness as a hard superfluidity phenomenon. *Nature*, 256:25–27, July 1975.

[37] M. A. Alpar, H. F. Chau, K. S. Cheng, and D. Pines. Postglitch Relaxation of the Crab Pulsar after Its First Four Major Glitches: The Combined Effects of Crust Cracking, Formation of Vortex Depletion Region and Vortex Creep. *Astrophysical Journal*, 459:706, March 1996.

[38] C. M. Espinoza, A. G. Lyne, B. W. Stappers, and M. Kramer. A study of 315 glitches in the rotation of 102 pulsars. *Mon. Not. R. Astron Soc.*, 414:1679–1704, June 2011.

[39] A.L. Potekhin. The physics of neutron stars. *Usp. Fiz. Nauk*, 2010.

[40] P. B. Demorest, T. Pennucci, S. M. Ransom, M. S. E. Roberts, and J. W. T. Hessels. A two-solar-mass neutron star measured using Shapiro delay. *Nature*, 467:1081–1083, October 2010.

[41] J. M. Lattimer and M. Prakash. Neutron Star Structure and the Equation of State. *Astro Physical Journal*, 550:426–442, March 2001.

[42] W.C.G. Ho & G.O. Heinke. A Neutron Star with a Carbon Atmosphere in the Cassiopeia A Supernova Remnant. *Nature*, (462):71–73, 2009.

[43] B. Haskell N. Andersson and G.L. Comer. r-modes in low temerature colour-flavour locked superconducting quark stars. *Physics Review D*, 82(023007), 2010.

[44] M. A. Alpar, D. Pines, P. W. Anderson, and J. Shaham. Vortex creep and the internal temperature of neutron stars. I - General theory. *Astrophysical Journal*, 276:325–334, January 1984.

[45] D. Pines and M. A. Alpar. Superfluidity in Neutron Stars. *Nature*, 316:27–32, July 1985.

[46] D. G. Yakovlev, W. C. G. Ho, P. S. Shternin, C. O. Heinke, and A. Y. Potekhin. Cooling rates of neutron stars and the young neutron star in the Cassiopeia A supernova remnant. *Mon. Not. R. Astro. Soc.*, 411:1977–1988, March 2011.

[47] S.K. Putterman. *Superfluid Hydrodynamics*. North Holland Publishing Company, London, 1974.

[48] W.H. Li and S.H. Lam. *Principles of Fluid Mechanics*. Addison-Wesley Publishing Company, Reading, Massachusetts, 1964.

[49] I.M. Khalatnikov. *An Introduction to the Theory of Superfluidity*. Perseus Publishing, Massachusetts, 1965.

[50] D.L. Goodstein. *States of Matter*. Prentice Hall, New Jersey, 1975.

[51] J. F. Allen and A. D. Misener. Flow Phenomena in Liquid Helium II. *Nature*, 142:643–644, October 1938.

[52] P. Kapitza. Viscosity of Liquid Helium below the λ-Point. *Nature*, 141:74, January 1938.

[53] L. Landau. Theory of the superfluidity of helium ii. *Phys. Rev.*, 60:356–358, Aug 1941.

[54] R. J Donnelly. *Quantised Vortices in Helium II*. Cambridge University Press, 1991.

[55] J. Serrin. Mathematical Principles of Classical Fluid Mechanics. *Handbuch der Physik*, 8:125–263, 1959.

[56] L. J. Campbell and R. M. Ziff. Vortex patterns and energies in a rotating superfluid. *Physics Review B*, 20:1886–1902, September 1979.

[57] D. T. Farley. Two-Stream Plasma Instability as a Source of Irregularities in the Ionosphere. *Physical Review Letters*, 10:279–282, April 1963.

[58] J. C. Weatherall. Streaming instability in relativistically hot pulsar magnetospheres. *Astrophysical Journal*, 428:261–266, June 1994.

[59] H Helmholtz. On the Discontiuous Movements of Fluids. *Monatsberichte der Königlichen Preussische Akademie Wissenschafen zu Berlin*, 23:215–228, 1868.

[60] G. Joos. *Theoretical Physics*. Dover Publications Inc, New York, 1986.

[61] N. Andersson and G.L. Comer. Entropy entrainment and dissipation in finite temperrature superfluids. *arXiv:0811.1660v3*, 2009.

[62] M. Prakash, J. M. Lattimer, and T. L. Ainsworth. Equation of state and the maximum mass of neutron stars. *Physical Review Letters*, 61:2518–2521, November 1988.

[63] M. Prakash, J. M. Lattimer, and T. L. Ainsworth. Equation of state and the maximum mass of neutron stars. *Physical Review Letters*, 61:2518–2521, November 1988.

[64] I. Hawke, G. L. Comer, and N. Andersson. The nonlinear development of the relativistic two-stream instability. *Classical and Quantum Gravity*, 30(14):145007, July 2013.

[65] N. Andersson, T. Sidery, and G. L. Comer. Superfluid neutron star turbulence. *Mon. Not. R. Astron. Soc*, 381:747–756, October 2007.

[66] T. Sidery, N. Andersson, and G. L. Comer. Waves and instabilities in dissipative rotating superfluid neutron stars. *Mon. Not. R. Astron. Soc*, 385:335–348, March 2008.

[67] N. Andersson and K. D. Kokkotas. The R-Mode Instability in Rotating Neutron Stars. *International Journal of Modern Physics D*, 10:381–441, 2001.

[68] R. Prix, G. L. Comer, and N. Andersson. Slowly rotating superfluid Newtonian neutron star model with entrainment. *Astronomy and Astrophysics*.

[69] L. Tisza. The Theory of Liquid Helium. *Physical Review*, 72:838–854, November 1947.

[70] G. Baym, C. Pethick, and D. Pines. Superfluidity in Neutron Stars. *Nature*, 224:673–674, November 1969.

[71] E. Lohsen. Second Speed-up of the Crab Pulsar. *Nature Physical Science*, 236:70–71, April 1972.

[72] D. S. Tsakadze and S. D. Tsakadze. Simulation of pulsar behavior in a low-temperature laboratory /Review/. *Astrofizika*, 15:533–547, July 1979.

[73] M. Ruderman. Long Period Oscillations in Rotating Neutron Stars. *Nature*, 225:619–620, February 1970.

[74] E. L. Andronikashvili and Y. G. Mamaladze. *Review of Modern Physics*, 38:567, 1966.

[75] L. D. Landau. On the theory of stars. *Phys. Z. Sowjetunion*, 1:285, 1932.

[76] A. B. Migdal. *Zh. Eskp. Teor. Fiz.*, 37:249, 1959.

[77] V. L. Ginzburg and D. A. Kirzhnits. *Zh. Eskp. Teor. Fiz.*, 47:2006, 1964.

[78] D. Pines. Proceedings of the twelfth international conference on low temperature physics. Kyoto(Japan), 1971.

[79] S.J. Tsakadze and J.S. Tsakadze. Measurement of the relaxation time on acceleration of vessels with helium ii and superfluidity in pulsars. *Soviet Physics - JEPT*, 37(5), 1973.

[80] J. S. Tsakadze and S. J. Tsakadze. Relaxation phenomena at accelaration of rotation of a spherical vessel with helium II and relaxation in pulsars. *Physics Letters A*, 41:197–199, September 1972.

[81] D. S. Tsakadze and S. D. Tsakadze. "Spontaneous" acceleration of freely rotating helium II and related phenomena in pulsars. *Soviet Journal of Experimental and Theoretical Physics Letters*, 22:139, September 1975.

[82] J. S. Tsakadze and S. J. Tsakadze. PHYSICS OF OUR DAYS: Superfluidity in pulsars. *Soviet Physics Uspekhi*, 18:242–250, March 1975.

[83] J.S. Tsakadze and Z.S. Nadirashvili. Investigation of the properties ot a rotating he3-he4 solution by the oscillating-disk method. *Soviet Physics JETP*, 45(1):96–100, 1977.

[84] C.J. Pethick and H. Smith. *Bose-Einstein Condensation in Dilute Gases*. Cambridge University Press, Cambridge, England, 2004.

[85] M. H. Anderson, J. R. Ensher, M. R. Matthews, C. E. Wieman, and E. A. Cornell. Observation of Bose-Einstein Condensation in a Dilute Atomic Vapor. *Science*, 269:198–201, July 1995.

[86] C. J. Myatt, E. A. Burt, R. W. Ghrist, E. A. Cornell, and C. E. Wieman. Production of Two Overlapping Bose-Einstein Condensates by Sympathetic Cooling. *Physical Review Letters*, 78:586–589, January 1997.

[87] E. A. Cornell and C. E. Wieman. Nobel Lecture: Bose-Einstein condensation in a dilute gas, the first 70 years and some recent experiments. *Reviews of Modern Physics*, 74:875–893, August 2002.

[88] D. S. Jin, J. R. Ensher, M. R. Matthews, C. E. Wieman, and E. A. Cornell. Collective Excitations of a Bose-Einstein Condensate in a Dilute Gas. *Physical Review Letters*, 77:420–423, July 1996.

[89] W. Vincent Liu. Theoretical Study of the Damping of Collective Excitations in a Bose-Einstein Condensate. *Physical Review Letters*, 79:4056–4059, November 1997.

[90] P. O. Fedichev, G. V. Shlyapnikov, and J. T. M. Walraven. Damping of Low-Energy Excitations of a Trapped Bose-Einstein Condensate at Finite Temperatures. *Physical Review Letters*, 80:2269–2272, March 1998.

[91] N.K. Glendenning. *Compact Stars*. Spinger-Verlag, New York, 2000.

[92] M. R. Matthews, B. P. Anderson, P. C. Haljan, D. S. Hall, C. E. Wieman, and E. A. Cornell. Vortices in a Bose-Einstein Condensate. *Physical Review Letters*, 83:2498–2501, September 1999.

[93] R. I. Epstein and G. Baym. Vortex pinning in neutron stars. *Astrophysical Journal*, 328:680–690, May 1988.

[94] N. Andersson. A New Class of Unstable Modes of Rotating Relativistic Stars. *Astrophysical Journal*, 502:708, August 1998.

[95] J. W. Reijnders and R. A. Duine. Pinning of vortices in a bose-einstein condensate by an optical lattice. *Phys. Rev. Lett.*, 93:060401, Aug 2004.

[96] M. P. Mink, C. M. Smith, and R. A. Duine. Vortex-lattice pinning in two-component Bose-Einstein condensates. *Physical Review A*, 79(1):013605, January 2009.

[97] R. Onofrio, C. Raman, J. M. Vogels, J. R. Abo-Shaeer, A. P. Chikkatur, and W. Ketterle. Observation of Superfluid Flow in a Bose-Einstein Condensed Gas. *Physical Review Letters*, 85:2228–2231, September 2000.

[98] R. G. Corro, I. Scott and A. M. Martin. Dynamics of two-component Bose-Einstein condensates in rotating traps. *PhysRevA*, **80**(3), 2009.

[99] H. Takeuchi, S. Ishino, and M. Tsubota. Binary Quantum Turbulence Arising from Countersuperflow Instability in Two-Component Bose-Einstein Condensates. *Physical Review Letters*, 105(20):205301, November 2010.

[100] C. Hamner, J. J. Chang, P. Engels, and M. A. Hoefer. Generation of Dark-Bright Soliton Trains in Superfluid-Superfluid Counterflow. *Physical Review Letters*, 106(6):065302, February 2011.

[101] M. A. Hoefer, J. J. Chang, C. Hamner, and P. Engels. Dark-dark solitons and modulational instability in miscible two-component Bose-Einstein condensates. *Physical Review A*, 84(4):041605, October 2011.

[102] H. Ishino, S. Takeuchi and M. Tsubota. Two-superfluid model of two-component bose-einstein condensate; first sound and second sound. *arxiv*, 1006.(4450v1), 2010.

[103] P. Ao and S. T. Chui. Binary Bose-Einstein condensate mixtures in weakly and strongly segregated phases. *Physical Review A*, 58:4836–4840, December 1998.

[104] S. T. Chui and P. Ao. Broken cylindrical symmetry in binary mixtures of Bose-Einstein condensates. *Physical Review A*, 59:1473–1476, February 1999.

[105] E. Tiesinga, B. J. Verhaar, and H. T. C. Stoof. Threshold and resonance phenomena in ultracold ground-state collisions. *Physical Review A*, 47:4114–4122, May 1993.

[106] S. L. Cornish, N. R. Claussen, J. L. Roberts, E. A. Cornell, and C. E. Wieman. Stable ^{85}Rb Bose-Einstein Condensates with Widely Tunable Interactions. *Physical Review Letters*, 85:1795–1798, August 2000.

[107] J. L. Roberts, N. R. Claussen, J. P. Burke, Jr., C. H. Greene, E. A. Cornell, and C. E. Wieman. Resonant Magnetic Field Control of Elastic Scattering in Cold ^{85}Rb. *Physical Review Letters*, 81:5109–5112, December 1998.

[108] S. Inouye, M. R. Andrews, J. Stenger, H.-J. Miesner, D. M. Stamper-Kurn, and W. Ketterle. Observation of Feshbach resonances in a Bose-Einstein condensate. *Nature*, 392:151–154, March 1998.

[109] P. Courteille, R. S. Freeland, D. J. Heinzen, F. A. van Abeelen, and B. J. Verhaar. Observation of a Feshbach Resonance in Cold Atom Scattering. *Physical Review Letters*, 81:69–72, July 1998.

[110] J. L. Roberts, N. R. Claussen, S. L. Cornish, E. A. Donley, E. A. Cornell, and C. E. Wieman. Controlled Collapse of a Bose-Einstein Condensate. *Physical Review Letters*, 86:4211–4214, May 2001.

[111] E. A. Donley, N. R. Claussen, S. L. Cornish, J. L. Roberts, E. A. Cornell, and C. E. Wieman. Dynamics of collapsing and exploding Bose-Einstein condensates. *Nature*, 412:295–299, July 2001.

[112] M. O. Borgh and J. Ruostekoski. Topological Interface Engineering and Defect Crossing in Ultracold Atomic Gases. *Physical Review Letters*, 109(1):015302, July 2012.

[113] M. O. Borgh and J. Ruostekoski. Topological interface physics of defects and textures in spinor Bose-Einstein condensates. *Physical Review A*, 87(3):033617, March 2013.

[114] P. P. Hofer, C. Bruder, and V. M. Stojanović. Superfluid drag of two-species Bose-Einstein condensates in optical lattices. *Physical Review A*, 86(3):033627, September 2012.

[115] S. Giorgini, L. P. Pitaevskii, and S. Stringari. Theory of ultracold atomic Fermi gases. *Reviews of Modern Physics*, 80:1215–1274, October 2008.

[116] A. Gezerlis and J. Carlson. Strongly paired fermions: Cold atoms and neutron matter. *Physical Review C*, 77(3):032801, March 2008.

[117] Vinen W.F. and Niemela J.J. Quantum turbulence. *Journal of Low Temperature Physics*, 128(513):167–221, 2002.

[118] W.W. Glaberson, W.I. Johnson and R.M. Ostermeier. Instability of a vortex array heii. *Physical Review Letters*, 33(20):1197–1200, 1974.

[119] R.M. Ostermeier and W.I. Glaberson. Instability of vortex lines in the prescence of axial normal fluid flow. *Journal of Low Temperature Physics*, 21(112):191–196, 1975.

[120] D. K. Cheng, M. W. Cromar, and R. J. Donnelly. Influence of an Axial Heat Current on Negative-Ion Trapping in Rotating Helium II. *Physical Review Letters*, 31:433–436, August 1973.

[121] C. E. Swanson, C. F. Barenghi, and R. J. Donnelly. Rotation of a Tangle of Quantized Vortex Lines in He II. *Physical Review Letters*, 50:190–193, January 1983.

[122] A. Kolmogorov. The Local Structure of Turbulence in Incompressible Viscous Fluid for Very Large Reynolds' Numbers. *Akademiia Nauk SSSR Doklady*, 30:301–305, 1941.

[123] A. N. Kolmogorov. Dissipation of Energy in Locally Isotropic Turbulence. *Akademiia Nauk SSSR Doklady*, 32:16, 1941.

[124] M. Tsubota. Quantum turbulence. *Journal of Physics: Condensed Matter*, 21(164):207–213, 2009.

[125] U. Frisch. *Turbulence. The Legacy of A.N. Kolmogorov*. Cambridge University Press, 1995.

[126] R. J. Donnelly. An Introduction to Experiments on Superfluid Turbulence. In C. F. Barenghi, R. J. Donnelly, and W. F. Vinen, editors, *Quantized Vortex Dynamics and Superfluid Turbulence*, volume 571 of *Lecture Notes in Physics, Berlin Springer Verlag*, page 17, 2001.

[127] C. J. Gorter and J. H. Mellink. On the irreversible processes in liquid helium II. *Physica*, 15:285–304, May 1949.

[128] R. P. Feynman. Application of quantum mechanics to liquid helium. *Progress in Low Temperature Physics*, 1:17–53, 1955.

[129] W. F. Vinen. Mutual Friction in a Heat Current in Liquid Helium II. II. Experiments on Transient Effects. *Royal Society of London Proceedings Series A*, 240:128–143, April 1957.

[130] W. F. Vinen. Mutual Friction in a Heat Current in Liquid Helium II. IV. Critical Heat Currents in Wide Channels. *Royal Society of London Proceedings Series A*, 243:400–413, January 1958.

[131] J. Maurer and P. Tabeling. Local investigation of superfluid turbulence. *EPL (Europhysics Letters)*, 43:29–34, July 1998.

[132] S. R. Stalp, L. Skrbek, and R. J. Donnelly. Decay of Grid Turbulence in a Finite Channel. *Physical Review Letters*, 82:4831–4834, June 1999.

[133] S. R. Stalp, J. J. Niemela, W. F. Vinen, and R. J. Donnelly. Dissipation of grid turbulence in helium II. *Physics of Fluids*, 14:1377–1379, April 2002.

[134] S. R. Stalp and R. J. Donnelly. Decay Of Grid Turbulence In Superfluid Helium 4. In *APS March Meeting Abstracts*, page D4156, March 1997.

[135] L. Skrbek, J. J. Niemela, and R. J. Donnelly. Four Regimes of Decaying Grid Turbulence in a Finite Channel. *Physical Review Letters*, 85:2973–2976, October 2000.

[136] K. W. Schwarz and J. R. Rozen. Anomalous decay of turbulence in superfluid ^{4}He. *Physical Review Letters*, 66:1898–1901, April 1991.

[137] S. W. Van Sciver. The Temperature Dependent Drag Crisis on a Sphere in Flowing Helium II. In C. F. Barenghi, R. J. Donnelly, and W. F. Vinen, editors, *Quantized Vortex Dynamics and Superfluid Turbulence*, volume 571 of *Lecture Notes in Physics, Berlin Springer Verlag*, pages 51–65, 2001.

[138] D. Kivotides, C. F. Barenghi, and Y. A. Sergeev. Interactions between particles and quantized vortices in superfluid helium. *Physics Review B*, 77(1):014527, January 2008.

[139] M. Kobayashi and M. Tsubota. Quantum turbulence in a trapped Bose-Einstein condensate. *Physical Review A*, 76(4):045603, October 2007.

[140] M. Kobayashi and M. Tsubota. Quantum Turbulence in a Trapped Bose-Einstein Condensate under Combined Rotations around Three Axes. *Journal of Low Temperature Physics*, 150:587–592, February 2008.

[141] P. Vollhardt, D. & Wölfle. *The Superfluid Phases of Helium 3*. Taylor and Francis, London, 2002.

[142] S. G. Sydoriak, E. R. Grilly, and E. F. Hammel. Condensation of pure he^3 and its vapor pressures between 1.2 k and its critical point. *Phys. Rev.*, 75:303–305, Jan 1949.

[143] J.C. Wheatley. Experimental properties of superfluid ^{3}He. *Rev. Mod. Phys.*, 47:415–470, Apr 1975.

[144] D. D. Osheroff, R. C. Richardson, and D. M. Lee. Evidence for a New Phase of Solid He^3. *Physical Review Letters*, 28:885–888, April 1972.

[145] D. D. Osheroff, W. J. Gully, R. C. Richardson, and D. M. Lee. New Magnetic Phenomena in Liquid He^3 below 3 mK. *Physical Review Letters*, 29:920–923, October 1972.

[146] P. M. Walmsley, V. B. Eltsov, P. J. Heikkinen, J. J. Hosio, R. Hänninen, and M. Krusius. Turbulent vortex flow responses at the *ab* interface in rotating superfluid ^{3}he-*b*. *Phys. Rev. B*, 84:184532, Nov 2011.

[147] E.P.S. Vilenkin, A. & Shellard. *Cosmic Strings and Other Topological Defects*. Cambridge University Press, 1994.

[148] T. W. B. Kibble. Topology of cosmic domains and strings. *Journal of Physics A Mathematical General*, 9:1387–1398, August 1976.

[149] M. B. Hindmarsh and T. W. B. Kibble. Cosmic strings. *Reports on Progress in Physics*, 58:477–562, May 1995.

[150] C. Bäuerle, Y. M. Bunkov, S. N. Fisher, H. Godfrin, and G. R. Pickett. Laboratory simulation of cosmic string formation in the early Universe using superfluid ^{3}He. *Nature*, 382:332–334, July 1996.

[151] D. I. Bradley, S. N. Fisher, A. M. Guénault, R. P. Haley, J. Kopu, H. Martin, G. R. Pickett, J. E. Roberts, and V. Tsepelin. Relic topological defects from brane annihilation simulated in superfluid ^{3}He. *Nature Physics*, 4:46–49, January 2008.

[152] S. N. Fisher, G. R. Pickett, P. Skyba, and N. Suramlishvili. Decay of persistent precessing domains in ^{3}He-B at very low temperatures. *Physics Review B*, 86(2):024506, July 2012.

[153] G Volovik. *The Universe in a Helium Droplet*. Oxford University Press, 2003.

[154] C. Raman, M. Köhl, R. Onofrio, D. S. Durfee, C. E. Kuklewicz, Z. Hadzibabic, and W. Ketterle. Evidence for a Critical Velocity in a Bose-Einstein Condensed Gas. *Physical Review Letters*, 83:2502–2505, September 1999.

[155] T.-L. Ho and V. B. Shenoy. Binary Mixtures of Bose Condensates of Alkali Atoms. *Physical Review Letters*, 77:3276–3279, October 1996.

[156] H. Pu and N. P. Bigelow. Collective Excitations, Metastability, and Nonlinear Response of a Trapped Two-Species Bose-Einstein Condensate. *Physical Review Letters*, 80:1134–1137, February 1998.

[157] P. A. Ruprecht, M. Edwards, K. Burnett, and C. W. Clark. Probing the linear and nonlinear excitations of Bose-condensed neutral atoms in a trap. *Physics Review A*, 54:4178–4187, November 1996.

[158] V. P. Mineev. The theory of the solution of two near-ideal Bose gases. *Soviet Journal of Experimental and Theoretical Physics*, 40:132, July 1974.

[159] Lecture Notes. Introduction to nuclear and particle physics ii. *Goethe Universtat*, Frankfurt am Main.

[160] J.D. Walecka. *Introduction to Modern Physics*. World Scientific Publishing Company, Singapore, 2008.

[161] R. Côté, A. Dalgarno, H. Wang, and W. C. Stwalley. Potassium scattering lengths and prospects for bose-einstein condensation and sympathetic cooling. *Phys. Rev. A*, 57:R4118–R4121, Jun 1998.

[162] C Gaul, N Renner, and C. A. Müller. Speed of sound in disordered bose-einstein condensates. *Phys. Rev. A*, 80(5):053620, Nov 2009.

[163] D. A. Butts1 and D. S. Rokhsar. Predicted signatures of rotating Bose-Einstein condensates. *Nature*, 397:327–329, January 1999.

[164] S. Tung, V. Schweikhard, and E. A. Cornell. Observation of Vortex Pinning in Bose-Einstein Condensates. *Physical Review Letters*, 97(24):240402, December 2006.

[165] M. Jahan-Miri. Glitches induced by the core superfluid in a neutron star. *Mon. Not. R. Astron Soc.*, 330:279–287, February 2002.

[166] N. Goldman, G. Juzeliunas, P. Ohberg, and I. B. Spielman. Light-induced gauge fields for ultracold atoms. *ArXiv e-prints*, August 2013.

[167] N. Andersson and G. L. Comer. Relativistic Fluid Dynamics: Physics for Many Different Scales. *Living Reviews in Relativity*, 10:1, January 2007.

[168] J. M. McGuirk, D. M. Harber, H. J. Lewandowski, and E. A. Cornell. Normal-Superfluid Interaction Dynamics in a Spinor Bose Gas. *Physical Review Letters*, 91(15):150402, October 2003.

[169] L.D. Landau and E.M. Lifshitz. *Fluid Mechanics, 2nd Edition*. Butterworth-Heinemann, Oxford, U.K., 1987.

[170] R. Prix. Variational description of multifluid hydrodynamics: Uncharged fluids. *Physics Review D*, 69(4):043001, February 2004.

[171] H. E. Hall and W. F. Vinen. The Rotation of Liquid Helium II. II. The Theory of Mutual Friction in Uniformly Rotating Helium II. *Royal Society of London Proceedings Series A*, 238:215–234, December 1956.

[172] R. Prix, G. L. Comer, and N. Andersson. Inertial modes of non-stratified superfluid neutron stars. *Mon. Not. R. Astron Soc.*, 348:625–637, February 2004.

[173] S. Yoshida and U. Lee. Relativistic R-Modes in Slowly Rotating Neutron Stars. In A. Krasnitz, R. Potting, A. M. Mourão, & M. Pimenta, editor, *New Worlds in Astroparticle Physics*, pages 245–251, April 2003.

[174] S. Yoshida and U. Lee. R-Modes of Neutron Stars with a Solid Crust. *Astrophysical Journal*, 546:1121–1125, January 2001.

[175] N. Andersson, G. L. Comer, and K. Glampedakis. How viscous is a superfluid neutron star core? *Nuclear Physics A*, 763:212–229, December 2005.

[176] K. Glampedakis, N. Andersson, and L. Samuelsson. Magnetohydrodynamics of superfluid and superconducting neutron star cores. *Mon. Not. R. Astron Soc.*, 410:805–829, January 2011.

[177] G. Mendell. Superfluid hydrodynamics in rotating neutron stars. I - Nondissipative equations. II - Dissipative effects. *Astrophysical Journal*, 380:515–540, October 1991.

[178] N. Andersson, K. Glampedakis, and B. Haskell. Oscillations of dissipative superfluid neutron stars. *Physics Review D*, 79(10):103009–+, May 2009.

[179] W. I. Glaberson, W. W. Johnson, and R. M. Ostermeier. Instability of a Vortex Array in He II. *Physical Review Letters*, 33:1197–1200, November 1974.

[180] W. I. Glaberson and R. J. Donnelly. Growth of Pinned Quantized Vortex Lines in Helium II. *Physical Review*, 141:208–210, January 1966.

[181] N Andersson. Gravitational waves from neutron star instabilities. *Conference Lecture*, 2006.

[182] D. Page, M. Prakash, J. M. Lattimer, and A. W. Steiner. Rapid Cooling of the Neutron Star in Cassiopeia A Triggered by Neutron Superfluidity in Dense Matter. *Physical Review Letters*, 106(8):081101, February 2011.

[183] P. S. Shternin, D. G. Yakovlev, C. O. Heinke, W. C. G. Ho, and D. J. Patnaude. Cooling neutron star in the Cassiopeia A supernova remnant: evidence for superfluidity in the core. *Mon. Not. R. Astron. Soc.*, 412:L108–L112, March 2011.

[184] N. Andersson and G. L. Comer. On the dynamics of superfluid neutron star cores. *Mon. Not. R. Astron. Soc.*, 328:1129–1143, December 2001.

[185] B. Haskell, N. Andersson, and G. L. Comer. Dynamics of dissipative multifluid neutron star cores. *Phys Rev D*, 86(6):063002, September 2012.

[186] K. D. Kokkotas and N. Stergioulas. Analytic description of the r-mode instability in uniform density stars. *Astron. Astrophysics*, 341:110–116, January 1999.

[187] W. C. G. Ho, K. Glampedakis, and N. Andersson. Magnetars: super(ficially) hot and super(fluid) cool. *Mon. Not. R. Astron. Soc.*, 422:2632–2641, May 2012.

[188] E. H. Gudmundsson, C. J. Pethick, and R. I. Epstein. Neutron star envelopes. *Astrophysical Journal*, 259:L19–L23, August 1982.

[189] D. N. Aguilera, J. A. Pons, and J. A. Miralles. The Impact of Magnetic Field on the Thermal Evolution of Neutron Stars. *Astrophysical Journal*, 673:L167–L170, February 2008.

[190] T. D. C. Bevan, A. J. Manninen, J. B. Cook, A. J. Armstrong, J. R. Hook, and H. E. Hall. Vortex Mutual Friction in Rotating Superfluid ^{3}He- B. *Physical Review Letters*, 74:750–753, January 1995.

[191] E. B. Sonin. Mutual friction force in rotating helium II at low temperatures and near the λ-point. *Journal of Low Temperature Physics*, 42:417–432, March 1981.

[192] N. Andersson and G.L. Comer. Variational multi-fluid dynamics and causal heat conductivity. *Physics Reports*, 96(4):205 – 250, 2009.

[193] L.D. Landau and E.M. Lifshitz. Course of Theoretical Physics. In *Fluid Mechanics*, volume 6. Butterworth-Heinemann Ltd., 1987.

[194] L. Onsager. Statistical hydrodynamics. *Il Nuovo Cimento*, 6, Supplement 2:279, Mar 1949.

[195] C. Lopez-Monsalvo. Covariant Thermodynamics and Relativity. *ArXiv e-prints*, July 2011.

[196] C. S. Lopez-Monsalvo and N. Andersson. Thermal dynamics in general relativity. *Royal Society of London Proceedings Series A*, 467:738–759, March 2011.

[197] N. Andersson and C. S. Lopez-Monsalvo. A consistent first-order model for relativistic heat flow. *Classical and Quantum Gravity*, 28(19):195023, October 2011.

[198] N. Andersson and G. L. Comer. A flux-conservative formalism for convective and dissipative multi-fluid systems, with application to Newtonian superfluid neutron stars. *Classical and Quantum Gravity*, 23:5505–5529, September 2006.

[199] Casas-Vázquez J. & Lebon G. Jou, D. *Extended Irreversible Thermodynamics*. Springer, Berlin, 1993.

[200] D. Lebon, G. Jou and J. Casas-Vázquez. *Understanding Non-equilibrium Thermodynamics*. Springer-Verlag, Berlin, 2008.

[201] Y.A. Cengel. *Thermodynamics and Heat Transfer*. McGraw-Hill, New York, 2008.

[202] L. Samuelsson, C. S. Lopez-Monsalvo, N. Andersson, and G. L. Comer. Relativistic two-stream instability. *General Relativity and Gravitation*, 42:413–433, February 2010.

[203] R. V. E. Lovelace, K. P. Jore, and M. P. Haynes. Two-Stream Instability of Counterrotating Galaxies. *Astrophysical Journal*, 475:83, January 1997.

[204] A. F. Cheng and M. A. Ruderman. Bunching mechanism for coherent curvature radiation in pulsar magnetospheres. *Astrophysical Journal*, 212:800–806, March 1977.